UNIVERSITÀ DEGLI STUDI DI PADOVA

DIPARTIMENTO DI INGEGNERIA DELL'INFORMAZIONE

UNIVERSITY OF PADOVA

DEPARTMENT OF INFORMATION ENGINEERING

MASTER'S DEGREE THESIS IN BIOENGINEERING

EXPERIMENTAL ANALYSIS OF RUNNING BIOMECHANICS OF ELITE PARALYMPIC AMPUTEE SPRINTERS IN TREADMILL AND TRACK TESTS

Supervisor: Prof. Nicola Petrone

Candidate: Sara Barbacane

Co-Supervisors: Eng. Andrea G. Cutti
Eng. Roberto Di Marco
Eng. Samira G. Breban

ACADEMIC YEAR 2021 – 2022

Date 13 / 12 / 2022

ABSTRACT

The study of biomechanics of running in amputees, in terms of kinematic and kinetic parameters, is crucial to gain a deeper insight of how the running gesture is performed by athletes wearing running specific prostheses. Knowledge of how the body moves and what forces are generated has implications for the design of prosthetic components, which must ensure the safety of athletes and help them improve their performance, with the aim of filling the gap between amputee and able-bodied sprinters.

The aim of this work is to contribute to the development of a biomechanical analysis software that allows the processing of data collected with different instrumentations in order to provide well-integrated and meaningful outputs.

Data collection is the first fundamental step in the analysis and requires careful design and planning of experimental sessions. Two in-vivo tests blocks have been carried out and each test session required specific protocols and specific instrumentations, including Motion Capture cameras, force platforms, wearable force sensors and inertial sensors. In each test session, two types of tests have been performed, one acceleration test and one constant speed test.

Afterwards, data must be processed to extract the desired biomechanical parameters. The analysis tool is made up of several interconnected sections. The first part is dedicated to kinematic analysis, aimed at joint angles, while the second part focuses on the analysis of Ground Reaction Forces, impulses, intersegmental forces and joint torques.

The results from each section are then compared to highlight the differences between types of tests, types of running surface and prosthesis configurations. All these outcomes should then be organized to provide trainers and orthopaedic technicians with a detailed and intelligible description of the athletes' tests, for a better qualitative but also quantitative evaluation of the performance.

Table of contents

Introduction

OLIMPIA project

The present work has been carried out in collaboration with INAIL (Italian National Institute for Insurance against Accidents at Work - *Istituto Nazionale Assicurazione Infortuni sul Lavoro*), a non-profit public entity whose aim is to reduce work-related accidents, protect workers who perform dangerous jobs and enable people to return to work after an injury [1].
In detail, the research is related to a specific division of INAIL, the Prosthesis Centre located in Vigorso di Budrio, near Bologna, where the most innovative techniques are applied to create custom-made prostheses and orthopaedic devices and to support patients in the rehabilitation process. In the Prosthesis Centre, sockets are modelled and assembled to create the prosthesis and then delivered to the patient, who is also assisted in terms of physical therapy and training. Helping injured people regain their autonomy and reintegrate into their social context is one of the main goals of INAIL, whose investigation also focuses on sport, which is considered key in this perspective. The experience gained in the design and manufacture of special prosthetic components, together with the use of new materials with high mechanical and elastic properties, enabled the Institute to address and solve the complex problems associated with the creation of sports devices, both for amateur and competitive athletes. INAIL is in fact the supplier of prostheses for the Italian Paralympic team.

My work relates to a research project in which University of Padua and INAIL collaborate. It is called 'OLIMPIA: *New technologies at paralympic athletes' service*' and addresses the development of new technologic innovative solutions aimed at improving the performance of Paralympic athletes and the safety in sport practice.
On the one hand the project focuses on the performance of prostheses and orthoses for running, long jumping and alpine skiing, on the other hand on their manufacture, and in particular it aims to the simplification and optimization of this process [2].

Regarding Paralympic running, in the course of the project it has being studied using many different approaches, which can be schematized in the table below.

Table 0.1 Approaches for the research project

	IN VIVO	IN VITRO	IN SILICO
INDOOR	Treadmill test	Test Bench	FEM, Neural Network
OUTDOOR	Track test		

Starting from top left, the *in vivo – indoor* approach indicates the condition in which athletes run on a treadmill in a laboratory equipped with several instrumentations, such as motion capture system and force platforms, which allow extensive data collection.

The *in vivo - outdoor* approach consists of performing tests with athletes running on an athletics track and having wearable sensors, like load cells and inertial sensors, and/or hitting instrumented portions of the track containing force platforms and surrounded by motion capture system.

In the box top right, the *in vitro – indoor* is the approach used to characterize the mechanical behaviour of the running prosthetic foot (RPF), which is mounted in a hydraulic test bench and then oriented and loaded reproducing the movement of the athlete.

Furthermore, there is the *in silico* approach, which consists in the creation of a finite element model (FEM) of the RPF starting from its geometrical and mechanical properties. The FEM model can then be used together with a mathematical model to simulate the foot elastic behaviour on varying loading conditions. Moreover, the *in silico* approach also includes the prediction of Ground Reaction Forces through artificial intelligence algorithms, such as neural networks.

There is another section of the OLIMPIA Project dedicated to the study of running specific sockets in terms of mechanical behaviour, in order to improve the design of these essential prosthetic components.

The focus in this Thesis will be on the *in vivo* approaches, both *indoor* or *outdoor* and deals with the processing of kinematic and kinetic data collected during experimental sessions in which elite Paralympic sprinters participated.

Motivation

Given the importance of sport as a means to improve physical and mental health and encourage social integration, both for able-bodied people and, even more so, for people with disabilities, it is essential to understand how the sport gesture is performed, in order to ensure the safety of the athletes. To this extent, many studies have focused on the description and analysis of sport activities, including also running.

The study of running biomechanics, in terms of kinematic and kinetic parameters, is aimed at the quantitative evaluation of the sport performance by providing objective measurements, such as propulsion forces or moments acting at joints. In addition, in the case of amputee athletes, biomechanics provides greater insight into how they compensate for replacement of active leg with a passive prosthetic implement [3] and so in the manner in which they regain running ability.

Collection and processing of experimental data play a fundamental role either in the development of new of training strategies or in the design of the prosthetic devices. On the one hand training should be improved for injury prevention and promotion of long-term musculoskeletal health; on the other hand prostheses should be optimized in terms of energy storage and release, also combining the advantages due to the use of new materials and the advancements in manufacturing technologies.

This knowledge then translates into improved performance, for example by enabling professional athletes to perform at elite levels. This is also evidenced by the growing number of Paralympic athletes, who not only provide clear evidence of engineering advances, but also exemplify resilience and determination. They thus become a great source of motivation both for other people living in their same physical condition and for other athletes and non-athletes.

Aim of the Thesis

The present work focuses on the study of running biomechanics of elite Paralympic sprinters and on the development of a method to extract quantitative parameters, which can be descriptive of their performance from an engineering point of view. The research has been built on the basis of previous studies, which investigated the effect of different prosthesis configurations on the performance, and it has been moulded on the basis of the instrumentation available.
In particular, there are three main research questions (RQ) which motivated this work and each RQ is targeting a specific aspect.

The first research question (RQ1) is: what are the differences between the Steady State Running and the Resisted Accelerated Running tests performed on treadmill by a single subject, wearing the same socket alignment?

The second research question (RQ2) is: what are the differences between running tests performed on treadmill and on track by a single subject, wearing the same socket alignment?

The third research question (RQ3) is: what are the effects of different socket alignments in running tests performed on treadmill by two subjects? For subject 1, are the results consistent with the outcomes obtained in a previous experimental session with a different instrumentation setup?

Each research question may have several dependent biomechanical variables, for instance joint angles, Ground Reaction Forces, joint moments or the power generated, but also subjective evaluation of the athlete can be considered. Only the most relevant biomechanical variables will be discussed. Moreover, since all athletes who took part in the experimental sessions are unilateral amputees, comparisons between the affected and the unaffected limb are also addressed. In some cases, if boundary conditions are similar, the inter-subject variability is also investigated.

The main steps developed in order to carry out the research were:

1. Planning and realization of experimental sessions for data collection. Three experimental sessions were performed and different instrumentations were employed.
2. Design and implementation of a tool for the biomechanical analysis. This tool has been implemented in MATLAB and it elaborates data gathered with different instrumentation to output numerical and graphical representations of the quantities of interest.
3. Discussion and critical comparison of the results obtained from the just cited software.

Chapter 1

Biomechanics Of Running

Running can be defined as the action to move the body forward at more sustained pace than walking, so that there is not a period in which both feet are simultaneously touching the ground, but on the contrary, there is a moment in which neither foot is touching the ground. The minimum speed required to mark the transition between walking and running is considered 2 m/s [4].

The analysis of running follows the same terminology used in the analysis of walking, since both belong to the same macro study area of gait analysis. In this context, the basic unit of measurement is the gait cycle, which begins with one foot touching the ground and ends when the same foot touches the ground again. In terms of time and space parameters, the time required to complete one gait cycle is defined as stride time and the distance travelled as stride length.

The gait cycle can be broken down into two main phases: stance and swing. Stance refers to the time period in which the foot is in contact with the ground, while swing to the period in which the foot is floating. In walking, the stance phase makes up nearly 60% of the stride time and swing the remaining 40%, whereas in running these percentages are inverted, so swing lasts longer than stance. In running, the stance-to-swing ratio ranges from 40/60 to 20/80, depending on the running speed. As speed increases, stance time decreases, double float time increases and, on the whole, cycle time shortens (Figure 1.1). Moreover, from a more technical point of view, as speed increases further, initial contact changes from being on the hindfoot, more similar to what happens in walking, to the forefoot, that is proper of sprinting.

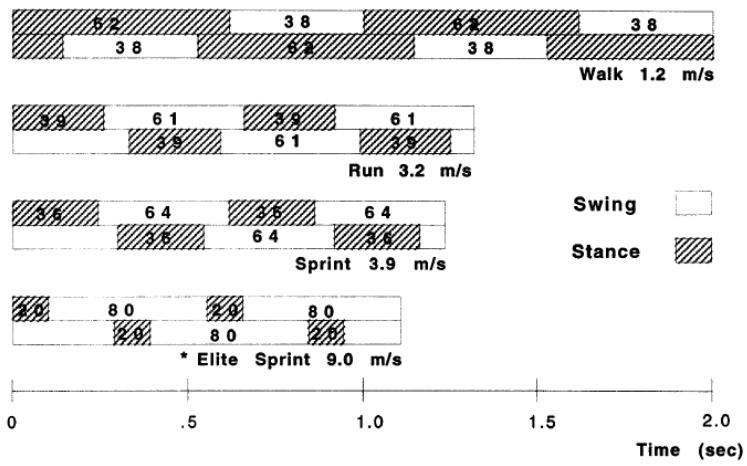

Figure 1.1. Variation in gait cycle parameters with speed of movement [The biomechanics of running, Novacheck [5]*]*

Initial contact, or footstrike, is the first sub-phase of stance, and it is followed by mid-stance and toe off. Swing can also be broken down into sub-phases, which are initial swing, mid-swing and terminal swing. At the toe off of the homolateral leg, the contralateral is just after mid-swing and straight after there is the 'flight' phase, in which both libs are floating.

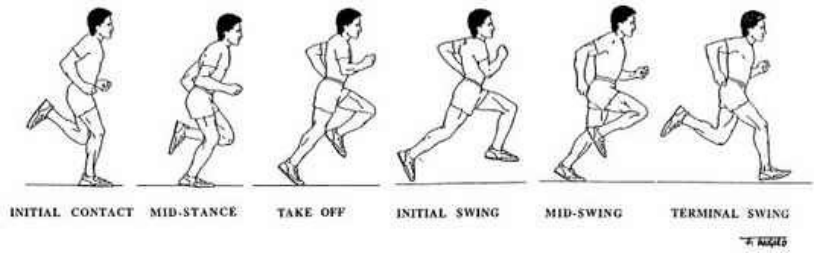

Figure 1.2. Running gait cycle. [Oandplibrary.org]

In the gait cycle there is an alternation of energy generation and absorption, to which contribute both potential and kinetic energy. In the absorption phase, that starts at mid-swing and end at mid-stance, the centre of mass of the body falls from its peak and decelerates horizontally, therefore loses potential and kinetic energy. After stance phase reversal, that is mid-stance, the generation phase begins. Kinetic and potential energy increase, since the centre of mass is propelled upward and forward until mid-swing, or swing phase reversal.

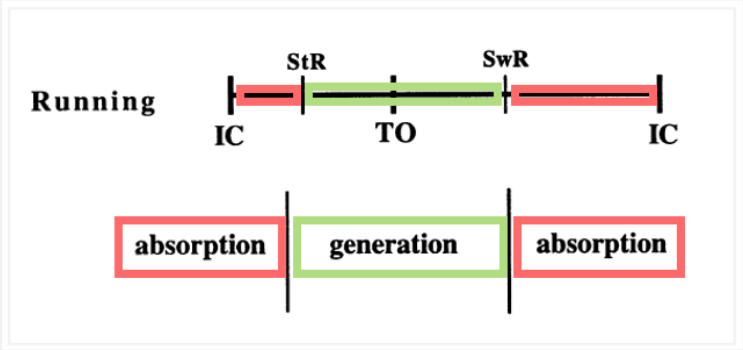

Figure 1.3. Energy absorption and generation phases in the running gait cycle [Adapted from: Biomechanics of running, Novacheck [5]*]*

There are several factors influencing the biomechanical parameters used to describe running. First of all, measures are affected by speed: to make a comparison between two individuals or between two running conditions, it is necessary to have a common speed, otherwise it would not be possible to distinguish whether the differences are due to speed or to other factors.
The second important factor is anthropometry (and gender), which may have an influence on the calculus of kinematic parameters, such as relative stride length.
The third point is the type of running surface, for example a running track or a treadmill.

Kinematics

Kinematics is the study of the motion of bodies without reference to mass or force. It aims to provide a description of the temporal and spatial parameters characterizing the moving body, including its orientation and the angles between its segments.

The basic parameters that can be derived from the spatial position of the body are stride length (SL) and step length, defined as the distance from one foot contact to the next contact of the same foot or of the other foot respectively. Relative stride length is the stride length divided by leg length, while contact length is the forward displacement of the centre of mass during the stance phase.

If the time axis is also considered, it is possible to calculate stride rate (SR), that is the number of strides per second, or its inverse, cycle time; the rate at which the body is moving (velocity V) and the rate at which velocity is changing, thus obtaining acceleration. One possible way to calculate velocity using the just cited parameters is the product of stride length and stride rate.

$$V = SL \times SR \tag{1.1}$$

It has been observed that both stride rate and stride length increase with increasing running speed, and running experience also makes a difference. Several studies highlighted that 'elite' distance runners usually have longer stride length and shorter support time than 'good' athletes running at the same speed.

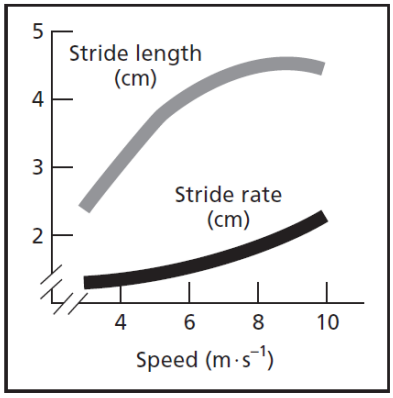

Figure 1.4. Changes in kinematic variables with increased running speed [The Dynamics of Running, Williams [4]*]*

In order to describe the relative orientation of body segments, simple instrumentation like the electrogoniometer can be used, which is a thin piece of wire sensitive to bending in up to three planes simultaneously. Despite being relatively accurate and unintrusive, its use may introduce

some errors when assessing human motion. The main source of error is the placement of the electrogoniometer in a plane different from the one of interest, thus adding some cross-talk between two planes of motion, e.g. frontal and sagittal. Errors in the signal could also be due to the relative movement of the end blocks of the electrogoniometer taped to the soft tissue around a joint. Another limitation to the use of electrogoniometers is the finite accuracy of angular displacement given by strain gauge wires. Moreover, if one is interested in studying multiple joint angles at a time, then needs to put many devices on the body and this may result in some discomfort for the athlete.

Accelerometers can be used to measure acceleration and deceleration of body segments. They allow direct and immediate signal output, but they do not give any direct information about the joint positions or on segment angles.

Movement analysis

To have an exhaustive description of gait kinematics, a movement analysis system is required, which is made up of cameras filming an activity with the subject having markers fixed on the skin with tape. Markers used in movement analysis are small spheres which can emit light (active markers) or just reflect light (passive markers). The instrumentation adopted during the present research work consists in cameras having infra-red light emitting diodes mounted around the camera lens and passive markers which reflect light back to camera lens. This way, in the images acquired by the cameras, markers are shown as bright spots on a dark background, while the rest of the body shape is not visible anymore (Figure 1.5). For a three-dimensional analysis, the minimum number of cameras is two, but usually at least four cameras are used, in order to increase the chances of tracking markers on the body during the entire movement [6].

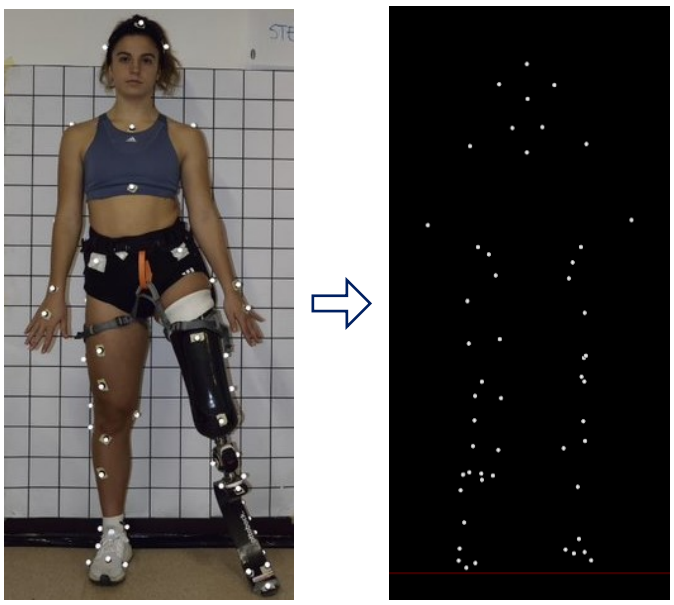

Figure 1.5. Image from digital camera (left) and from an infra-red camera-based system (right)

The rationale for this method is to replace the complex morphology of body segments with a simpler one. More precisely, the body segment is approximated to a rigid body defined by at least three markers that are assumed to have fixed relative distances. Each rigid body can then be associated with a coordinate system and its movement described with respect to a global coordinate system.

A coordinate system (CS) is an orthonormal right-handed triad composed of three unit vectors. The global CS is usually relative to the laboratory, or to the environment in which the observed motion takes place, while the local CS is relative to each body segment. Local CSs are defined using the markers placed on the body, either on anatomical landmarks or on "technical" points, it is to say points not related to the anatomy of the body segment.

Given a local CS, its position and orientation, with respect to the global CS, fully describe the movement of the related segment.

The position is defined as a vector connecting the local origin ${}^{glo}O_{loc}$ to the origin of the coordinate system ${}^{glo}O_{glo}$.

$$ {}^{glo}\vec{p}_{loc} = {}^{glo}O_{loc} - {}^{glo}O_{glo} \qquad (1.2) $$

The orientation is defined by a 3 x 3 matrix, called direction cosine matrix or orientation matrix, whose columns represent the unit vectors of the local CS projected onto the global axes. Therefore, the matrix ${}^{glo}\boldsymbol{R}_{loc}$ transforms the local frame into the global frame and its elements represent the cosine of the angle between the axes in the local reference frame and the axes in the global one.

Orientation matrix and position vector are usually expressed together in a 4 x 4 matrix, named rototranslation matrix or 'transformation matrix', which represent the pose of the coordinate system with respect to the global CS.

$$ {}^{glo}\boldsymbol{T}_{loc} = \begin{bmatrix} {}^{glo}\boldsymbol{R}_{loc} & {}^{glo}\vec{p}_{loc} \\ 0 \quad 0 \quad 0 & 1 \end{bmatrix} $$

(1.3)

Cardan and Euler angles

The orientation matrix is made up of nine elements, but due to the orthonormality of the vectors representing its columns, the number of degrees of freedom reduces to three. Therefore, only three parameters are actually needed to represent the orientation of a body.
The most used are:

- Cardan angles (φ, θ, ψ)
- Euler 'Aeronautical' angles (Roll – pitch – yaw)

Cardan and Euler 'Aeronautical' angles are alternative ways to express the sequence of elementary rotations the body should make to reach its final orientation. Elementary rotation is the rotation of a vector around the axis x, y or z of a reference frame and its mathematical representation is a 3-by-3 matrix. If the vector rotates of a generic θ angle, the three possible elementary rotations can be expressed by the following matrices:

$$ R_x(\theta) = \begin{bmatrix} 1 & 0 & 0 \\ 0 & \cos\theta & -\sin\theta \\ 0 & \sin\theta & \cos\theta \end{bmatrix} \quad R_y(\theta) = \begin{bmatrix} \cos\theta & 0 & \sin\theta \\ 0 & 1 & 0 \\ -\sin\theta & 0 & \cos\theta \end{bmatrix} \quad R_z(\theta) = \begin{bmatrix} \cos\theta & -\sin\theta & 0 \\ \sin\theta & \cos\theta & 0 \\ 0 & 0 & 1 \end{bmatrix} $$

Figure 1.6. Rotation matrices

Cardan angles define three subsequent elementary rotations around moving axes and the final orientation matrix is obtained by post-multiplication of the three elementary rotation matrices. However, in movement analysis, the inverse procedure must be done, that is the extraction of the angles from the orientation matrix. Formulas used to obtain angles involve resolution of a sequence of trigonometric equations and the order in which equations are computed depend on the precise sequence of axes adopted. The sequence should have the axis of main rotation in the first place. One of the most used Cardan sequences, at least in gait analysis, is $Z\ x'\ y''$, because the focus is usually on the flexion/extension movement, which takes place about the Z axis. The single apex indicates that the second rotation happens about the once rotated x axis, while the double apex notifies that the third rotation happens about the twice rotated y axis.

Euler ‘Aeronautical’ angles correspond to three rotations executed about three different fixed perpendicular axes. For example, Roll, Pitch, Yaw are the angles of rotation about X, Y and Z axis respectively. In this case, the final orientation matrix is obtained by pre-multiplication of the three elementary rotation matrices. The procedure to obtain the angles from the orientation matrix is analogous the one described for Cardan angles.

Prior to calculation of angles and to give such angles a physiological meaning, it is necessary to define the coordinate systems of the segments using anatomical landmarks, either physical (individuated by markers), or virtual (reconstructed in the data processing phase). According to ISB recommendations [7], the longitudinal axis (y) of a limb will be approximated to the vector joining the centre of the distal joint to the centre of the proximal joint, the medial-lateral axis (z) will be approximated to the vector joining a medial and a lateral bone prominence, e.g. the epicondyles, and the antero-posterior axis (x) will be the vector completing the orthogonal triad.

Kinetics

Kinetics focuses on the study of forces and moments that result in the movement of body segments. The main goal of kinetic analysis, often called also dynamic analysis, is deriving joints moments and powers from Ground Reaction Forces and therefore estimating the internal forces, which are the forces exerted by muscles. In this respect, kinetic analysis makes an important contribution to understanding the metabolic expenditure and the fatigue process and to evaluation of athletic performance.

Ground Reaction Forces

The focus of kinetics is on Ground Reaction Forces (GRFs), which are the reaction forces generated as a result of the body hitting or resting on the ground [6]. According to the Newton’s third law, when the runner exerts a force on the ground, he/she receives an equal and opposite reaction force that drives him/her up and forward. GRF is represented as a vector, which goes from the ground on the foot. In a three-dimensional space, such vector can be decomposed into its horizontal, vertical and transversal components.

In order to determine the effects of GRF on the body, it is necessary to know its point of application, also known as centre of pressure (COP). It can be assessed through force platforms or baropodometric platforms. The former measures the total force applied by the foot to the ground and the moments about the axes, thus enabling the calculation of the COP location; the latter measures only the vertical component of the force and divides it by the active area of each

sensor to gives in output a pressure map.

The direction and magnitude of the Ground Reaction Force is determined by the position and the acceleration of the centre of mass of the runner. For example, during sprinting the trunk is leaned forward, therefore the centre of gravity falls ahead of the contact point and GRF allows forward acceleration. When reaching maximum velocity, the body returns upright, the centre of mass moves backward and the GRF do not cause any acceleration [5].

Ground Reaction Forces are usually analysed in their three cartesian components. The greatest contribution to the total vector is given by the vertical component. There is not a unique pattern representative of vertical GRF in runners, since the shape of this curve varies whether the subject is a rearfoot (Figure 1.7-a), midfoot (Figure 1.7-b) or forefoot (Figure 1.7-c) striker.

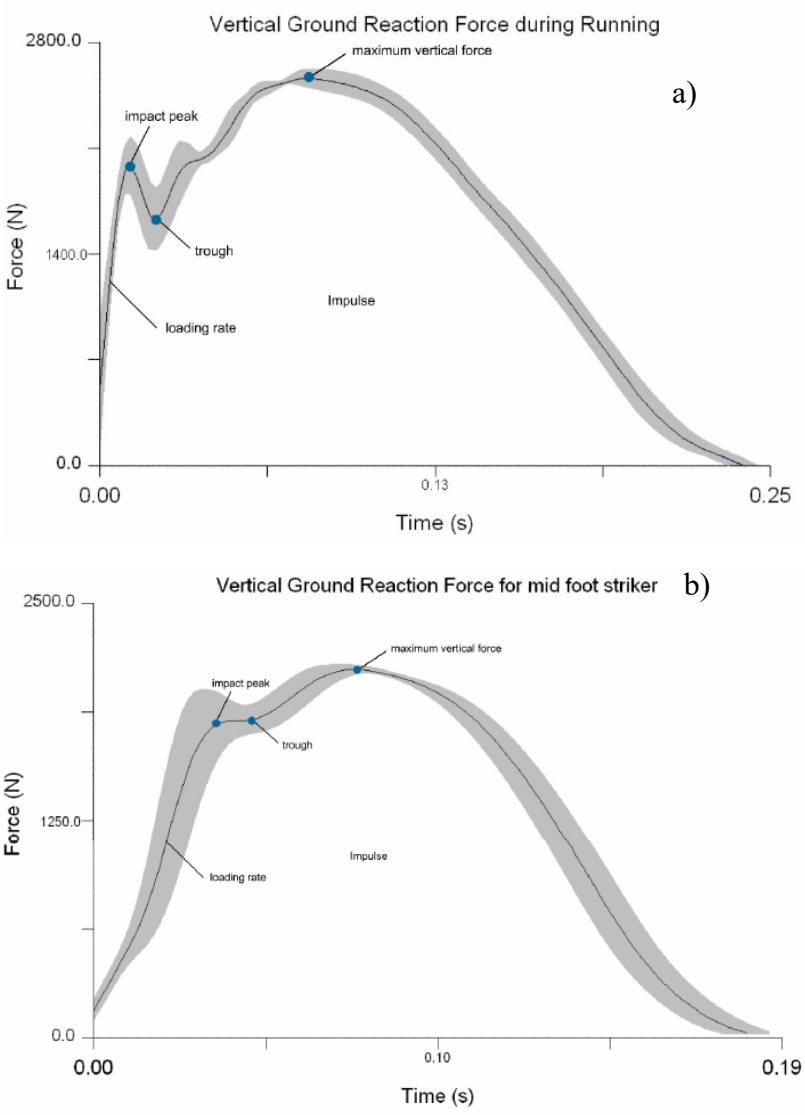

Figure 1.7 Vertical Ground Reaction Force patterns: a) Typical Rearfoot striker, b) Typical Midfoot striker [Biomechanics in Clinics and Research, Richards [6]]

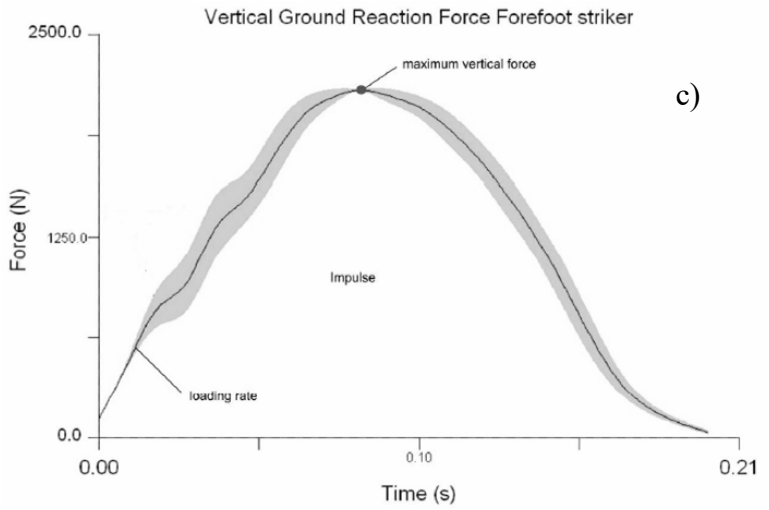

Figure 1.7.c) Vertical Ground Reaction Force: typical Forefoot striker pattern [Biomechanics in Clinics and Research, Richards [6]*]*

In rearfoot strikers, vertical force typically shows two peaks separated by a valley, named 'trough' phase. The first peak, called impact or loading peak, represents how hard the person is hitting the ground, while the second peak, higher than the former, is referred to as propulsive or active peak and it is mainly related to body deceleration downwards and the simultaneous muscle activity. Its magnitude can reach and sometimes exceed 2.5 times the person's body weight, which is twice the maximum value of vertical GRF reached in walking, but it is very dependent on the running speed. In midfoot strikers the first peak is usually still present but much attenuated, whereas in forefoot strikers there is only the propulsive peak.

The trough phase is clearly discernible only in rearfoot strikers and corresponds to the reduction in force after the initial impact, in which the ankle moves rapidly into plantarflexion and then to the foot flat position.

The initial rate of loading, obtained by dividing the difference between two force measurements during initial loading by the time elapsed, is a way to describe the quality of shock absorption during initial contact. The lower the value of this rate, the better the ankle and knee joint work to absorb the initial impact. The lowest values of impact loading rate can be observed in forefoot strikers, while the highest values belong to rearfoot strikers.

The pattern of antero-posterior force shows three main elements: two consecutive negative peaks during the loading phase and one positive peak during the propulsion phase. The first one is the impact peak, and it is the counterpart of the vertical impact peak in the antero-posterior direction. The magnitude and amplitude of this peak are related to the running style, with rearfoot strikers having the highest (in absolute value) and sharpest peak, while in midfoot and forefoot strikers the peak reaches smaller values with a smaller loading rate. The second negative peak denotes the maximum posterior breaking force, which is developed while the

subject slows down after the impact. The magnitude of the peak depends again on the running speed and type of footstrike. Thereafter, force reduces to zero and then grows until reaching the third peak, which represents the maximum of the anterior thrusting force developed during the second half of support, when speed increases forward. The zero-crossing point nearly corresponds to the point of midstance, which is usually defined in kinematics as the instant of stance phase in which the greater trochanter is vertically above the COP or the mid-point of the foot.

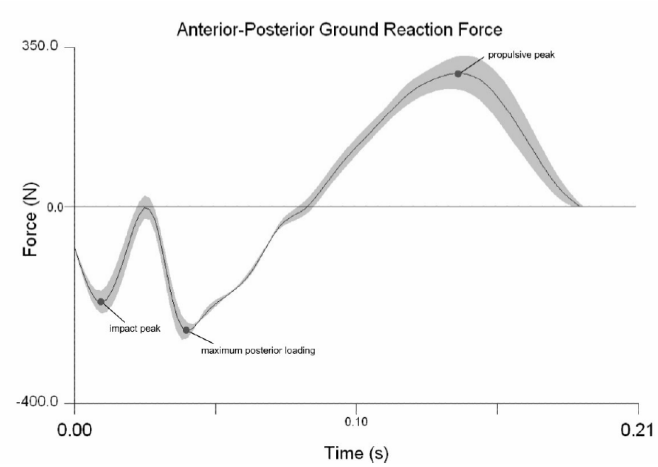

Figure 1.8. Anterior-Posterior Ground Reaction Force [Biomechanics in Clinics and Research, Richards [6]*]*

Medial-lateral force is the third and smallest component of Ground Reaction Force and it relates to the amount of pronation and supination of the foot during stance phase. At the initial contact, the foot is usually pronated, to a greater extent in the case of rearfoot strikers than midfoot and forefoot strikers. The force graphic indeed shows at the beginning a medial impact peak, followed by a lateral peak, with a variable timing between these two peaks. The force then oscillates around zero and it remains predominantly medial in the remaining part of the stance.

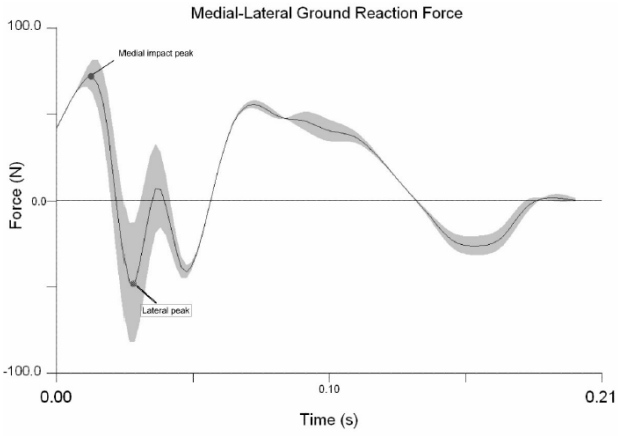

Figure 1.9. Medial-Lateral Ground Reaction Force [Biomechanics in Clinics and Research, Richards [6]*]*

Impulse

Impulse expresses the change in momentum, which is given by the product of the mass of a body and its change in velocity. Impulse is also defined as the integral of force (F) over time (t), so the bigger the force or the longer it acts, the greater the impulse. Its units is [Ns].

$$Impulse = \int F\, dt \qquad (1.4)$$

The graphical representation of the impulse consists in the area under the force-time graph and its value is obtained by integration of the force curve between two points.

Calculation of impulse is useful to compare the GRFs of different subjects or of the same subject doing different running trials. For example, braking and propulsive impulses, corresponding to the area under the anterior-posterior force graph in its negative and positive part respectively, should be of the same magnitude if the person is running at constant speed. Conversely, if the person is accelerating, the propulsive impulse will be greater than the negative impulse, which may even be absent in some cases, and therefore the net impulse will be positive.

Joint Moments

The combination of segmental kinematics with Ground Reaction Forces allows the estimation of joint reaction forces and moments and internal muscle forces.
There are basically two approaches for the calculus of joint moments: on the one hand the simplified method or GRF vector method, which takes into consideration only the location of the ankle, knee and hip joints, their distance from the COP and the magnitude and direction of GRF at any given time; on the other hand, the inverse dynamics method, which is based on solving the rigid body equilibrium problem considering inertial forces too.
In order to compute the inverse dynamics, some anthropometric data are required, such as height and weight of the subject, centre of mass, length, mass distribution, and radius of gyration of body segments.

Centre of mass (COM) or centre of gravity is the point where all mass of a body can be considered to act. Theoretically, it could be found experimentally: one suspends an object from position close to one of its edges, drops a plumb line, marks the line on the object and then repeats the procedure at least one more time after changing the suspension edge. The intersection between the lines defines the COM. In practice, for geometrical solids mathematical formulas are used, whereas for the human body the COM can be approximately located within the pelvis when the person is standing, but its position changes as the person

moves.

To find the exact position of the COM, either during stance or movement, it is necessary to know the location of the centre of mass of each body segment and then combine them together. The procedure is based on the use of anthropometric tables, which contain the coefficients for calculating the length of each body segment starting from the subject's height and the position of the COM of each segment in relation to its proximal end. Various versions of these tables exist in the literature and one of the most widely used is the one developed by W.T. Dempster, who studied the properties of body segments starting from cadavers.

There are other reference tables that can be used, such as that from Zatsiorsky- de Leva, who used images from individual in vivo obtained with gamma-ray scanning technique, or from Vaughan, Davis and O'Connor who used both data from cadavers and from in vivo measurements to obtain regression equations.

Anthropometric tables are also used to calculate the mass of each body segment as percentage of the total body mass, the radius of gyration and the moment of inertia.

To calculate joint moments according to the simplified method, only the magnitude and direction of the Ground Reaction Force and the distance at which it acts from the joint are required. Underlying this method is the assumption that body segments are not accelerating or decelerating and that their inertial properties can be neglected.

Moment or torque ($\vec{M}$) is calculated as the cross product of the lever arm vector ($\vec{b}$) connecting the joint about which the torque is being measured to the point of force application, and the force vector ($\vec{F}$).

$$\vec{M} = \vec{b} \times \vec{F}$$

(1.5)

Attention must be paid to nomenclature and sign conventions. The general rule adopted by some authors [6] is to use the suffix *-ing* when referring to the external moments, which are the moments produced by the Ground Reaction Force, while the internal moments, which are produced by the muscles to counterbalance the external moments, are called with the suffix *-or*. For example, if the Ground Reaction Force acting on the ankle joint has an anticlockwise turning effect and tries to dorsiflex it, it is referred to as dorsiflex-*ing* moment. Calf muscles will act with an equal and opposite clockwise moment, which is referred to as plantarflex-*or* moment [6]. Provides a schematic representation the moments and their nomenclature.

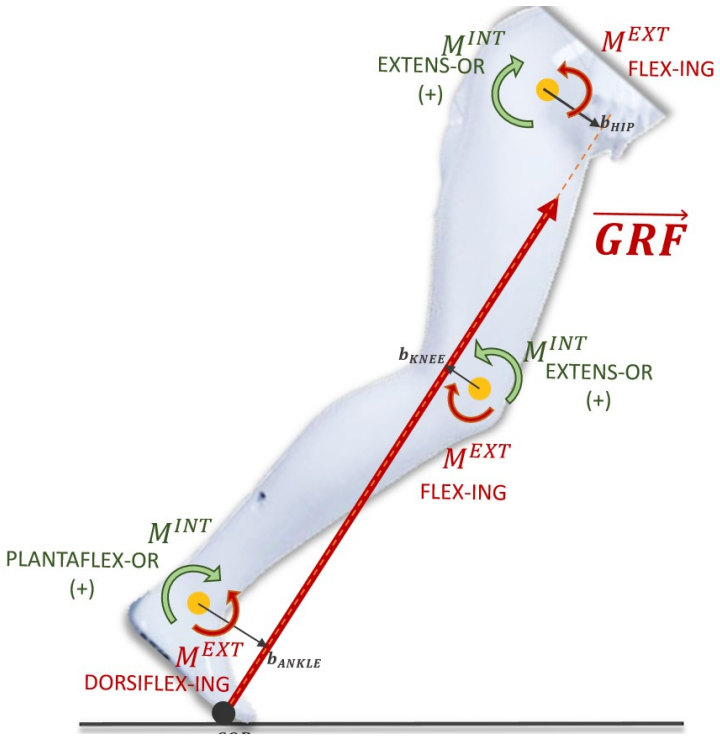

Figure 1.10. External (red) and internal (green) joint moments with relative sign conventions adopted in the present work.

As far as the sign convention is concerned, there is great variability in the literature. According to International Society of Biomechanics, intersegmental moments acting to flex, dorsiflex, intra-rotate and adduct the joint are considered as positive, while their opposites as negative [8].

Inverse dynamics method takes into consideration not only GRFs and weight of body segments, but also their inertial properties. The Moment of Inertia (I_{COM}) describes the unwillingness of a body to change its angular velocity and it is equal to the product of the mass of the body (m) and its radius of gyration (k), which is the distance between the axis of rotation and a single point where all of the body's mass is concentrated.

$$I_{COM} = m\,k^2 \tag{1.6}$$

If the reduction point for the equilibrium problem is not the centre of mass, but for example the joint, the moment of inertia of the body segment must be calculated according to the Huygens-Steiner theorem, which considers the distance (d) between the axis passing through the centre of mass and the new reference axis. Therefore, the total moment of inertia is equal to:

$$I_{TOT} = I_{COM} + m\,d^2 \tag{1.7}$$

This way, in the final expression of moment balance, inertial force ($\overrightarrow{IF}$) is considered too. It represents the effect of the tangential linear acceleration ($\vec{a}$) at centre of mass of the segment. Linear acceleration is indeed the product of angular acceleration ($\vec{\alpha}$) and the distance between the point of reduction and the centre of mass, that is the same above cited distance (d).

$$\overrightarrow{IF} = m\vec{a} = m\,\vec{\alpha}\ \times\ d$$

(1.8)

The complete equation describing the moment acting at a certain joint, in a bi-dimensional case is:

$$\vec{M}_{xy,joint} = -\left(\overrightarrow{b_d}\ \times \overrightarrow{F_d}\right) - \overrightarrow{M_d} - \left(\overrightarrow{b_{COM}}\ \times m * \vec{g}\right) +\ (I_{TOT} * \vec{\alpha})$$

(1.9)

where:

$\overrightarrow{F_d}$ is the distal force, which can be either the GRF or the joint force at the distal joint;

$\overrightarrow{b_d}$is the lever arm vector from the point of application F_d to the pole;

$\overrightarrow{b_{COM}}$ is the distance between the COM and the pole. It is the same as d .

In the three-dimensional case it is preferable to use the centre of mass as point of reduction, otherwise many additional terms related to the variation of the Moment of Inertia must be added. The equation, for the three-dimensional case becomes:

$$\vec{M}_{xyz,COM} = -\left(\overrightarrow{b_d}\ \times \overrightarrow{F_d}\right) - \overrightarrow{M_d} - \left(\overrightarrow{b_p}\ \times \overrightarrow{F_p}\right) +\ (I_{COM} * \vec{\alpha}) + (\vec{\omega} \times I_{COM}\vec{\omega})$$

(1.10)

where:

$\overrightarrow{b_p}$ is the lever arm vector from the point of application F_p to the pole

$(\vec{\omega} \times I_{COM}\vec{\omega})$ is the term coming from the derivative of the angular momentum.

The difference between the two methods is minimal in the case of ankle, where I_{COM} is small, but in the case of the hip, where the contribution of inertial components is much higher, the difference is significative.

In addition to joint moments, joint forces can be calculated. They depend on all the forces acting horizontally and vertically around a joint and can be computed either considering or omitting muscle forces. In the first case, Ground Reaction Force and weight of the distal body segments are the only terms put in the equilibrium equation, while in the second case the vertical and horizontal components, sometimes called also rotary and stabilizing components, of force

produced by active muscles must be also included. Despite being more accurate, the second method is rarely used in biomechanics.

The measurement of internal forces produced by muscles and other soft tissues, tendons and ligaments, would require invasive instrumentation, like intramuscular or surface electromyography and surgically implanted tendon buckles. To avoid these methods, musculoskeletal models have been developed. Once given some assumptions, for example relative to insertion point and line of pull of the muscle, its cross-sectional area and the force ratio factor for agonist muscles, musculoskeletal models allows the estimation of internal muscle forces.

However, when talking about performance, the term muscle strength is more recurring than the term muscle force. Strength is related to the amount of force a particular muscle can produce or to the amount of weight that can be lifted. It depends on many factors, such as the speed and type of muscle contraction, the angle of pull of the muscle, its insertion and the body segment inclination.

Power

The mechanical work done during running is related to the changes in energy levels of the body centre of mass or the changes in segmental power derived from joint forces and moments.

In general, power (P) is defined as the derivative of work with respect to time, and if angular work is considered, power is obtained as the product of the net moment about a joint (M) and the angular velocity ($\dot{\varphi}$) of that joint. Angular work is the product of force and arc length, i.e. the distance travelled through an arc. To obtain work from power, the integral of power over time is calculated.

$$Power = M \cdot \dot{\varphi}$$
$$Work = \int P \, dt$$

(1.11)

Negative power should correspond to the periods of eccentric contraction of muscles or energy absorption, while positive power to periods of concentric contraction of muscles and energy generation. The total amount of power generated increases as speed increases, and the relative contribution from each muscle group increases when going proximally. Furthermore, it can be noted that muscles stretch eccentrically just before generating their burst of power [5]. This way, both tendons and muscles can operate in the most efficient way, since the stretch-shortening cycle aids power production.

Another important parameter closely related to biomechanical analysis of running is the running economy**,** term often used to refer to the submaximal oxygen uptake per unit body mass (V_{O2} [ml · kg^{-1} · min^{-1}]). V_{O2} usually reaches its minimum when an individual runs at the freely chosen stride length and it is generally considered linearly related to the running speed. Moreover, some studies found that a better economy is aided by greater forward trunk lean, longer support time and lower medially directed ground reaction force, but there is no widespread agreement on these considerations.

Regarding energy optimization, while in walking the potential and kinetic energy are out of phase, thus allowing a good energy efficiency, in running they are in phase.
Both kinetic and potential energy increase during the generation phase, when the centre of mass accelerates upward and forward, and they reach their peak in mid-swing. Thereafter, energy decrease as the centre of mass falls to the ground and foot contacts the ground. The main source of energy optimization are elastic structures like tendons and ligaments, which can store elastic potential energy during the absorption phase and release it in the following phase, thus reducing the amount of metabolic work done by active muscles.

Lumped parameter models

The biomechanics of running can be effectively explained through a mass-spring-damper model, which depicts the runner during the stance phase. The point mass in the model represents the body, which is reduced to its centre of mass, the massless linear spring connecting the ground to the COM represents the leg hitting the ground and the damping element represents tendons, ligaments and other soft tissues that have visco-elastic properties. For sake of simplicity, the damper will be neglected, without introducing major approximation errors.

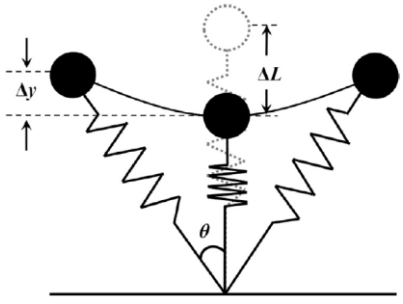

Figure 1.11. Spring–mass model for running. Δy is the maximal vertical displacement of the centre of mass; ΔL is the maximal leg compression; θ denotes half of the angle swept by the leg during the ground contact [[9]*]*

A linear spring is characterized by its spring constant $\boldsymbol{k}$, which is a measure of the spring's stiffness and is defined as the ratio between the applied force and the variation of its length.
In the context of gait analysis, the stiffness of the spring is called Leg Stiffness k_{leg}, at it is

calculated as the ratio of maximal Ground Reaction Force (GRF_{max}) to maximum leg compression (ΔL) during the stance phase [9].

$$k_{leg} = \frac{GRF_{max}}{\Delta L}$$

(1.12)

In addition to leg stiffness, it can be defined also vertical stiffness k_{vert} , which is another crucial parameter to determine the spring-like behaviour of the leg in running. k_{vert} is the ratio of maximal vertical Ground Reaction Force to maximum vertical displacement of the centre of mass (Δy) in the middle of the stance phase.

$$k_{vert} = \frac{vGRF_{max}}{\Delta y}$$

(1.13)

On the one hand, the overall stiffness of the leg is related to the mechanical behaviour of soft and hard tissues, contraction speed and viscoelastic properties of the muscle, delay in reflex and activation under CNS control; on the other hand, the biomechanical parameters that influence k_{leg} are stride frequency and speed. As stride frequency increases, vertical displacement of COM reduces; as speed increases, force and contraction speed of the muscle increase. These elements lead to an increase in leg stiffness. The stiffer the leg, the more elastic energy can be returned. However, high leg stiffness also means that Joint Reaction Forces increase, which may cause injuries to bones. Conversely, if k_{leg} decreases, there is higher risk of damages to soft tissues [10].

For this reason, the estimation of the leg stiffness plays a key role in the assessment of the sport performance and in the subsequent improvement of training methods.

The simplest mathematical model that can be used to calculate leg stiffness analytically is the unidimensional model, in which only vertical component of GRF is considered.

According to a previous Thesis work, in literature there are several mathematical models which allow the estimation of leg and vertical stiffness. Their implementation in the MATLAB environment and their testing using a public dataset of non-elite athletes [11] has already been done. Among the goals of the project Olimpia is the adaptation of these codes in order to estimate the leg stiffness using the data acquired during the experimental sessions and afterwards to implement new models which better represent running in amputee athletes.

Chapter 2

Amputee Running

Several studies have been carried out in order to investigate the running biomechanics, and in the last decades there has also been growing interest on running biomechanics of individuals with lower limb amputation.

Limb amputation

The surgical removal of body lower extremities (toes, foot, leg) can be the consequence of many factors. The most common causes are diabetes mellitus and peripheral arterial disease, which are usually close related. Circulatory disorders imply reduced blood flow and reduced oxygen supply to the lower limbs and so they cause the person feeling pain during walking and the affected extremity being cold and bluish [12].
The reduced perspiration also causes the limb to dry out and crack. In case of diabetic patients, the high sugar deposit in the nerves also inhibits feeling of pain related to wounds or cracks, so patients sometimes do not even notice them. This way wounds might get bigger if sores are subjected to stress and tissues might become more inflamed with cells dying off.

Other causes for limb amputation are traumas caused by accident, infections, tumours, severe burns or wounds that do not heal. In some other cases amputation is necessary because of some congenital malformations of the limbs [13].

In Italy, the number of hospitalizations due to lower limbs amputation between 2015 and 2020 exceeds 3000 [14], while in the United States people undergoing lower extremity amputation each year amount to 150000 [15]. The majority of them (80%) is related to the diabetic foot syndrome or peripheral vascular disease, whereas a smaller but still significative percentage (16%) is due to traumatic events, that often involve young and athletic people.

Lower extremity amputation often involves significant perioperative morbidities, physiological complications and a general impairment in quality of life. However, a well-designed healing process including physical therapy and rehabilitation can enable amputees to regain their mobility and independence and to return to sport practice [16], which is actually highly recommended to reduce risk of cardiovascular and other chronic diseases.

The use of sports activities for rehabilitation of amputees was first introduced in 1944 at Stroke Mandeville Hospital thanks to the neurosurgeon Ludwig Guttman. In 1948 the first games for

British injured military personnel took place in Stroke Mandeville Hospital. This event grew year by year and numerous international competitors started participating. In 1960 the competition was held alongside the official Summer Olympics in Rome and it was recognised as the first Paralympic Games. Thereafter, the development of peculiar sporting prostheses has aided sport participation and the public interest has increased noticeably [17].

It became necessary a classification system for athletes with different disabilities, in order to facilitate fair competition. Today there are seven disabilities included in the categorization system. They are amputation, deafness, cerebral palsy, intellectual impairments, spinal cord injuries, blindness and Les Autres, which includes all those athletes with different disabilities from the ones included in the previous categories [18]. Each category is identified by an alphanumeric code, made up of one or two letters, describing the type of disability and a number that indicates the severity of the disability.

For what concerns athletics, there are three subcategories, Track, Field and Pentathlon, represented by letter 'T', 'F' and 'P' respectively. The letter is followed by a number going from 11 to 64. According to the Classification Rules of the World Para Athletics which took effect since 2018 season, the group 42-44 is composed of athletes affected by lower limb deficiency, leg length difference, impaired muscle power or impaired passive range of motion competing without prosthesis, while the group 61-64 is composed of athletes with lower limb/s amputation or leg length difference competing with prosthesis [19] .
Here are presented the categories relative to different levels of lower extremity amputation [20].

- T/F 61: Bilateral through knee amputation (knee disarticulation KD) or above knee (AK) limb deficiency (transfemoral amputees TFA)
- T/F 62: Bilateral below knee (BK) limb deficiency (transtibial amputees TTA)
- T/F 63: Unilateral through knee or above knee limb deficiency (TFA)
- T/F 64: Unilateral below knee (BK) limb deficiency

Running prosthetic foot

Among sport activities, running is one of the most convenient and cost-effective forms of cardiovascular exercise to increase physical activity level [21]. Achieving a good level of locomotion is crucial for a good quality of life, both for able-bodied people and, even more so, for individuals with lower extremity amputation (ILEA). Although it is also possible to run with daily-use prostheses (DUPs), which are originally designed for walking, the performance achieved by using running specific prostheses (RSPs) is significantly superior.

Historical development of prosthetic foot

The first modern foot prosthesis, which distinguishes from the devices developed from the Roman to the Post-Industrial Revolution Era, is the Solid Ankle and Cushioned Heel (SACH) foot, introduced in the late 1950s. Its simple design consists of a soft material moulded over a more rigid inner piece that mimics the shape of a human foot. It allows pseudo plantar-flexion thanks to a mechanical ankle and its large heel cushion provides sufficient shock absorption for limited walkers, but it is not suitable for moderate to high activity prosthesis users [22].

Figure 2.1. SACH foot [Accessprosthetics.com]

Lower-limb prostheses remained quite basic in the design and functionality until the ‘80s, when the expansion of plastic and composite industries made new materials like carbon fiber, titanium and graphite available. Prostheses became stronger and more durable, and at the same time lightweight and with increased energy-storing capability. In 1984 Van Philips created the ‘Flex-Foot’, which was then used in the Paralympic Games held in Seoul in 1988, even if it was not designed for running [23] [24].

Shortly thereafter, in 1992, the first specialized Running Specific Prosthesis (RSP), the ‘Flex-Sprint I’ was introduced. It had no heel and it had a singular stiffness configuration, due to the lay-up sequence of carbon. Many other specialized running feet were developed after that

moment and they became more and more efficient and lighter, still recalling the basic shape of 'Flex-Sprint I'.

Figure 2.2. Flex-Foot Modular II (left) and Flex-Sprint Cheetah (right) [From Conventional Prosthetic Feet to Bionic Feet. Chiriac et al. 2020]

It is important to stress that there are some strict rules established by the International Paralympic Committee (IPC) regarding the prostheses that can be used in races. For example it is stated that the technology or equipment used must not '*provide an unrealistic enhancement of stride length*', it must be '*commercially available to all athletes*' (and not exclusively produced by manufacturers) and it must not '*contain materials or devices that store, generate or deliver energy designed to provide an athlete with a competitive advantage over an athlete not using such technology*' [25].

Components of RSPs

The main components crucial to the design and performance of the prosthesis are the socket, the prosthetic knee, the connecting organs, like the pylon, the pyramidal attack, the clamp, and of course the foot (Figure 2.3).

Socket is the custom element representing the interface between the residual limb and the distal prosthetic components. It must be lightweight, but at the same time ensure the proper mechanical strength to avoid any harm for the patient, have adequate load transmission and ensure stability and control.

The basic steps required to make a socket are the creation of a negative cast of the residual limb, filling that cast with plaster to obtain a positive mould, optimizing the shape of the mould and then doing the lamination using carbon fibre, resin or nylon materials. The quality of the sockets depends on its capacity to distribute forces over the residual limb avoiding pressure sensitive

areas and limiting force on pressure-tolerant areas. Another crucial factor in the design of a prosthesis is the suspension system, which has to provide a close fit for the residual limb and keep the socket in place during locomotion. Among the different suspension techniques, one of the most used is suction, which is realized thanks to an expulsion valve on the socket. Once the residuum is in the socket, the valve is opened to let air out and then is closed to maintain a negative pressure. By opening or pushing the suction valve, the air will return, breaking the seal and thereby allowing the prosthesis removal.

Another suspension option is the pin-locking system. It consists in a pin applied at the bottom of the liner which has to go into a locking mechanism at the bottom of the socket. A release mechanism can then be pressed to unlock the pin [26].

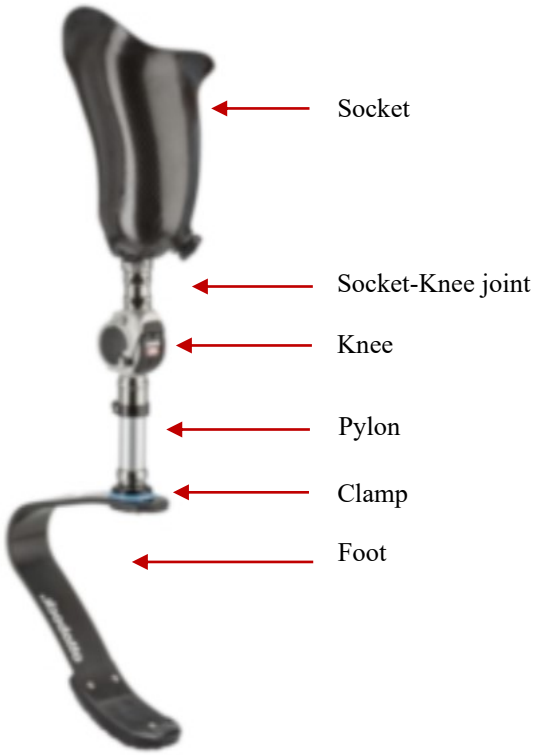

Figure 2.3. Running Prosthesis components [Adapted from Ottobock.com]

The mechanical prosthetic knee used in running is a single-axis mechanism that works like a hinge. It is made of aluminium and can bear the high loads developed while running. It allows athletes to make a more natural swing movement and so have a more symmetrical running, otherwise they would have to perform a compensation movement, such a hip circumduction, to take a step forward. Sport knee joints have a stability mechanism which automatically locks the

knee when it has to support loads, for example in the phase of stance, but they can also be locked manually, to prevent the knee from buckling in certain circumstances. The level of friction of the prosthetic knee, which controls the damping in flexion and extension motion, can be adjusted according to the running speed of the athlete. In addition, mechanical prosthetic knees have a fluid control system which provides variable resistance during swing. This system consists of pistons inside cylinders containing a fluid, usually silicone oil, in the case of hydraulic systems, or air in the case of pneumatic systems, which is compressed as knee is flexed, stores energy, and then returns it when the knee moves into extension [27].

Figure 2.4. Mechanical Prosthetic Knee, Ottobock Sport Knee joint 3S80 [Ottobock.com]

The pylon is a rigid tubular member connecting the socket to the knee unit or directly to the foot. It helps the prosthesis in the weight bearing and shock-absorption [28].

The pyramidal attack consists of a pyramid receiver and a pyramid adapter in titanium, which allow to quickly fix the foot to the pylon and adjust the angles of alignment of the foot by acting on four fixing screws.

The Running Prosthetic Foot (RPF) is characterized by its shape, category and height.
The shape, which is referred to as ‘C’ or ‘J’, depends on the type of running performed and on whether the prosthesis is attached directly to the socket or below it [28].

‘C’ shaped RSPs attach distal to the socket and they are mainly used by above knee amputees or KDs. They are very effective at storing and releasing energy over time, thus they are more commonly used for a jogging pace and distance running.

Figure 2.5. Flex-Run, Össur [Össur.com]

‘J’ shaped RSPs attach posterior to the socket and are more common in transtibial amputees. Their design allows a quicker return of energy and helps to achieve higher speeds, thus they are frequently used by sprinters. However, in order to have good performance in terms of energy return, the blade must be compressed a lot, and this requires higher energy than in the case of ‘C’ shaped RPF.

Figure 2.6. Cheetah Xtend, Össur [Össur.com]

The category is a number representing the relative stiffness of the blade. The stiffer the foot, the bigger the category number. The category of RPF prescribed by the prosthetist is based on manufacturer's recommendation, which in turn depends on an athlete's body mass and activity level. The choice of the category is also based on the visual inspection of symmetric ground contact time between legs [29].

In the end, height of the prosthesis is based on the unaffected leg and residual limb length. For a C-shaped RSP, height is adjusted by shortening or lengthening the pylon that connects the foot to the socket, while for a J-shaped RSP, height is adjusted by changing its mounting position posterior to the socket. The total height of the affected limb, when unloaded, is usually

set to be about 5 cm longer than the intact limb to compensate for blade deflection during loading [30] [31].

Socket alignment

The position of socket with respect to knee and foot, also called 'alignment', is essential for the athlete to have a good feeling while running and thus also to achieve better results. The alignment procedure should be done in the condition of midstance, which is reproduced on a bench during the design phase and in vivo during test sessions.
Midstance is defined as the instant of the stance phase in which the projection of the Greater Trochanter on the ground overlaps the fifth metatarsal head for the sound side or passes through the prosthetic knee centre for the prosthetic side. The use of reference points on the RPF to define midstance is usually to be avoided, since in stance phase the foot is deformed.

Prior to bench alignment, the subject's thigh orientation and hip mobility should be measured. To this extent, the Thomas' test has to be performed, which consists in a manual muscle test aimed at measuring the degree of hip flexion shortness called *Thomas' Angle*, or in other words the flexibility of hip flexors muscle group.
All prosthetic components are pre-assembled on the perch and subsequently the prosthetist adjusts them starting from the top, that is from the socket.
First of all, the socket axis, which can differ from the anatomical axis of the femur, is identified as the intersection between frontal and sagittal planes of the socket. The lateral axis of the socket has also to be marked and it represents the incidence of frontal plane with the socket.
Second, a plumb line is used to obtain the 'Alignment Axis', which is the vertical axis passing through the Greater Trochanter (GT), approximating the Hip Joint Centre and which, in condition of midstance, should pass through the Knee Joint Centre (KJC).
Once identified these axes, the socket is first rotated around the articular centre on the frontal plane to establish the normal physiological hip adduction and then around the GT on the sagittal plane to have the same hip flexion at heel strike and the same orientation of the femur at midstance of an able-body athlete. The entity of this rotation, which is basically the angle in the sagittal plane between the lateral axis of the socket and the Alignment Axis, is referred to as $\boldsymbol{\gamma}$ angle (Figure 2.7). For a walking prosthesis, the socket tilt should range from 3° to 5° plus the patient-specific *Thomas' Angle*, but for sockets used in sprinting, this angle should range from 5° up to 15 °, plus the *Thomas' Angle*.

The socket is then moved upward or downward so that the absolute height of the GT is 5 cm higher than the GT on the sound side, in order to balance the compression of the prosthetic foot.

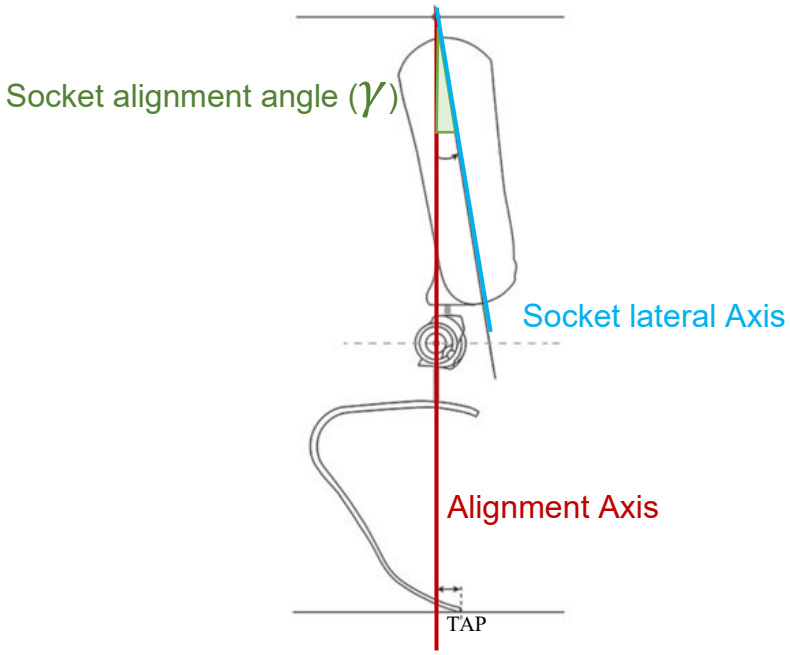

Figure 2.7. Alignment Axis and socket lateral axis used in RPFs assembly to individuate alignment angle (γ)

The regulation of the prosthetic knee in the antero-posterior direction must be done to place the knee centre vertically under the GT. It is essential that the position of the knee is at maximum on the frontal plane, but not further, to ensure an extension moment during whole stance phase. If the knee is placed too anteriorly, at the toe off the hip should exert a significative extra extensor moment to prevent the knee from flexing due to the direction of GRF.
In the transverse plane, knee should be extra-rotated of about 5-7°, which compensates the internal rotation of the socket during the swing phase. The height of the prosthetic knee can also be adjusted by acting on the pylon connecting it to the socket. The correct height is about 5 cm higher than the knee of the unaffected limb.

In the end, the foot can be rotated forward or backward in the sagittal plane, so that distal tip of the foot is positioned at a certain distance, called 'TAP' from the projection of GT on the ground.

In the course of the latest studies [32], including the experimental sessions that will be described later in this work, different socket alignments have been tested with Paralympic sprinters and they will be referred to as A<n>, with <n> ranging from 0 to 3 and they differ from each other for the socket tilt angle and the TAP distance.

The first alignment, A0, is characterized by a socket tilt of 5° and a horizontal distance between the tip and the vertical line connecting GT and KJC (TAP) conventionally equal to 3.5 cm. Passing to A1, which is considered the 'transition alignment', the TAP is reduced to 0 cm, to obtain a possible higher propulsive boost due to the smaller resistance surface. The socket tilt progressively increases from 9° to 15°, to mimic possible different orientation angles of the sound thigh. The features of each alignment are listed in the table below.

*Table 2.1. Socket Alignments features (*Socket tilt angle has to be added to the Thomas' Angle)*

	Socket tilt* (γ)	**TAP**
A0	5°	3.5 cm
A1	9°	0 cm
A2	12°	0 cm
A3	15°	0 cm

Differences in running between amputee and able-bodied athletes

Despite replicating the macro-function of a biological leg, RSPs introduce some differences in the running performance of amputee sprinters if compared to able-bodied (AB) runners.

Looking at the world records in athletics, it can be observed that amputee athletes run slower than able-bodied athletes, even though the time gap has become quite smaller over the years, decreasing to less than one second for men (9.58 s AB record vs 10.57 s amputee category T62 record) and nearly two seconds (10.49 s AB record vs 12.79 s amputee category T62 record) for women [33], [34].
In addition, it can be noted that, among amputee athletes, runners belonging to class T62 (previously called T43), which are bilateral below-knee amputees, run faster than the ones belonging to T64 (previously T44)[23], which are athletes with unilateral below knee amputation.

Several authors have investigated the variables that characterize the running of amputee athletes, but there is no widespread agreement on all of them.

It has been found that shorter swing time enhances faster running, but different authors explain this information relative to amputee athletes in opposite ways. On the one hand shorter swing

time is seen as the consequence of the lower mass and smaller moment of inertia of the RSP if compared to the human shank-foot segments [23] , on the other hand it is explained as a result of the training technique [23]. Moreover, in an experimental study conducted with unilateral transtibial athletes, it was found that adding mass to the RSP does not increase the swing times for the affected limb (AL) at top speed [35], but only made flight time more symmetrical between legs.

Regarding contact length, it is well established that it is greater at faster speeds, but while some argued that there are no significant differences between the intact and the prosthetic leg in unilateral amputee athletes [23], others noted that contact length of the affected limb is greater than that of the intact limb, in case of unilateral transtibial amputees [21], or than that of able-bodied athletes, in case of double-transtibial amputee [23].
Step frequency increases with speed, but it is found to have a greater increase in the unaffected limb (UL) [36].

The vertical component of GRF is another important factor determining speed. In this case, several studies agree on the fact that the vertical force produced by the prosthetic limb is smaller (-9%) than the vGRF exerted by the intact limb (Figure 2.8) and this is the main constraint to top speeds.

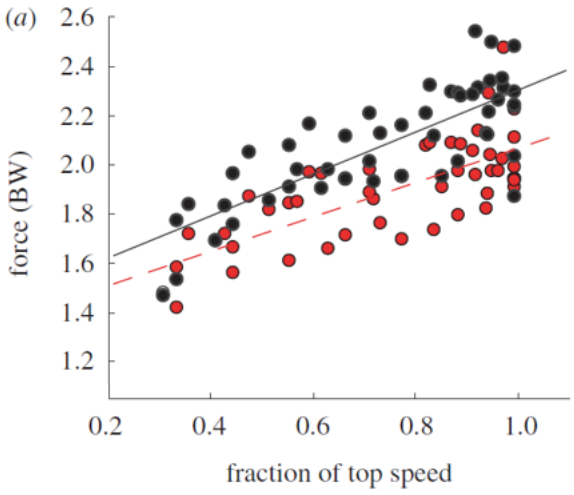

Figure 2.8. Stance average vertical GRF across speed for the UL (filled black circle) and AL (filled red circle). Lines are linear regressions for the AL (dashed line) and UL (solid line) [Grabowski, 2010 [35]*]*

The impairment in force generation comes from the fact that people with transtibial and transfemoral amputations are missing part of their foot and ankle musculature, which provides much of the energy used to accelerate the body [21]. RSPs cannot generate new mechanical power, but only behave like springs which store and release elastic energy [36]. In addition, the asymmetry in average GRF and peak vertical GRF between intact and affected limb could be

also related to leg length discrepancies [30]. Nevertheless, the higher GRF values, together with a higher vertical average loading rate in the intact limb compared to the prosthetic limb or to the values recorded in able-bodied runners, might be an increased injury risk in the intact limb [21].

Looking at anteroposterior GRFs, it can be noted that the prosthetic limb generates lower braking forces and impulses compared to intact limbs [21], [30], probably due to the different toe landing of the RSP, while propulsion is similar for both legs. Moreover, it has been found that the net impulse is consistently positive in the affected limb and negative in the unaffected limb.

As for mediolateral forces, some studies highlighted that the medial GRF is lower for AL than for UL, due to the absence of fine muscular control. This suggests that running with RSPs may reduce the ability to maintain dynamic balance and stability [21], [37].

Asymmetries between limbs in unilateral amputees has been found also in joint kinematics. Ankle must be excluded from comparisons, since there is no standard method to define ankle joint in RSPs, which do not resemble the ankle complex of an intact foot [21]. Regarding knee kinematics, some studies reported that the residual knee (in transtibial amputees) is more flexed than intact limb knee both at foot contact and at toe off [21]and then it overextends in late swing. Hip joint behaviour in the intact limb is comparable to that of AB runners, except for a decreased flexion prior to toe-off, while the residual hip shows increased flexion at foot contact than the intact limb.

Joint moments also present some differences between UL and AL. For example, the peak of extension moment in stance phase in the residual limb knee is smaller in magnitude than that of the intact limb, which could be due to the smaller range of motion of the prosthetic knee [21]. On the other hand, the greater extension moment in the intact knee joint during stance may reflects an increased reliance on the intact limb during running [30].

In addition, since RSP has lower mass and moments of inertia than intact limbs, the eccentric flexor moment at terminal swing is smaller too, because the muscles are required less effort to slow the knee extension prior to foot contact

For the hip, the extension moment during initial stance phase is prolonged in the residual limb compared to the intact limb, but its peak is smaller [21].

Biomechanical factors affecting running with RSPs.

In addition to the alteration of spatiotemporal, kinetic and kinematic parameters, among the strategies employed to improve performance there is also stiffness regulation. The stiffness of the prosthesis blade is prescribed by the prosthetist, and therefore it is fixed, but the modulation of the stiffness of the intact and residual limbs can vary according to running speed.
Many studies reported that the prosthetic leg has lower stiffness (k_{leg}) than the sound leg, in particular during running at submaximal speeds, from 2.5 to 3.5 m/s [23], [35]. At these speeds, the k_{leg} of prosthetic leg remains constant, whereas when speed exceeds 6 m/s, it increases non-linearly [30].
The category and the height of the RSP could be expected to have an effect on the stiffness of the affected leg, but it came out that the main influence is on the k_{leg} of the sound leg. [23]

The characteristic of RSP that most influences maximum running speed is the shape, and in particular the J-shaped foot allows to run faster compared to C-shaped foot. This result may be due to the fact that the 'J' RSP has a wider base and a lower hysteresis, which provide greater mediolateral stability and greater vertical COM velocity at the end of the stance phase. Moreover, J-shaped RSPs resulted in greater stance average vertical GRF and longer aerial time, which cause also slower step frequencies compared to C-shaped RSP [38].
Finally, RSP height does not contribute to an increase in top speed; on the contrary, it produces a greater moment of inertia and decreases step frequency.

Research approaches

The study of running of amputee athletes can be conducted in several different ways and some of the research approaches that can be found in literature will be briefly discussed in this section.

Force platforms

One of the most common approaches is to use force platforms placed on the ground in an indoor or outdoor athletics track. The acquisition system can be coupled with motion capture cameras, which collect additional data relative to body posture.
In many cases, less than ten platforms are used – often seven –, meaning that the number of "good" steps, that are steps occurring within the platform boundaries, is about two or three, depending on the running speed of the athlete and on the position of the platforms with respect to the starting point of the run. In case that a step overlaps two force platforms, the data can be

discarded [39] or cumulated [40], depending on the processing method adopted. The use of force platforms is not invasive for the athletes and does not require them any specific preparation. However, if the number of platforms is limited as in the cases cited above, the risk of "bad" steps is quite high. To overcome this problem, some authors, like Nagahara, adopt another approach, which consists in increasing the number of platforms up to fifty-four [41]. In this case, the percentage of correctly acquired steps is much higher, as is the cost of the total instrumentation. In spite of the improvements in statistics achieved with more data, the problem of repeatability between different trials or between different subjects remains, as running speed is self-regulated by the runner, who tries to maintain a set speed.

Instrumented treadmill

Instrumented treadmill is an effective approach which both solves the problem of repeatability and of correct steps. The force plates embedded in the treadmill are used to collect GRF data. Treadmills can be either split belt [42], which collect data of the left and right limb separately and thus can be used also in walking, or single belt [35], which collect data either from the right or left side.

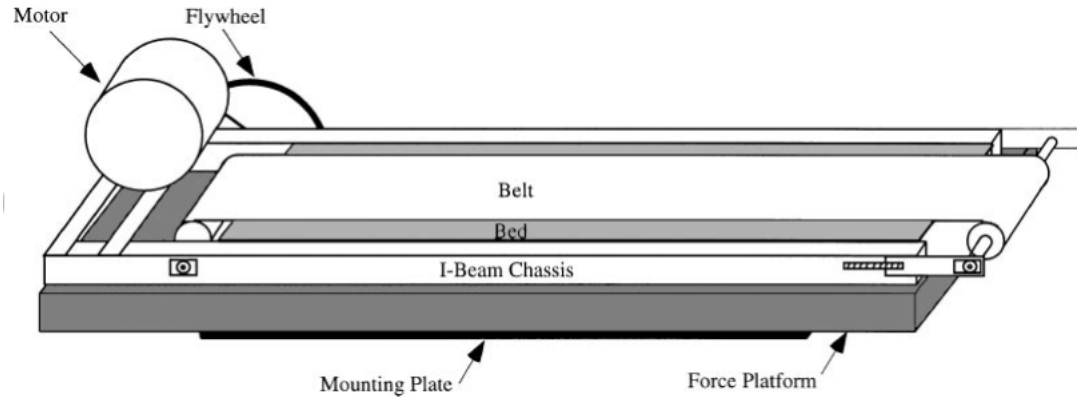

Figure 2.9. Schematic view of force-treadmill. [Force treadmill for measuring vertical and horizontal ground reaction forces. Kram et al. 1998]

In addition to commercial instrumented treadmill, a customized treadmill can also be used to measure Ground Reaction Forces, which is the approach adopted during the first and second experimental session described later in this work. It consists in using a common treadmill as running surface and force platforms placed below the treadmill to measure forces. The main advantages of using the (instrumented) treadmill are that speed can be set and maintained identical among trials and that the number of steps collected just depends on the duration of the trial. However, also this method has some drawbacks, which are related to the unfamiliarity of

the athletes with the instrument and thus the impossibility of reaching speeds as high as those of overground running.

Wearable sensors

An additional limitation of the above listed methods is that tests are performed indoor, unless force platforms are placed outdoor, but in this case the issue of limited number of steps still remains. In order to overcome these problems wearable sensors can be used, which allow continuous measurement of the running gesture and can be used in whatever environment, including the outdoor athletics track.

The first strategy developed at University of Padua in the last years is the instrumented Running Prosthetic Foot (iRPF). This is a system of strain gauge bridges are attached to the prosthetic foot which allow measuring the forces acting on the foot clamp on multiple steps without modifying the RSP behaviour [43].

Figure 2.10. Instrumented RPF: strain gauge bridges applied to a Ottobock Runner Cat. 4 RPF [Petrone et al., 2020 [44]*]*

Two strain pure bending bridges are applied to the straight portion of the upper stiffer part of the foot, while the third pure bending bridge is applied on the curved portion of the blade (Figure 2.10). This configuration allows decoupling the effects of forces along two axis and measuring the bending moment. The cables of the strain gauges are then connected to a portable data logger, contained in a small backpack that the athlete wears during the running trial. A meticulous calibration procedure is needed in order to have accurate and reliable measurements of the vertical and horizontal ground reaction forces and of the bending moment acting at foot clamp. The calibration has been done using a multi-component test bench, which has been newly designed for this purpose [45]. The bench can apply loads parallel and perpendicular to the foot clamp axis at different angles to the ground. Afterwards, the iRPF system is validated

on field, with the athlete running and making a clean step over a force platform placed under the athletics track.

Figure 2.11. Athlete running on track with iRPF over the force platform [Petrone et at., 2020 [43]*]*

The second strategy related to wearable sensors consists in mounting a small and lightweight 6-axis load cell between the foot clamp and the prosthetic knee, in order to measure the forces applied to the clamp, which represent in turn the effect of the Ground Reaction Forces transferred through the RPF. Furthermore, a high-speed inertial sensor has been taped on the inner surface of the upper stiffer part of the foot and it gives information about the linear acceleration and angular velocity of the foot. The detailed description of this setup will be addressed in Chapters 3 and 4, and the results of the processing of the data coming from these devices will be reported in Chapter 6.

Neural networks

One of the latest and most innovative approaches in running gait analysis involves the indirect measurement of Ground Reaction Forces through inertial sensors and neural networks. One of the proposed methods [46], consists in using one sacral- and two shoe- mounted biaxial accelerometers and giving the acquired data in input to a recurrent neural network, which predicts continuous normal GRFs.

Data relative to the vertical and horizontal acceleration of the sacrum and of the right foot have been collected with subjects running on an instrumented treadmill at different speeds and slopes. Raw data have been downsampled, filtered and the mean, standard deviation and range have been calculated for both acceleration components of the sacrum (3 x 2 = 6 variables), while data coming from accelerometers on the foot have been used just to classify foot strikes as either rearfoot, midfoot or forefoot strikes (3 variables). Additional input variables are mass and height of the subject (2 variables) and the slope and speed of the treadmill (2 variables), for

a total of 13 variables. The type of recurrent neural network chosen in the study is the long short-term memory (LSTM) network, as it is particularly suitable for the prediction of sequential data. The accuracy of the network was established by comparing the predicted GRFs with the values measured by the instrumented treadmill, with very promising results.

The main innovative aspect of this method is that kinetic and kinematic variables can be predicted outside the laboratory environment, since input data are not constrained by other temporal variables, such as the duration of stance phase, which depend on additional laboratory instrumentation. However, the robustness of this method may be altered if accelerometers are placed and fixed on the body in different ways, if the running surface is softer than the treadmill and also if the subject runs in conditions different from the ranges of slope ad speed used to train the network.

Chapter 3

Experimental Tests: Materials

The main focus of the present work is the elaboration of data acquired during experimental sessions. Therefore, a description of the materials, tools and subject is here provided.
In the time period from November 2021 to October 2022, three test sessions were executed. They have been called Olimpia Session 1, Olimpia Session 2 and Olimpia Session 3 and they will be referred to as OS1, OS2 and OS3 respectively.

OS1 and OS2 tests took place in the Sports Engineering Laboratory in the Industrial Engineering Department of University of Padua in November 2021 and December 2021 respectively, while OS3 took place in October 2022 in the Palaindoor of Padua.

Olimpia sessions 1 and 2

The instrumentation adopted during OS1 and OS2 consisted in:

- *Technogym Skillrun* treadmill;
- 8 *BTS Smart Capture-DX 6000* cameras for motion capture;
- 4 *BTS P 6000* force platforms;
- *CCT TF02* uniaxial load cell
- *SoMat eDAQ-lite* acquisition unit;

Additional instrumentation used during the tests consists in high-speed cameras and smartphones used to record videos of the athlete running on the treadmill, both from sagittal and frontal view. Those videos have not been actually used in the data processing, but they are useful to have a visual feedback when analysing results.

Treadmill

The treadmill used during the tests is a *Technogym Skillrun*. It can reach maximum speed of 30 km/h, it can be used either with positive or negative incline, which range from +25% to -3% and it can also operate at controlled resistance. The treadmill is 55 cm wide, that is 30% wider than common running treadmills and this enables athletes to run in total safety and comfort.

Figure 3.1. Tecnogym Skillrun Treadmill [Technogym.com]

In order to adapt the treadmill to the tests, some changes were needed. First of all, the monitor and the handrail were removed because their natural oscillation frequency was in the same range as the running frequency of the athlete, so they would introduce additional noise in the recorded signals. The screen was placed on a table nearby, so that the view on the athlete legs was not obstructed and another person –not the runner - could set the treadmill speed. A custom frame made of steel and covered with neoprene rubber was placed around the treadmill, standing on the floor externally to the treadmill, to support the athletes and ensure their safety.

BTS acquisition system

The Sport Engineering laboratory is provided with a *BTS* acquisition system, which consists of force platforms, motion capture cameras and a set of sensors for surface electromyography (EMG) analysis, called *FREEEMG*. All these devices are controlled by the same workstation. For these tests, only force platforms and motion capture cameras have been used and they are described in detail in the following sections.

Force platforms

The treadmill was not placed directly on the ground, but on four force platforms, that were positioned to have their centre aligned with one foot of the treadmill.

The force platform model is *BTS P-6000* and its dimension is 60x40 cm. Force platforms are typically used in gait analysis, because they allow the measurement of ground reaction forces, moments and the centre of pressure. Each force platform works as a six-axis load cell, which has eight output signals that are converted through a calibration matrix into six load components Fx, Fy, Fz, Mx, My, Mz. From these quantities, the three-dimensional vector representing the total Ground Reaction Force and its point of application, or centre of pressure, located on the

surface of the force platform can be obtained. These force platforms have a maximum acquisition frequency of 1000 Hz and a maximum vertical load capacity of 3500 N.

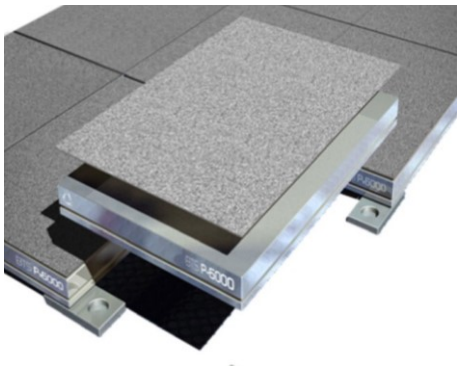

Figure 3.2. Force platform BTS P-6000

Motion Capture cameras

The *BTS Smart Capture-DX 6000* is a system of digital cameras having a maximum acquisition frequency of 340 Hz. For these tests, an acquisition frequency of 250Hz has been chosen. Cameras hang from the ceiling and surround half of the laboratory, where the target measurement volume is identified. Each camera emits infrared light, which is reflected off the markers applied on the athlete's body. Light reflection is caught by the camera sensor, which has a resolution of 2.2 Megapixels, and that converts the light signal into a two-dimensional image. Then the algorithm combines the image coming from the camera with information regarding focal length and lens distortion, called intrinsic parameters, and information regarding the position and orientation of the camera, which are the extrinsic parameters. This way it creates a 3D vector connecting the marker to the camera. The intersection of 3D vectors relative to different cameras allows the determination of the three-dimensional location of the marker in the space. For this reason, each marker must be seen at least by two cameras. This process is called triangulation.

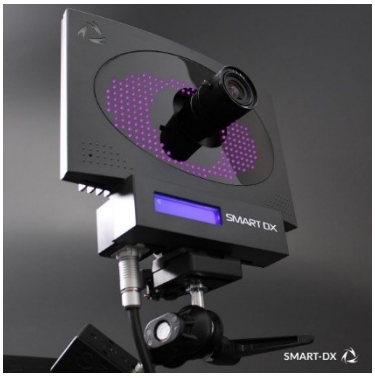

Figure 3.3. BTS Smart DX Camera

The markers are placed in specific positions on the body and prothesis, according to an established protocol. 'Protocol' is actually a wide term, which defines the biomechanical model, the procedures for data collection, processing, analysis and reporting of the results. In the Appendix B, the part of the protocol relative to markers placement is presented in detail. Depending on the dimension of the anatomical/prosthetic area, two different marker sizes can be employed, 10 mm or 15 mm diameter, and they can be spherical or hemispherical.

Prior to data acquisition, calibration is required to establish a 3D reference for the cameras, that is to determine the X, Y and Z axes along which the three dimensions of the markers position is measured. Cameras must be in a fixed position and the capture volume should be clear from people, markers or reflective surfaces creating phantom markers. If there are light reflections that cannot be eliminated, masks can be applied in the camera settings, but this will prevent the cameras to capture markers in that area. Once completed this preliminary check, the calibration procedure is carried out in two steps.

As a first step, a wand with three markers is moved through the capture volume at a moderate speed and in a variety of directions. The movements must cover as much of the volume of interest as possible, but especially in the specific area where the activity to record will take. During this process the system takes 2D images from each synchronised camera and then the software reconstructs the position of the markers and the position of cameras with respect to each other [47], because it knows exactly the size of the wand and the distance between markers.

As a second step, a physical triad made by three orthogonal wands is placed in the acquisition volume, with the intersection of the three wands corresponding to the origin of the capture volume. Each wand has a different number of markers on it and represents one of the three axes of the absolute reference frame. During the tests the following schema was adopted:

4 - marker wand: X axis = antero-posterior axis (gait direction).

3 - marker wand: Y axis = vertical axis.

2 - marker wand: Z axis = medio-lateral axis.

Figure 3.4. Calibration of the system with global reference triad

The position and orientation of the cameras relative to the ground reference system defined by the triad is then computed.

Since the tests also include the use of force platforms, an additional calibration step is required. A second smaller L-frame is placed on one force platform at a time to get its location in the capture space.

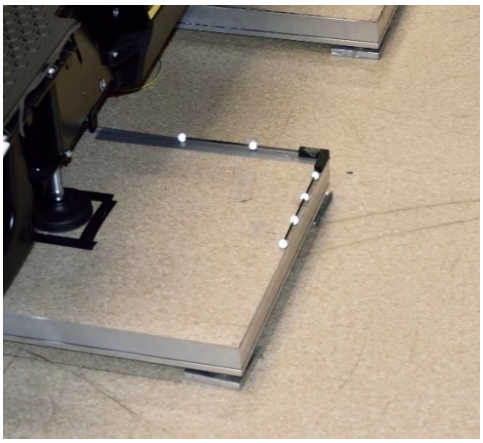

Figure 3.5. Localization of force platforms in the acquisition volume

This way, kinematic and kinetic data can be combined to estimate joint moments and corresponding forces generated by muscles.

Portable data acquisition system

The **SoMat eDAQ-lite** is a portable data acquisition system which has the capability to perform signal conditioning, on-board data processing and storage. The eDAQ-lite consists of one base processor layer and a variable number of optional add-on layers, including layers for bridge

channels, digital input and output and battery. The system collects data at the desired sampling rate, from 0,1 Hz to 100 kHz and stores them in a variety of formats, which can be then analysed with InField or MATLAB or Excel software

Figure 3.6.Acquisition System Somat eDAQ-lite [Hbm.com]

Load cell

In order to measure the traction force applied by the athlete during one of the tests, a monoaxial load cell has been tied to the waist belt of the harness through an elastic band. The load cell must be then connected to the first channel of the first bridge of the SoMat eDAQ-lite.

Before the tests, the sensor has to be calibrated by hanging it to the ceiling and loaded with increasing weights. Once obtained some value pairs of known load and corresponding signal (N; mV), it is possible to calculate the slope of the line that best fits experimental data. The inverse of such value corresponds to the calibration constant.

Figure 3.7. Uniaxial Load Cell

Olimpia session 3

The third test session was carried out in a totally different environment. While in the Sports Engineering Laboratory the athletes ran on a treadmill, so they were running actually always on the same spot, in Palaindoor athletes ran on a real athletics track and therefore they moved along the space. Therefore, different instrumentation was needed.

The instrumentation adopted in session OS3 consisted in:

- 28 *Vicon* cameras for marker-based motion capture (25 *Vicon Vero v2.2*, 2 *Vicon Vantage v16*, 1 *Vicon Vantage v5*);
- *DTS Slice Nano* acquisition system;
- Triaxial accelerometer + triaxial gyrometer *DTS 6DX PRO-A;*
- 6-axis load cell *SRI M3564F1*;

Some additional instrumentation was part of the total set up, but the data acquired with the following devices are not elaborated in the present work.

- 7 *Vicon Vue* cameras, used for markerless motion capture;
- Dynamometric starting blocks equipped with load cells (*Gefran CU K5D* and *CU K1C*);
- Optical system for movement detection *OptoGait;*
- Three-axis logging accelerometer *AX3 Axivity.*
- 2 high-speed cameras for the sagittal and frontal recording.
- Smartphones for slow-motion videos and for recording complete trials.

Palaindoor

Palaindoor of Padua is one of the two sport facilities for indoor athletics in Italy, opened in 2015. It is essentially an indoor arena in which there is a 200 m track with six lanes, 60 m straight runway with eight lanes and multiple platforms for high jump, pole vault, long jump and weight throw.

Among the goals of Olimpia project is the sensorization of the running track to carry out biomechanical analyses aimed at studying and improving sport performance of athletes, either able bodied or with disabilities, letting them train in a much more confident environment than a laboratory. The intention is to build a moving 13 x 7 x 3.5 m framework, on which ten optoelectronic cameras for motion capture are anchored; place eight 60 x 90 cm and two 40 x

60 cm force platforms on the ground in order to acquire kinematic and kinetic data while the athletes are performing either a sprint or a long jump.
During OS3 the framework and the platforms were not installed yet, therefore some different instrumentation has been brought on site.

Figure 3.8. Palaindoor Padua

Vicon Motion Capture cameras

Vicon cameras have been used for marker-based motion capture and their operating principle is the same as the *BTS* cameras.

Figure 3.9. Motion Capture Cameras. Vicon Vero (left) and Vicon Vantage (right)

6 out of 28 *Vicon* cameras were placed on a square framework in the middle of the track, while the remaining cameras were placed on tripods placed along the eighth lane of the straight runway.
The very first step required to prepare cameras for the acquisition is adjusting the position and tilt of each camera to have the intended framing. *Vero* and *Vantage* cameras have varifocal lens. As such, there are three dials to be adjusted. The closest to the body of the camera is the zoom, which acts on the focal length and gives a field of view ranging from 44° to 98°; the middle dial is the aperture, which controls the amount of light allowed through the lens; the last dial is for the focus. Each of these dials has an effect on the 2D image and has to be regulated camera

by camera by loosening the corresponding screw and moving it carefully to one side or the opposite. To perform this operation correctly, some markers have to be placed in the acquisition volume and then one checks the view of each camera from the *Nexus* software. The camera is optimized when, if zooming on a marker, a tight circular image is shown, with a cross exactly in the centroid of the marker blob, the centre of the blob is bright white and towards the edges there is a gradient of grayscale.

Once all cameras are correctly aimed, acquisition frequency has to be set from the software. This parameter is critical for camera optimization, as it affects shutter speed and thus the amount of reflected light reaching the sensor.

Additional parameters that can be selected from the software are the strobe intensity, which is the intensity of the light emitted from the camera strobe units, and the threshold strobe, which is the minimum grayscale value required for a pixel to be displayed within the camera view and so to be part of a marker centroid. Lowering strobe intensity makes the noise related to unwanted reflections in the volume decrease, but at the same time it reduces the brightness of markers and therefore the number of its corresponding pixels in the image.

Once this preliminary step is completed, calibration can be performed, which is done in the same way as the for the *BTS* cameras, i.e. first wanding in the acquisition volume and then placing an L-frame or a triad in the point of the volume where the origin is to be located.

DTS Acquisition system

DTS SLICE NANO is an ultra-small, standalone acquisition system with microprocessor, memory, sensor excitation and signal conditioning and it can be connected to multiple sensors. This acquisition system has a modular design, called *SLICE* 'Stack', which consists of one Base+, one battery and up to 8 additional sensor input modules having three input channels each. Dimension of the single SLICE is 31 x 26 mm and its height varies in the range 5.5 to 6.5 mm. It runs on DC power, which must range from 9V minimum to 15V maximum and can be supplied either by a converter connected to a power socker or by a Lithium-Polymer rechargeable battery.

Base+ SLICE lies at the bottom of the SLICE Stack and contains a microprocessor, 16 GB flash data memory, USB cable to connect it to PC, power conditioning and control signals.

Battery SLICE is only a back-up battery in case main power is lost.

Sensor input SLICEs can be either Bridge or IEPE. During the current tests, four Bridge modules were employed: two were connected to the six-axis load cell and the remaining two were connected to the 6DX PRO-A, which is a triaxial accelerometer + triaxial angular rate sensor.

Figure 3.10. Acquisition System DTS Slice NANO

The system is provided also with an End Of Chain terminal, which enables attaching the battery, sending a trigger signal or monitoring the status of the SLICE system. In order to make the system easier to use, especially in the case of recording repetitive trials, a push button panel has been designed and produced by addictive manufacturing. In the panel there is a button for switching on and off the system, another button to for the start and stop of the record input, a button for event input signal and a LED showing the status of the system.

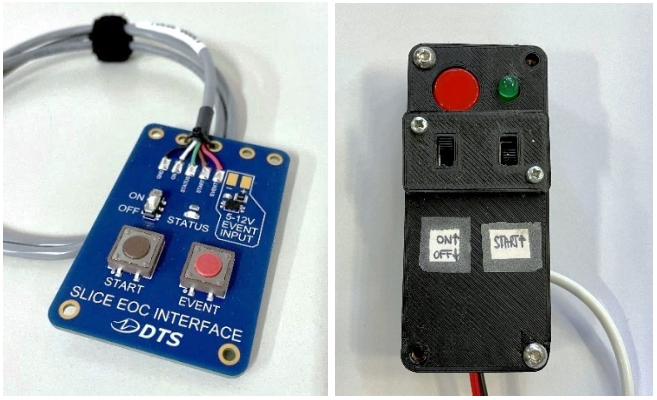

Figure 3.11. Button panel of the DTS Acquisition system (left) and custom case (right)

To prepare the system for the acquisition and to visualize data afterwards, the *SLICEWare* software is required. It allows the management of sensor database, the real-time sensor check-out, the definition of the test set-up, the execution of the test and the export of the data acquired.

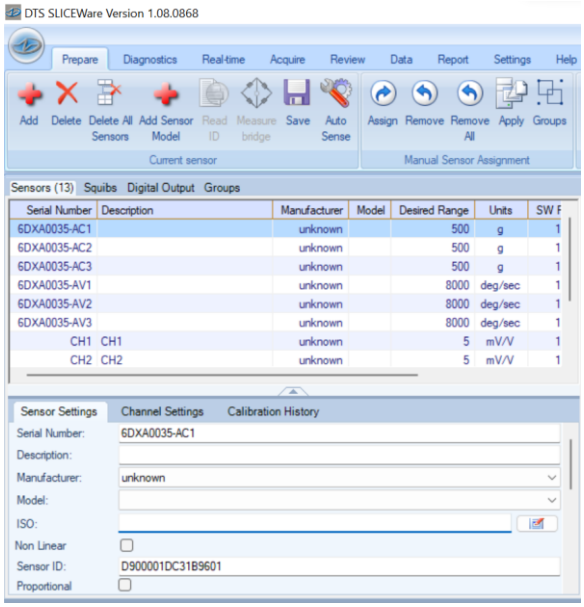

Figure 3.12. Software Interface of DTS SLICEWare

During the current session, SLICE NANO was placed inside a trail-running backpack that the athlete had to wear during the tests. In addition to the acquisition system, the backpack contained the battery, the button panel and the powerbank used to power the load cell connected to the acquisition system.

Figure 3.13. Backpack containing the instrumentation

Load cell

Due to the lack of force platforms and in order to validate a new method to measure forces with wearable sensors, a six-axis load cell was placed between the prosthetic knee and the prosthetic foot (Figure 3.16), so that it could measure the Ground Reaction Forces transferred to the knee and then to the socket.

The model of load cell chosen is M3564F1, produced buy the *SRI sensors* company. It is a circular, extra thin load cell of 10 mm height and 65 mm diameter and its mass is only 190 g. It has six coupled output channels, which can be then decoupled thanks to calibration matrices

to obtain three components of force, Fx, Fy, Fz and three components of moment, Mx, My and Mz.

The maximum measurable value along X and Y directions is 2500 N, while along Z direction the maximum is doubled. Regarding Mx and My the maximum value is 200 Nm and for Mz it is 100 Nm.

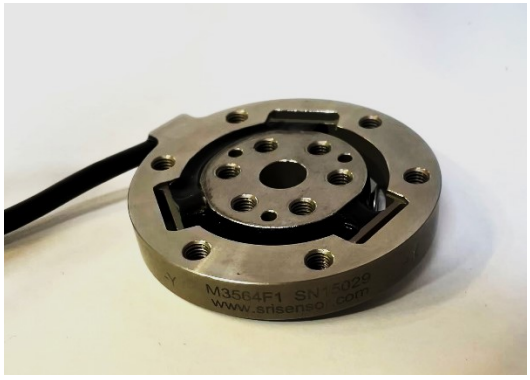

Figure 3.14. 6-Axis Load Cell

Inertial sensor

6DX PRO-A is a small, high-shock tolerant six degrees of freedom sensor package, which includes three angular rate sensors plus three accelerometers. It is 19 x 19 x 17.4 mm big and weighs 14 g. This is a very versatile sensor, since it has large bandwidth options available and multiple sensor ranges. The triaxial accelerometer can measure linear accelerations in the range ±500 g along the three axes, while the triaxial angular rate sensor works in the range ±8000 deg/sec. The unit has two long cables which terminate with a triaxial connector. One cable serves the accelerometer sensor and one cable the gyroscope sensor.

Figure 3.15. Six degrees of freedom inertial sensor package 6DX PRO-A

The sensor was fixed on the inner surface of the proximal portion of the prosthetic foot, almost under the clamp, while the load cell was fixed between the clamp and the prosthetic knee.

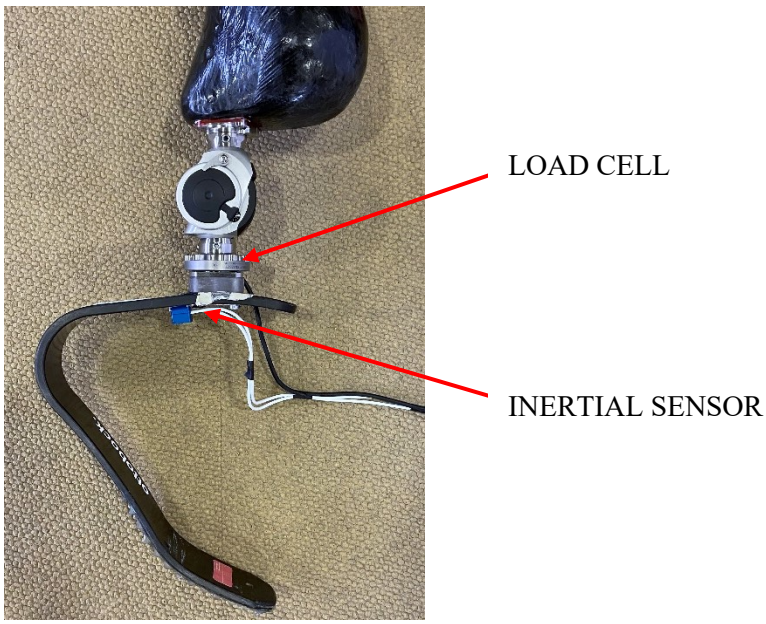

Figure 3.16. Load cell and sensor set up

Starting blocks

Dynamometric starting blocks are identical to common starting blocks, but they measure forces generated by the sprinter thanks to a set of load cells (CU K5D and CU K1C models, *GEFRAN* SpA, Brescia, Italy), which enable the measurement of the magnitude and direction of forces with a maximum acquisition frequency of 1 kHz. Each block is equipped with four monoaxial load cells with 0.01 N sensitivity: three cells were used to measure the vertical loads and one to measure the horizontal loads. The force data are temporally stored in the data logger enclosed in the box connected to the starting blocks (Figure 3.17) and afterwards transferred to a PC for signal processing and resolution of data into horizontal and vertical components for each foot [48].

Figure 3.17. Dynamometric starting blocks

OptoGait

The *OptoGait* system from *Microgait* is made up of transmitting and receiving bars positioned parallel on the floor, which communicate each other through LEDs. When the subject passes through the corridor identified by the bars, the communication between the infrared optical sensor is interrupted and the system calculates some parameters relative to the position and duration of the movement, such as contact time, flight time, speed, step and stride length and asymmetry between legs. The maximum time resolution is 1 millisecond, while the maximum space resolution is 1.041 cm.

OptoGait is a modular system, with 1 meter-long bars that can be assembled in series. In this experimental session ten bars have been employed.

Figure 3.18. OptoGait system [Optogait.com]

Accelerometer

The *AX3* by *Axivity* is a small and lightweight data logger that contains a MEMS with a 3-axis accelerometer and 512 Mb non-volatile flash on-board memory. The accelerometer has a sample rate ranging from 12.5 to 3200 Hz and a configurable full-scale range varying from ± 2 to ± 16g. If choosing specific recording options, the battery can last up to six months, thus allowing long-term data collection. Such data can be elaborated to highlight different patterns of acceleration while doing different tasks, like standing, walking, running or sprinting and also to extract information useful for fatigue testing.

Figure 3.19. Accelerometer Axivity

Subjects

A total of three **subjects** participated in the test sessions: Martina Caironi, Ambra Sabatini and Maxcell Amo Manu.

Subject 1 (59 Kg, 1.65 m): Martina Caironi (MC), 100 m and long jump silver medallist in Tokyo Paralympic Games 2020 for category T63. She participated in OS1 and she was wearing the Running Prosthetic Foot Ottobock 1E91 standard, category 4 (Figure 3.20-a).

Subject 2 (53 Kg, 1.60 m): Ambra Sabatini (AS), 100 m gold medallist in Tokyo Paralympic Games 2020 for category T63. She participated in both OS2 and OS3 and in both cases was wearing the Running Prosthetic Foot Ottobock 1E91 standard, category 3.5, which is the same shown in Figure 3.20 - a.

Subject 3 (85 Kg, 1.87 m): Maxcel Amo Manu (MM) is the fastest Italian sprinter in Paris World Para Athletics Grand Prix 2022 for category T64. He participated in OS3 and he used two different Running Prosthetic Feet: Össur Cheetah Xtreme category 6 (Figure 3.20-b) and Össur Cheetah Xcel category 5 (Figure 3.20-c).

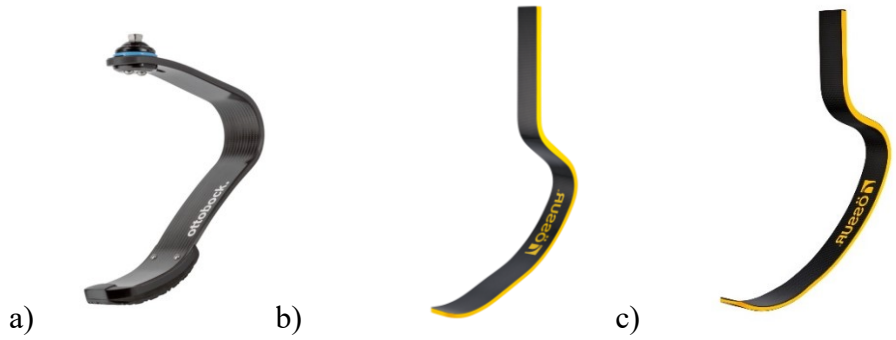

Figure 3.20. Running Prosthetic Feet: a) Ottobock 1E91 standard. [Ottobock.com]; b) Össur Cheetah Xtreme; c) Össur Cheetah Xcel [Ossur.com]

The detailed description of the procedures carried out during the experimental tests is provided in the following Chapter.

Chapter 4

Experimental tests: Methods

One of the main goals of this Thesis is the development of a data processing tool to perform biomechanical analysis. The deep knowledge of the type of data to elaborate and how they have been collected are basic requirements for any kind of data processing.
In this chapter the description of test preparation and test execution for the three test sessions will be provided.

Olimpia sessions 1 and 2

In test sessions OS1 and OS2 two types of tests have been executed:

- Steady State Running (SSR): the treadmill is operating in controlled speed mode. The athlete hangs on the handrails of the external frame while the treadmill reaches a speed of 10 km/h. The athlete then jumps on the belt and starts running. The treadmill speed is quickly led to a maximum value (16 or 18 Km/h), agreed with the athletes during the pilot test, and the athlete has to continue running at this constant speed for at least 7 seconds.

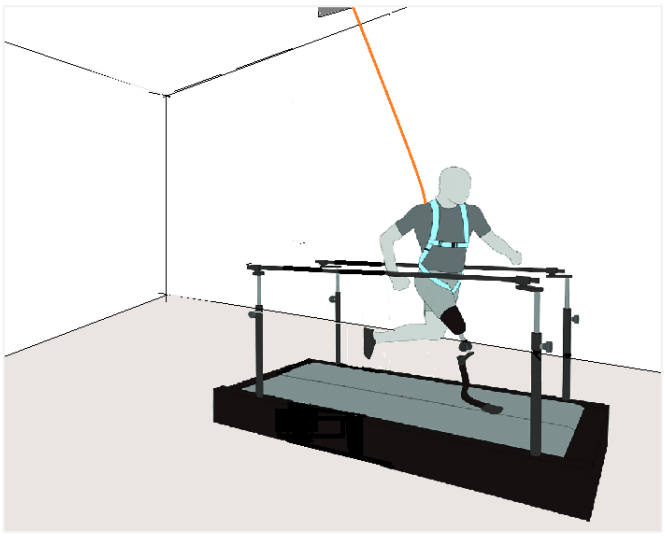

Figure 4.1. Schematic representation of Steady State Running (SSR)

- Resisted Accelerated Running (RAR): the treadmill is switched off, so that it works in passive mode to simulate inertial and air resistance. This operation mode has been preferred to the activation of the resistance mode on the treadmill, which simulates sled training, because the resistance opposed to athlete's push was too high, despite the minimum resistance level was selected. The athlete starts running from zero and

accelerates until reaching the maximum personally sustainable speed, that has to be maintained for at least 5 to 7 seconds. In this case, the athlete is tied with an elastic rope to the load cell, which measures the force exerted at pelvis height.

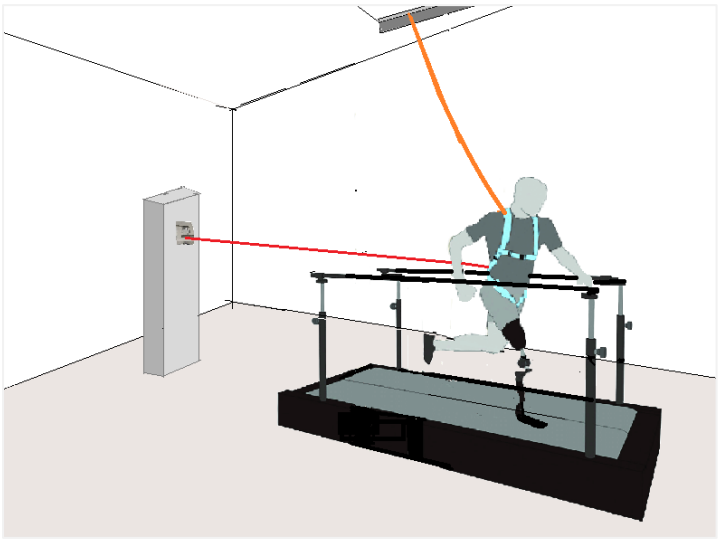

Figure 4.2. Schematic representation of Resisted Accelerated Running (RAR)

Athletes had to test four different socket alignments, A0, A1, A2, A3, which have been described in Chapter 2 and are reported in Table 4.1, together with the TAP distance used in the tests (for both athletes).

Table 4.1. Alignments features used in OS1 and OS2

	Socket tilt (γ)	**TAP**
A0	5°	5.5 cm
A1	9°	5.5 cm
A2	12°	5.5 cm
A3	15°	5.5 cm

For each alignment both types of tests, SSR and RAR, have been performed.

Test preparation

- The treadmill has to be correctly placed on the force platforms with each support of the treadmill in the centre of one force platform. *BTS* force platforms and *BTS* cameras are connected to the workstation through ethernet cables.
- BTS workstation is switched on and the software *SMARTClinic* opened.
  Once clicked on 'New Patient' button, some demographic data regarding the athlete

have to be filled in. Next, pressing on 'SMART Activation' button, the calibration file for the kinematics (cameras) and dynamic (platforms) instrumentation can be loaded. If no calibration file exists, then the calibration must be performed. First, the wand has to be moved all around the acquisition volume, in particular in the treadmill area. Second, the reference triad with reflecting markers has to be placed on the treadmill, on the point chosen to be the origin of the three-dimensional volume. Third, the small L-frame with reflecting markers is placed on the corner of each platform, one at a time. Once completed the calibration, the user clicks on 'Close' and exits this window.

The following steps are the creation of a new session, by clicking on the homonymous button, and afterwards the creation of a new trial. Each trial must have a different name.

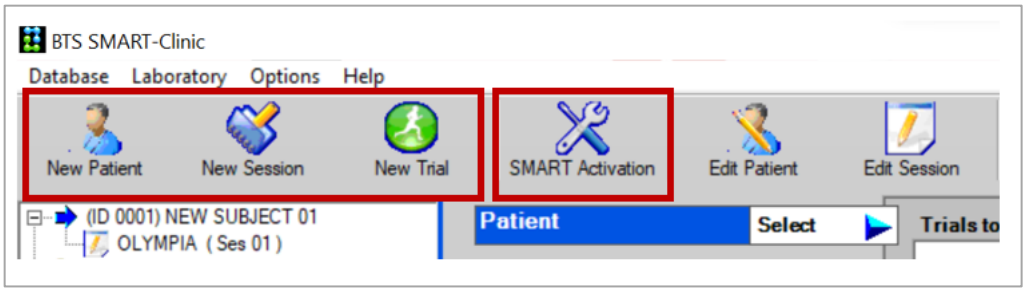

Figure 4.3. Database creation in BTS SMARTClinic

- After clicking on 'Acquire', the software *Smart Capture* opens automatically. Here the user can select 'Monitor' and check what are the cameras looking at and what load is measured by the platforms. When no subject is on the treadmill, the force measured by the platform should be only the weight of the treadmill, which can be set as the new zero value.
- SoMat acquisition system has to be connected to the load cell through an input cable and to a PC through wi-fi. The software *TCE* has to be opened and the user has to insert the data relative to the load cell and initialize the test.

If everything is properly working, then the systems are ready for the acquisition.

- Before the athlete gets on the treadmill to run, she has to wear the socket, which has been previously prepared in terms of alignment angle and TAP. Afterwards, she has to wear a safety harness, which secures her to the ceiling in case of fall.
- In the end, markers are attached to the body, including the markers on the medial anatomical landmarks (such as femoral epicondyles) and on the face.

The full markerset is composed of 56 markers: 23 markers are applied on the upper part of the body, 4 markers on the pelvis and 33 on the lower part of the body. Among them, the most critical markers are the ones on the prosthetic leg. They include:

- GTL (Greater Trochanter Left);
- S1L, S2L, S3L (Technical markers: placed on the socket, 2 lateral and 1 frontal);
- FLEL and FMEL (Left Femoral Epicondyle Lateral and Medial: placed on the socket);
- KML and KLL (Left Knee Lateral and Medial: placed on the prosthetic knee);
- FP1, FP2, FP3, FP4 (Technical markers: placed on the proximal end of the prosthetic foot);
- FD1, FD2, FD3 (Technical markers: placed on the distal end of the prosthetic foot).

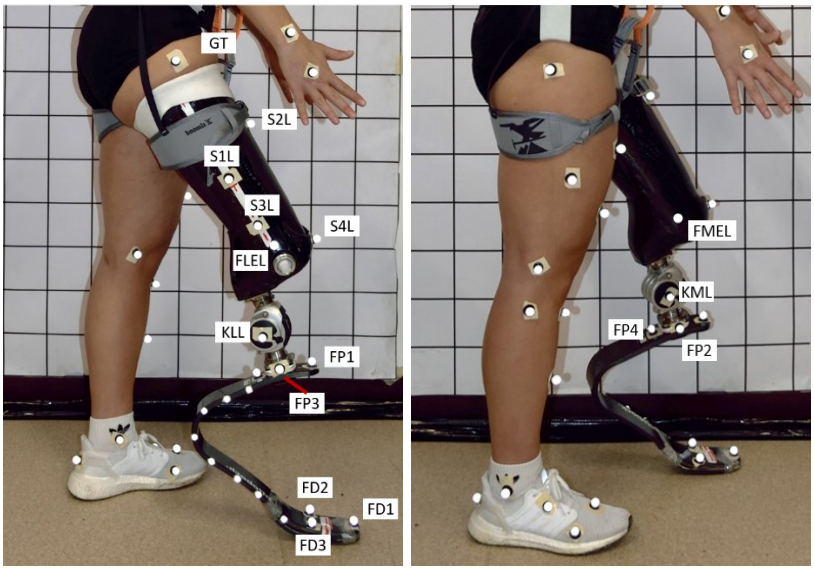

Figure 4.4. Markerset applied on prosthetic limb in OS1 and OS2

Static trials

The athlete gets on the treadmill and the static trials take place. In the software *Smart Capture*, as the button 'Start' is pressed, acquisition starts and the athlete has to maintain a standing still position for few seconds. The acquisition is then stopped and saved.

Static trials also include the acquisitions in which the athlete maintains the same standing position and another person points at some anatomical landmarks or at specific points on the prosthesis with a wand. This wand has two markers in known positions with respect to the wand tip, so that cameras acquire the location of the two markers and then the tip can be reconstructed geometrically. Each pointed landmark requires a separate acquisition. This procedure is called 'Static Calibration' and it is needed to locate the position of some landmarks, which would not

be clearly visible otherwise or which are too small to be correctly located with a marker. In the end, the hip functional calibration is performed. The athlete makes circumduction of the hip, three in clockwise direction and three in anticlockwise direction, once for the left and once for the right limb, during two separate acquisitions. Once completed this procedure, markers not required for the dynamic acquisitions are removed.

Dynamic trials

For both types of tests, before acquisition starts, the athlete has to suspend on the handrails for few seconds, so that the signal recorded by the platforms starts from zero loading condition.

For the Steady State Running tests, no additional preparation steps were required. The treadmill is switched on and accelerated while the athlete is standing on the external borders or hanging on the handrails. Then she jumps on the belt and starts running with the treadmill increasing the speed until reaching 16 or 18 Km/h, depending on the single trial. This maximum speed was maintained for 7 seconds, then she suspends again on the handrails and the acquisition is stopped.

For the Resisted Accelerated Running tests, the uniaxial load cell has to be positioned. The load cell is fastened to a solid vertical frame placed behind the treadmill at a safe distance to prevent any harm to the athlete in case of fall of from the treadmill. The load cell is then attached to a rigid cable in series with an elastic rope, which is then attached to the waist belt of the harness. The cell position is adjusted to be at the same height of the athlete's waist, so that the rope joining her to the cell is almost horizontal. Once the athlete is ready, the acquisition is started in the BTS software and just thereafter a trigger signal is generated by a dedicated Trigger Box Unit, in order to start the acquisition also in the TCE software. The same signal is sent to the BTS workstation and this allows the synchronization of the signals.

During OS1, tests were conducted with the athlete Martina Caironi. She performed a total of 29 tests, including both static and dynamic. Table 4.2 is a synthetic list of the trials performed, where the trials relative to Static Calibration with the wand, repeated trials or not valid trials have been omitted. 'Test number' refers to the progressive number given to BTS acquisitions.

Table 4.2. Tests performed by MC during OS1

SUBJECT	TEST NUMBER	TEST TYPE	SOCKET ALIGNMENT
MC	2	STATIC	A2
MC	14	SSR	A2
MC	16	RAR	A2
MC	19	STATIC	A1
MC	20	SSR	A1
MC	21	RAR	A1
MC	22	STATIC	A0
MC	23	SSR	A0
MC	24	RAR	A0
MC	25	STATIC	A3
MC	27	SSR	A3
MC	29	RAR	A3

In OS2 participated the athlete Ambra Sabatini. She performed a total of 35 trials, which have been reported in Table 4.3. Test performed by AS during OS2according to the same criteria explained above.

Table 4.3. Test performed by AS during OS2

SUBJECT	TEST NUMBER	TEST TYPE	SOCKET ALIGNMENT
AS	02	STATIC	A2
AS	13	SSR	A2
AS	16	RAR	A2
AS	19	STATIC	A1
AS	22	SSR	A1
AS	24	RAR	A1
AS	27	STATIC	A3
AS	28	SSR	A3
AS	30	RAR	A3
AS	33	STATIC	A0
AS	35	SSR	A0

Olimpia session 3

In test session OS3, the following two test types have been performed:

- Steady State Running on track (TSSR): the athletes start either from standstill or from the starting blocks and have to reach a constant speed, equivalent to the 60% of the personal maximum speed (nearly 15 km/h for AS and 20 km/h for MM), in about 15 meters and then maintain that speed for about 20 meters, which corresponded to the part of the track included in the acquisition volume.
- Start from starting blocks (START): the athletes start from the starting blocks, placed in the acquisition volume, and are asked to reach the 60% of the personal maximum speed in about 15 meters.

Test preparation

- *Vicon* Motion Capture cameras are mounted on temporary tripods which needed to be placed in the desired area of track, which was the central portion of the 8th lane of the straight runway. To mount the camera on the tripod, a plastic plate has to be screwed into one of the mounting points on the camera body and then fixed to the pan/tilt head of the tripod. Then each camera is connected to the *Vicon* workstation through Ethernet cables. The workstation is provided with a computer, from which the software *Nexus 2.13* can be opened. In the *Resource* pane, acquisition frequency was set at 300 Hz. In the central *View* pane, it can be visualized what each camera is seeing, and it can be assessed whether aperture, zoom and focus are correctly set. Afterwards, all markers and any source of unwanted reflection have to be removed from the volume and then calibration takes place.

  From the *Tools - System Preparation* pane, 'Active Wand' must be selected from the list of calibration devices and 'Full Calibration' from the list of calibration types. Once clicked on 'Start', an operator has to wave the wand throughout the area to be captured. If 'Auto Stop' is selected, the acquisition ends when every camera has collected enough data to be calibrated successfully. During calibration, the software creates a *.xcp* file containing the calibration parameters for each camera and the description of the capture volume necessary to produce accurate 3D data.

  In order to complete the system setting, the volume origin must be set, either with a calibration device, in this case the Active Wand, or with three makers placed on the ground, and the position of the floor plane must be adjusted using some markers placed along the volume, so that the coordinate system is accurately aligned with the floor. This

last operation is necessary in case the acquisition volume is very long, as it is in the case of the athletics track, otherwise in some areas markers trajectory could have a biased vertical coordinate.

The following step is the creation of a hierarchical structure for storing and managing all data associated with the trial. In the *Communication* pane, on the *Data Management* tab, there is the button 'Manage Eclipse Database', which allows to make a new folder for the database or to select an existent one. The first sub-layer in the database is the 'Patient Classification', then there is the 'Patient' and in the end the 'Session'.

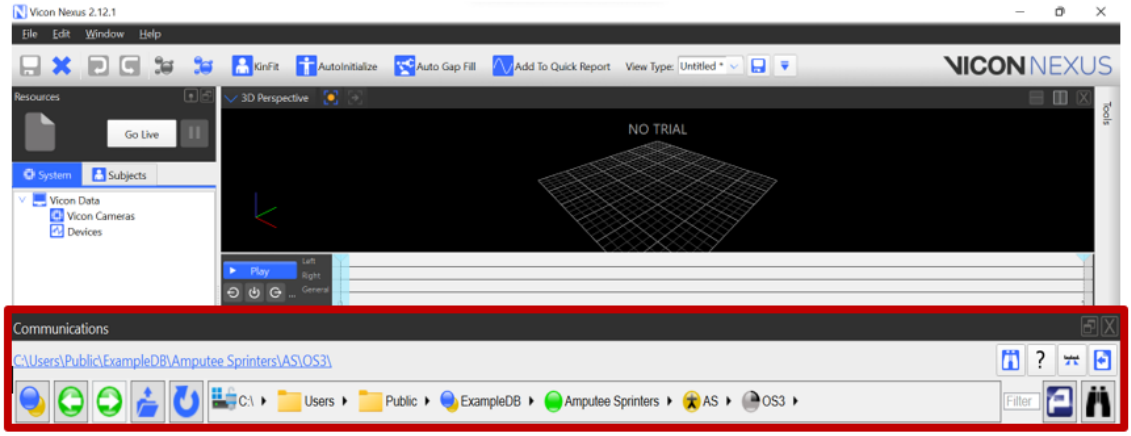

Figure 4.5. Database creation in Vicon Nexus 2.12.1

Now the system is ready to capture data.

- The *OptoGait* system has to be placed on the ground with the two 10-meter-long rails parallel, switched on and connected to a PC. In the software *OptoGait*, a new 'Patient' and a new 'Test' must be created.
- Regarding the preparation of the instrumented prosthesis, which was realized for the athlete AS only, the *SRI* 6-axis load cell is placed between the pyramidal attack below the knee and the clamp of the foot, then it is screwed in four points. In the proximal end of the foot, on the inner surface and just behind the clamp, it is placed the second sensor, which is the *6DX-PRO A* inertial sensor. It is fixed with tape so that its cables are projected forward. The cables of the sensor, together with the cable of the load cell, are strapped laterally to the socket, so that they stay tight to the body and are not dangerous for the athlete's movement.

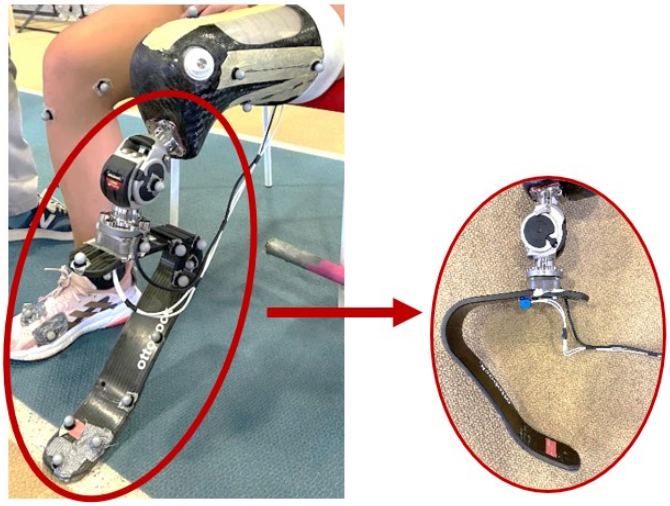

Figure 4.6 Wearable sensors on RPF setup

- Sensors are then connected to *DTS*. The acquisition system, its battery, the button panel and the powerbank needed to power the load cell are placed in a running backpack, with the button panel at the top. The athlete then wears the prosthesis and the backpack and to avoid excessive shaking of the backpack, the shoulder straps were tied together on the chest. In the case of athlete MM, no instrumentation was placed on the prosthesis, therefore the backpack was not necessary.
- The last preparation step consists in attaching the markers on the athlete's body and prosthesis according to the chosen protocol. The location of the markers slightly differs from the one used in OS1 and OS2, mainly for the prosthetic side.

  In particular, the number of technical markers applied on the socket increased, while the markers applied on the socket which should reproduce anatomical landmarks have been removed.

  - LFAP, LFAD, LLAP, LLAD, LPAP, LPAD (Technical markers: placed on socket).

  Some additional markers have been placed on the prosthetic foot.

  - LFPA, LFPP (Technical markers placed on the proximal end of the foot, ahead and behind the clamp);

  - LFP1, LFP2, LFP2 (Technical markers placed on the 'T frame' taped to upper stiffer part of the foot).

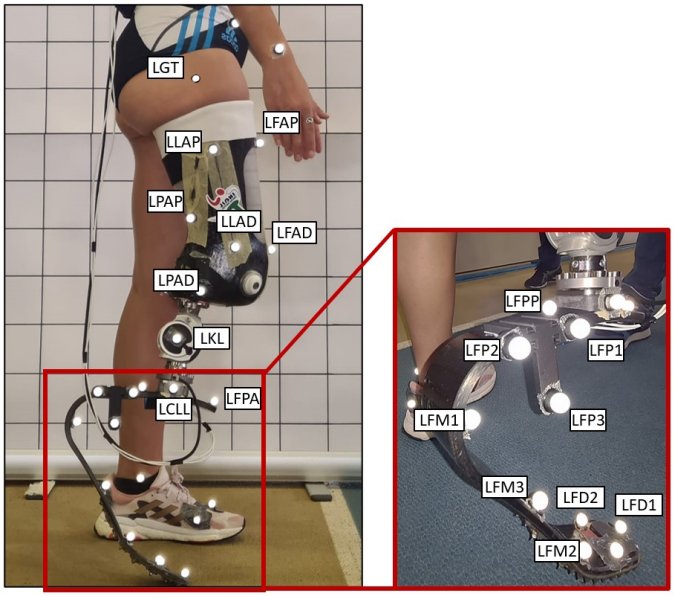

Figure 4.7. Markerset applied on prosthetic limb in OS3 (athlete AS)

The screws of the socket used to connect it to the knee have been pointed with the wand, and so the four reference points indicating the two main axes of the load cell (X and Y).

Static trials

In the *Nexus* software, the operator has to ensure that the active session where to store data is correct and that the system is in 'Live' mode.

- The athlete AS goes in the middle point of the acquisition volume and has to stay standstill while the operator clicks on 'Start' form the *Tools – Capture* section and after a couple of seconds clicks on 'Stop'. Due to the fact that the backpack inhibits the view of the markers on the back of the athlete, the first static capture is made with the backpack off, so that all markers were visible. Some markers are not placed directly on the body, for instance the marker on the ears, chest, load cell and socket screws, but they have been calibrated with a wand, according to the static calibration procedure described for OS1 and OS2.
- Once all markers required for the static model have been captured, the markers not required for the dynamic trials are removed, the backpack is put on and another acquisition with the updated markerset is recorded.

The procedure is similar for the athlete MM, except for the absence of the backpack.

Dynamic trials

The athlete goes to the start of the lane and prepares for the run and once ready the operator can click on '*Start*' in *Nexus*. For athlete AS, since she was wearing the sensors, the following sequence of steps must be iterated before each test.

- An operator opens the backpack, turns the acquisition system on and puts it into acquisition mode.
- The athlete then lifts the prosthetic leg for three seconds and thereafter performs three kicks on the ground. This is useful to have distinctive peaks in the sensors signal.

The button 'Execute' is then clicked in *OptoGait* to have the system start the acquisition.

During TSSR tests the subject accelerates for about 15 metres and then maintains a constant speed while running across the acquisition volume.
When the athlete exits the volume, she/he can decelerate and then stops. The acquisition is stopped both on *Nexus* and in *OptoGait.* At the end of the lane there is another operator who waits for the athlete to do the same sequence of movements performed before starting, that is three seconds with the prosthetic leg lifted and three kicks on the ground, then opens the backpack and stops the acquisition of the *DTS* by turning off the corresponding button on the panel.

In START tests, after doing the preparation sequence, the athlete sets on the starting blocks, placed inside the acquisition volume, and then sprints at the acoustic signal given by the device. She accelerates and once out of the capture volume she slows down and repeats the sequence of leg lifting and kicks.

Figure 4.8. Example of TSSR test (left) and START test (right) for athlete AS

The procedure described above applies to the athlete AS. In the case of MM, he has performed TSSR tests only, but he has always used the starting blocks placed on the start line of the track. Two tests have been executed with one type of RSP, while the third with a different RSP.

During OS3, the athlete AS performed 18 tests, wearing the same socket alignment, that is A3. The features relative to the alignment are reported below:

Table 4.4.Alignment A3 features during OS3

	Socket tilt* (γ)	**TAP**
A3	15°	5.5 cm

Table 4.5 contains a summary of the trials performed, where the test number is the same progressive number given to Vicon acquisitions.

Table 4.5. Tests performed by AS in OS3

SUBJECT	TEST NUMBER	TEST TYPE
AS	2	STATIC
AS	8	TSSR
AS	11	TSSR
AS	13	TSSR
AS	15	START
AS	17	START
AS	18	START

The athlete Maxcel Manu performed 7 tests including both static and dynamic. In the dynamic trials he always used the starting blocks placed outside of the acquisition volume, therefore the acquisitions are relative only to the steady state running. The list of trials is presented in Table 4.6.

Table 4.6. Tests performed by MM in OS3

SUBJECT	TEST NUMBER	TEST TYPE	RSP
MM	1	STATIC	Ossur Cheetah Xtreme cat6
MM	3	TSSR	Ossur Cheetah Xtreme cat6
MM	5	TSSR	Ossur Cheetah Xtreme cat6
MM	6	STATIC	Ossur Cheetah Xcel cat5
MM	7	TSSR	Ossur Cheetah Xcel cat5

The following Chapter describes the biomechanical analysis tool that has been developed. So far, it has been used to process data for MC and AS athletes only, but the calculation pipeline would be the same for other athletes.

Chapter 5

Biomechanical Analysis Tool

The large amount of data collected must be processed in order to obtain meaningful quantities describing the running gesture. The present work has contributed to the development of a software for the biomechanical analysis, which calculates the kinematic and kinetic parameters starting from raw data.

The flowchart in Figure 5.1 depicts the macro-blocks of operations done by the software.

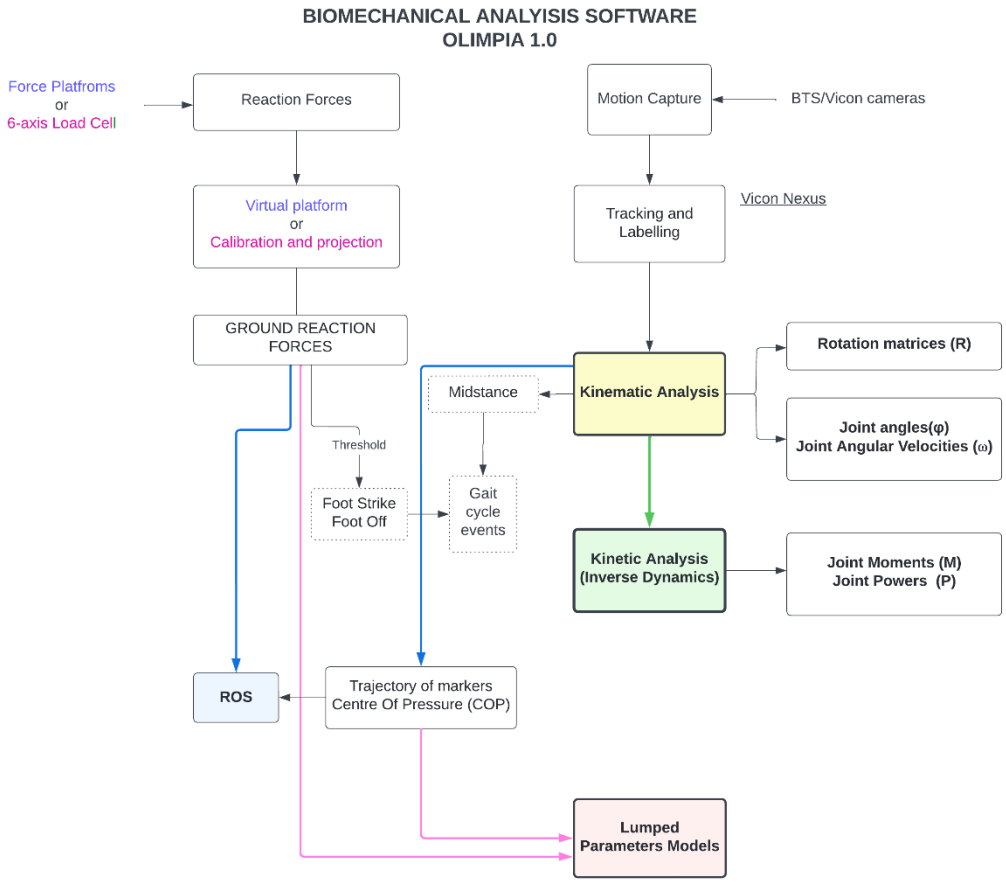

Figure 5.1. Workflow of Biomechanical Analysis

Starting from the top, there are the main two input sources, which are the data from Motion Capture cameras and the data from the force platforms or from the wearable load cell. On the one hand, data from the force platforms need to be processed to obtain a single resultant Ground Reaction Force vector and data from the load cell must be converted into the desired force components through a calibration matrix; on the other hand, data from Motion Capture need to be 'labelled'. These procedures will be described in detail in the following sections.

Once obtained the markers trajectories, the kinematic analysis can be carried out. It gives in output the matrices describing the orientation of each body segment in the three-dimensional space, the joint angles and the joint angular velocities. All these data, together with the filtered and segmented GRF and the gait cycle events are the inputs for the kinetic analysis, which in turn calculates the joint moments and powers. Furthermore, from COP trajectory and pose of body segments, the Roll-Over-Shape (ROS) can be calculated.
In the end, given the trajectory of specific markers on the lower limb and their mutual distance, the location of the Centre of Pressure and the Ground Reaction Forces, the lumped parameters models can be implemented. Such models are aimed at representing the running movement through simple elements like springs, masses and cams, but they should also consider the differences between the prosthetic and the sound limb, the influence of socket alignments and the multidimensionality of the prosthetic foot stiffness. This last topic will not be addressed in this work.

Pre-processing using *Vicon Nexus 2.12.1*

The data acquired with Motion Capture cameras, either with *BTS* or *Vicon* cameras, needs some pre-processing prior to be used for the kinematic and kinetic analysis.

When using *BTS*, stereophotogrammetry data of each trial are saved in a file *.tdf*. This file needs to be converted in a the *.c3d* format, which is a public domain file format containing all the information needed to read, display and analyse 3D motion data with additional analog data from force plates, if available. The format conversion is done by opening the *.tdf* file in the software *BTS Smart Tracker*, then clicking on 'Export → C3D format' and selecting in the relative window which trajectories to export (all trajectories have to be selected), whether to include or not data from force plates and the orientation of the coordinate system. In order to facilitate the reading of the file in the software *Vicon Nexus*, 'Z-UP' is selected. This way the global coordinate system will have X as the medio-lateral direction, Y as the antero-posterior direction and Z as the vertical direction.

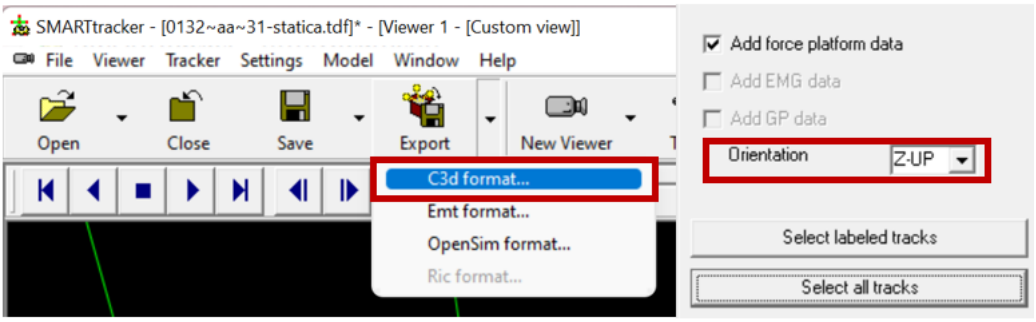

Figure 5.2. File opening and conversion in BTS SMARTtracker

Conversely, when using *Vicon*, raw data acquired from the cameras are saved in a file format *.x2d*. They can be directly loaded in *Nexus*, but to visualise markers in the virtual 3D space, it is necessary to click on the 'Reconstruct' button, which computes the three-dimensional location of each marker starting from the bidimensional data of the cameras.

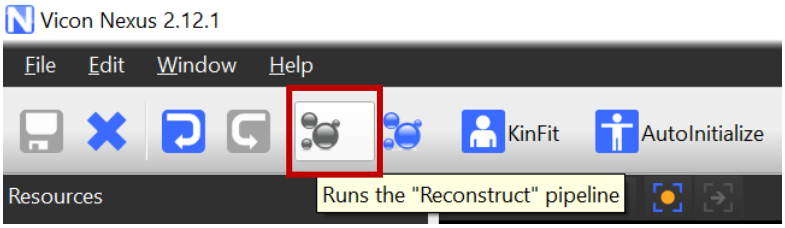

Figure 5.3. 'Reconstruct' pipeline in Vicon Nexus

Subsequent steps are invariant whether 3D data are obtained through the first or second method. They are relative to the software *Vicon Nexus 2.12.1*

- Creation of a new 'Blank Subject' from the 'Resources – Subject' pane toolbar.
- Creation of a 'Labeling Skeleton Template', which describes the generic relationship between physical marker attached to a subject and the skeletal structure to which the markers are attached. The purpose is to define how markers move with respect to each other and it does not pretend to be an anatomically correct template. In detail, the user goes to the 'Tools – Subject Preparation' pane and in the 'Labeling Template Builder' section enters the name of a body segment in the dedicated box, i.e. 'Trunk'. Then the user selects in the 'View' pane the markers belonging to that segment and clicks on the confirmation button. It is essential to create all segments on the same frame, regardless it is the first frame. Afterwards, the name and the colour of the markers of a segment can be edited, otherwise all segments have the same colour, and the markers are named using the name of the segment and progressive numbers. In the case of right and left limbs, if the word 'Left' or 'Right' is written at the beginning of the segment name, the software will automatically assign to that segment the colour red or green respectively.

- If the user wants to perform the ‘Labeling’ operation automatically, the template must be completed by linking the segments by joints. For each pair of segments, a type of joint must be chosen among hinge, hardy spicer, ball and free joint and then the two segments have to be selected according to the parent-child order. Afterwards, the ‘Static Skeleton Calibration’ operation can be executed, which computes and saves the distances between markers in a dedicated file.
- Save the just created ‘Skeleton Template’ and attached it to the current subject by right clicking on the same of the subject in the ‘Resource’ pane.

At this point, whether the automatic labelling has been performed or not, it is necessary to scroll through the test frame by frame and check that at each instant each marker has the correct label. It may happen that markers, which are very close, as in the case of the prosthetic foot, are swapped or that the trajectory of some markers has some gaps because in those instants the marker was not seen by the minimum number of cameras, usually three. In the first case it is necessary to unlabel the trajectory and re-assign the correct label to the marker, while in the second case, *Nexus* provides some tools to interpolate trajectories. These steps are quite time consuming, but they are of paramount importance to proceed with the analysis of the data, since errors in the labelling procedure may cause major errors in the following phases.

The graphical interface of *Nexus* allows the visualization not only of the 3D location of the markers, but also of the force platforms and the Ground Reaction Force vector, whether platforms are present. This way is it is possible to individuate the time instants in which initial contact and toe off take place. This procedure can be done also automatically, by running a pipeline which detects gait cycle events using vertical GRFs and adds them to the time bar. In this case, the detection of events has been done in a separate phase, through a dedicated MATLAB function. Once all pre-processing operations are completed, the trial data can be exported in as a *c3d* or ASCII file. The file format and some further preferences, like the initial and end frame and the option to include or not the events, can be set from the ‘Tools - Pipeline’ pane. The format chosen has been always *.c3d.*

Kinematic analysis

The goal of the kinematic analysis is the calculation of joint kinematics, that is the description of the relative movement between two adjacent body segments. To this extent, a reference system for each body segment has to be defined using the physical or virtual markers placed on the subject’s body. While in static trials it is quite easy to get the exact location of the anatomical landmarks, because the trajectory of the markers placed on them is constant – or possibly

reduced to a single time instant – in dynamic trials there are many sources of error. The low precision of the instrumentation, the inaccuracy in markers placement and the soft tissue artifact make the signal noisy or discontinuous.

In order to minimize experimental errors, two possible methods can be adopted, the 'non-optimal' or the 'optimal' method. According to the 'non-optimal' method, only three markers are applied on each body segment, or if there are more than three markers, their location has to be expressed as a function of three markers. This way, a triangle is individuated and it is used to define the pose of the segment, which highly depends on the specific location of the triangle, which may be affected by some noise. During the static trial, the inaccuracies can be considered very small or negligible, therefore the 'non-optimal' procedure can be adopted. However, in the dynamic trials, the entity of errors increases and distances between markers are not more time invariant. To make the analysis more robust, the second method has to be used, which is based on the minimization of an objective functional that expresses the experimental error, calculated as the sum of squared differences between the location of each point measured in the dynamic trial (P_i) and the location estimated ($\hat{P}_i$) from the static trial.

$$f = \sum_{i}^{n} \left|e^i\right|^2 = \sum_{i}^{n} \left|P_i - \hat{P}_i\right|^2$$

(5.1)

The minimum of this functional is reached when the cross-covariance between the two signals is maximum. Cross-covariance is a measure of similarity of two signals, commonly used to find features in an unknown signal, in this case the pose of markers in dynamics ($\tilde{P}_{di}$), by comparing it to a known one, which is here the pose of the same markers in static ($\tilde{P}_{si}$).
Cross-covariance between two signals X and Y is mathematically defined as:

$$C_{XY} = cov(X, Y) = E[(X - \mu_X)(Y - \mu_Y)^T]$$

(5.2)

In this case, given $(X - \mu_X) = \tilde{P}_{di}$ and $(Y - \mu_Y) = \tilde{P}_{si}^T$, cross-covariance is calculated as the product $\tilde{P}_{di}\tilde{P}_{si}^T$. The matrix C is then broken down into three components according to the Singular Value Decomposition (SVD) principle, and by the multiplication of the two resulting orthonormal matrices, the matrix expressing the orientation of the local coordinate system in dynamics is obtained.

$$C \overset{SVD}{\Longrightarrow} U \cdot W \cdot V^T$$
$$R = UV^T$$

(5.3)

Kinematic analysis implementation

The proper data processing takes place in the programming platform MATLAB.
In order to extract data from the *.c3d* files, the open-source MATLAB library *Biomechanical ToolKit - BTK* is employed. This library contains many functions useful to read and write.*c3d* files, to get specific information like the number of markers, the number of analog channels (relative to force platforms), the acquisition frequency either for the stereophotogrammetry or the dynamic data, and many others.

In the following description, vectors and matrix dimensions are expressed using the following terminology:
- nF is the number of frames;
- nP is the number of markers (points).

Static trial processing

First, the *c3d* file containing the location of markers during static acquisition is loaded. It is important to exactly load the file corresponding to the static trial recorded just before the dynamic trial that will be analysed. It is essential if the socket alignment has changed between dynamic trials and is it useful also to get the exact location of markers in case some of them have fallen and then have been re-positioned.

The global reference frame used in *Nexus Vicon* is a right-handed triad having the x-axis pointing rightward, the y-axis pointing forward and the z-axis vertical. However, according to ISB (International Society of Biomechanics) recommendations, the global reference frame is '*a right-handed orthogonal triad fixed in the ground with the + Y axis upward and parallel with the field of gravity, X and Z axes in a plane that is perpendicular to the Y axis*' [49] . Therefore, a 90° anticlockwise rotation about X axis and then a 90° anticlockwise rotation about the new Y axis are necessary to make the *Nexus* coordinate system consistent with the one proposed by ISB.

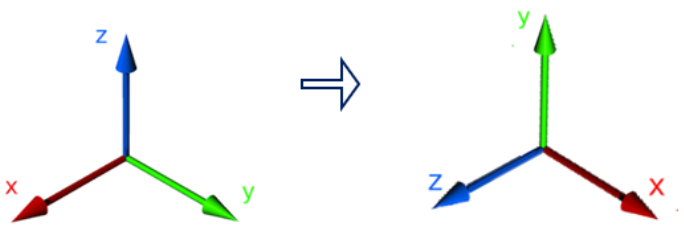

Figure 5.4. Global reference systems. From GCS of Vicon (left) to ISB notation (right)

This result can be achieved either by pre-multiplication of each maker trajectory [nF x 3] by the rotation matrix [3 x 3] obtained as product of two basic rotation matrices, or, more easily, by changing the coordinates order. In detail:

- the second coordinate becomes the first [Y → X];
- the third coordinate becomes the second [Z → Y];
- the first coordinate becomes the third [X → Z].

In order to make this passage quicker, a custom MATLAB function called `swapCoord` has been developed.

Afterwards, for each body segment, the following general steps are performed.

1. Group the markers belonging to the selected segment by creation of a tensor [nF x 3 x nP], called `cluster_<S>_gnd_st`, where "<S>" stands for the specific segment (trunk, pelvis, thigh, shank, foot, socket, prosthetic knee, prosthetic foot). For some segments, an additional cluster is defined by grouping only the markers kept during the dynamic trial. This cluster is then used for the dynamic optimization.
2. Define the anatomical (or local) coordinate system of the body segment through custom functions specific of the segment. The function receives in input the markers – at least three – needed to build the reference frame and gives in output the 'pose matrix', which is a tensor sized [4 x 4 x nF] and named `gnd_T_loc_<S>_st`. The first three columns of the tensor contain the three-dimensional components of x, y and z axes of the anatomical CS with respect to ground CS and the fourth column is composed of the homogeneous coordinates of the CS origin referred to ground CS in each instant frame. The general procedure to obtain a local coordinate system is:
   - Select a marker as origin of the CS or calculate the origin as midpoint between two or more markers. Its coordinates make up the position vector.
   - Define the distance between two markers to obtain the first vector, possibly temporary, and do the same to obtain the second vector. Vectors are then normalized to obtain unit vectors. These two vectors identify a plane.
   - Compute the cross product between the unit vectors to obtain a third vector, perpendicular to their plane. Re-define one of the previous vectors by computing another cross product, to obtain an orthogonal triad, having x-axis in the antero-posterior direction, y-axis in the cranio-caudal direction and z-axis in the left-to-right direction, both for left and right limbs.
   - Arrange the three unit vectors as columns of a matrix [3x3] and add the position

vector as fourth column of the matrix, which becomes [3 x 4]. In the end, a row vector [0 0 0 1] is added to complete the tensor.

3. Map the global coordinates of the cluster(s) of markers into the local reference system. Here the custom function `points2local` is used. It requires in input the cluster in ground coordinates and the coordinate system of the segment. It gives in output either the local coordinates of the markers frame-by-frame or their average location over time, which is the [3 x nP] tensor called `cluster_<S>_loc_st`.

The representation of the local anatomical CSs for the body segments can be found in Figure 5.5 and the detailed description of how the Coordinate Systems are computed is provided in the Appendix C.

The local coordinate system of the prosthetic knee and of the load cell are crucial to obtain a meaningful calculation of joint angles and reaction forces for the affected limb, so they are described in detail.

Prosthetic knee requires two coordinate systems: the first is integral with the socket and the second is the same as the previous but it is centred either on the foot proximal tip (FP1/LFPA) or on the clamp centre, depending on what markers are available and it is associated to a cluster of markers applied on the knee and proximal foot.

The first prosthetic knee CS, `gnd_T_loc_LprosthKnee_st`, is so defined:

- Centre (O_{knee}) is the midpoint of the markers placed laterally (KL) and medially (KL) to the prosthetic mechanical knee;
- Z axis (z_{knee}) is defined as the frontal axis pointing rightward, that is going from KL to KM;
- X axis (x_{knee})is the axis pointing forward obtained as cross product of a temporary vector joining the origin to HJC and Z axis;
- Y axis (y_{knee}) is the cross product of Z and X axes, pointing upward.

This CS is used to get the local coordinates of the technical markers placed on the socket, so it is related to the movement of the thigh.

The second CS relative to prosthetic knee, `gnd_T_loc_LfunctKnee_st`, is defined identically to the previous ($x_{knee}, y_{knee}, z_{knee}$) except from the origin ($O_{distKnee}$) and it is used for the projection of the coordinates of marker placed on the prosthetic knee and on the proximal foot.

Load cell reference system, `gnd_T_LoadCell_st` is built as follows:

- Centre (O_{lc}) in the centroid of the load cell, calculated as midpoint between the four (virtual) markers placed around the load cell (LO1, LO2, LO3, LO4);

- Z axis (z_{lc}) is the mediolateral axis, pointing rightward, defined with the markers LO2 and LO3, placed medially and laterally respectively;
- Y axis (y_{lc}) is the axis pointing upward, defined as the cross-product of Z axis and a temporary vector connecting the anterior (LO1) and the posterior (LO4) markers
- X axis (x_{lc}) is defined as the cross-product of Y and Z, pointing forward.

In Figure 5.6 there is a schematic representation of the reference systems created for the unaffected limb and for the trunk, while in Figure 5.6 the CSs of the prosthetic limb are represented.

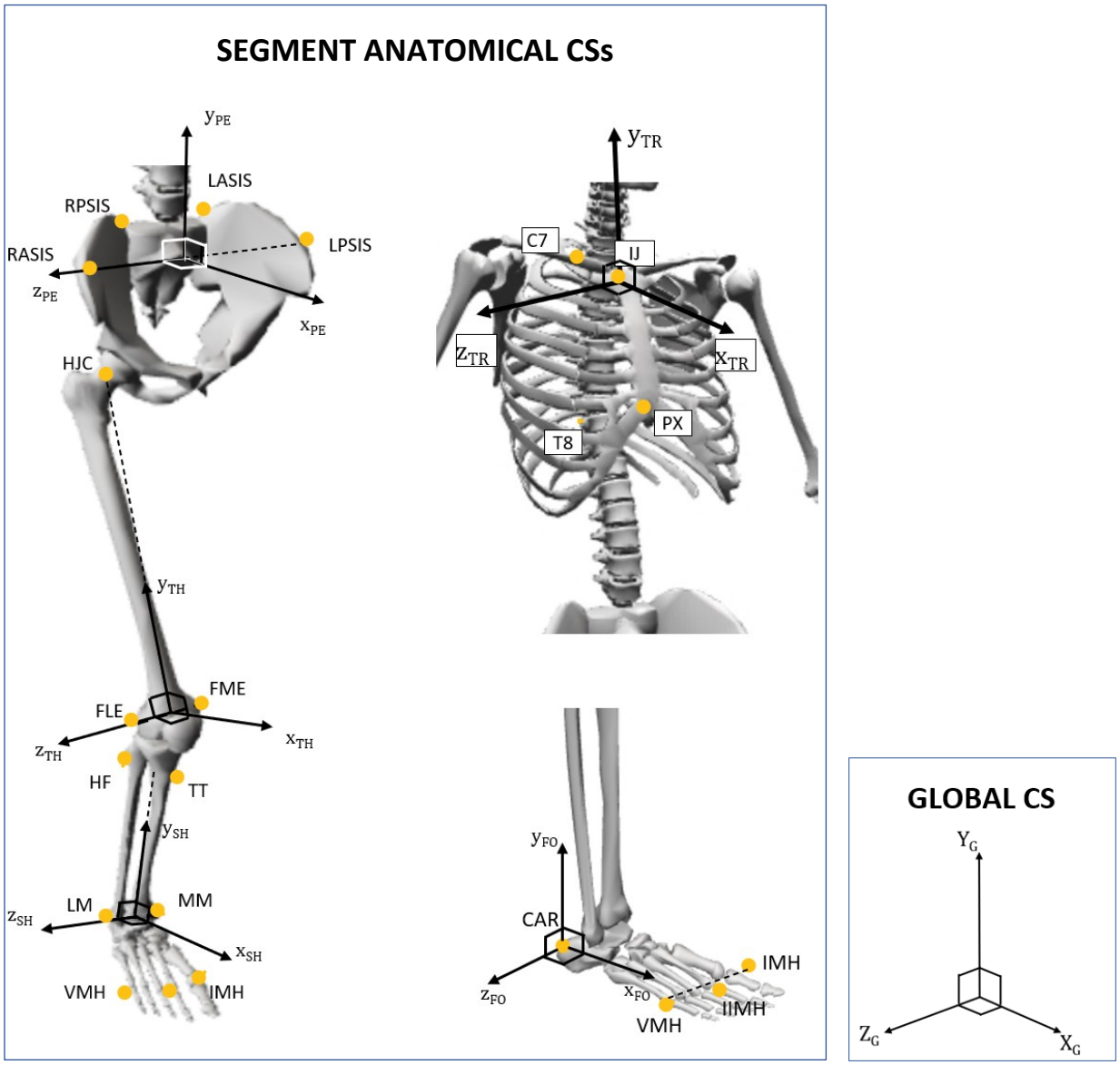

Figure 5.5. Anatomical markers and segment anatomical Coordinate Systems (see Appendix C)

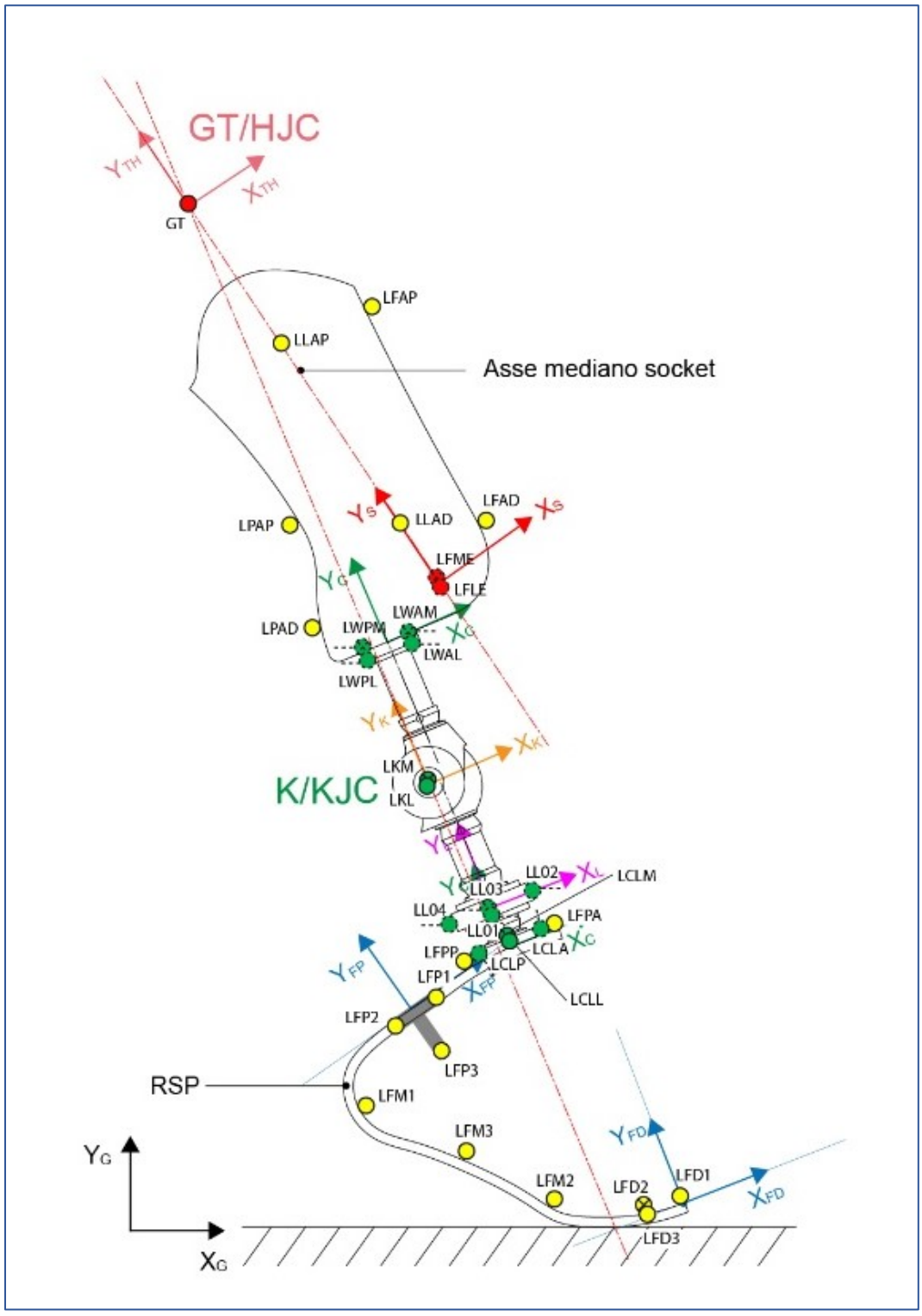

Figure 5.6. Technical markers and technical Coordinate Systems (see Appendix C)

There are some segments which need further processing. In detail, the reference system of the thigh or the socket require a virtual marker, which is the hip joint centre (HJC). 'Virtual' means that it does not correspond to a marker physically attached to the body, but its location can be retrieved from other physical markers. There are mainly two methods to obtain the coordinates of HJC: predictive and functional. The former is based on regression equations that estimate HJC from easily measurable anthropometric quantities, the latter calculates HJC through an algorithm which first requires the subject to perform leg circumduction and then uses the trajectories of markers applied on the pelvis and on the lower limb to compute the instant centre of rotation of the leg. In the present work, the predictive method, commonly called also 'Bell's method' from one of its authors, is used. Attempts have been made also with the second method, also called 'Gamage's method' or 'Cappozzo's method', and have driven to similar results, but it has then been discarded because it was more time consuming.

Bell's method has been implemented in the custom function `bellHJC`, which first calculates pelvis width as Euclidean distance between the markers placed on the superior anterior iliac spines, then multiplies it for three regression coefficients to obtain the three-dimensional coordinates of HJC expressed in the pelvis local reference frame.

$$PW\ (pelvis\ width) = |RASIS - LASIS|$$
$$RHJC^{LOC} = [-0.10 * PW;\ -0.30 * PW; +0.36 * PW]$$
$$LHJC^{LOC} = [-0.10 * PW; -0.30 * PW;\ -0.36 * PW]$$

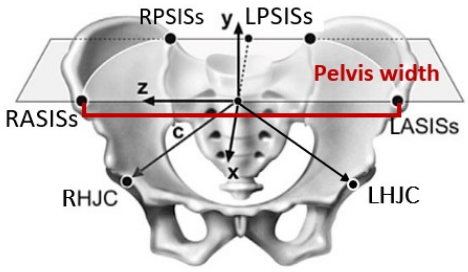

Figure 5.7. Hip Joint Centre with respect to Pelvis Coordinate System

Afterwards, HJC coordinates are mapped into the ground reference system, using a function named `movepoint,` which does operation inverse to `points2local`, that is it 'moves' the point from the local to the global CS. To do so, it pre-multiplies the vector of local HJC [1 x 3] by the pose matrix [4 x 4 x nF] of the pelvis and gives in output a matrix sized [nF x 3], which is consistent with the dimension of the matrices of the other markers.

Since the location of the hip joint centre is required both for hip and knee angles calculation, it is useful to refer it not only to pelvis, but also to thigh and socket. Once obtained the coordinate systems of thigh and socket, HJC is first projected onto the reference systems of these segments, thus obtaining a new HJC^{LOC} and then referred again to the global CS. The matrix now

employed to ‘move’ the point is the pose matrix of the thigh or of the socket respectively. The global coordinates are very similar to the ones obtained when using pelvis pose, but not identical. The choice to use the one or the other can be due to the fact that in some patients, especially if they are overweight, the iliac spines are not clearly visible and therefore referring HJC to the pelvis reference system would introduce additional errors in the subsequent angles calculation. In this case, using HJC coordinates relative to the socket instead of the ones relative to the pelvis is preferable in the definition of the prosthetic knee CS to reduce the errors relative to socket oscillation relative to pelvis.

Some issues occurred during the definition of coordinate systems in static. The main problems are relative to the absence of some markers, for example the markers placed on the medial side of the segments. As far as the sound side is concerned, two possible strategies can be applied.

- The first one consists in using another static trial where all markers are visible to define the coordinate system. This can be done because markers on the unaffected limb are placed on precise anatomical landmarks, which do not vary their mutual distance between different static acquisitions.
- The second option is the so-called “solidification” procedure, which consists in ‘moving’ a marker from the complete static trial into a different static trial. To do so, a technical reference system has to be defined in both trials using the same markers. Afterwards, the coordinates of the target marker, e.g. FMER (femoral medial epicondyle - right) are referred to the local CS and in the end, through the function `movepoint`, they are transformed again into global. The same procedure is adopted to reconstruct the tip of the wand used during the Static Calibration, however in this case the identification of the wand tip through geometrical formulas is also necessary.

On the contrary, for the prosthetic leg none of these procedure is applicable, because the relative position of markers can vary when changing socket alignments. This point remains an open issue, but to go further with data processing, ‘solidification’ of FMEL (femoral medial epicondyle – left) has been done, possibly introducing some errors.

Dynamic trial processing

Once the definition of CSs for all body segments and prosthetic components in the static trial is completed, one can go further with the dynamic trial. Once loaded the corresponding file (or files in case of trials split in multiple files), markers trajectories which have some gaps at the beginning or at the end of the trial are added a padding by replicating the first or the last non-

zero value respectively. To fill other possible gaps in the middle of the acquisition, interpolation is performed using the MATLAB function `spline`. Signals are low-pass filtered using a Butterworth filter having a cut-off frequency equal to 10 Hz and then they are given in input to `swapCoord`, to re-order the coordinates. The following operations are then executed for each body segment.

1. Definition of cluster of markers. It is essential that all and only the markers used to define the cluster in static are here employed and that the order in which they are stacked is the same order used in static. The tensor representing the cluster is named `cluster_<S>_gnd_dyn`.
2. Calculation of local coordinate system in dynamics through the function `OptDynLoc`, which implements the 'optimum' method cited above, here also called 'Dynamic Optimization'. The function takes in input the average local coordinates of the cluster gathered from the static trial and the global coordinates of the same cluster gathered from the dynamic trial, computes the centroid of both clusters (μ_Y, μ_X) and the instantaneous vector joining the centroid to each point of the cluster. Afterwards multiplies the matrix of such vectors in dynamics (X) by the transpose of matrix of vectors in static (Y), thus obtaining the cross-covariance matrix `C`. Singular value decomposition is applied to such matrix and then the product of the first and last component of the decomposition give the matrix describing the orientation of the segment in dynamics. To complete the reference system, the definition of its origin is mandatory. Origin of the CS is obtained by adding the local coordinates of the static centroid multiplied by the orientation matrix to the global coordinates of the dynamic centroid. Orientation matrix and origin vector are then packed into the pose matrix `gnd_T_loc_<S>_dyn` [4 x 4 x nF].

Coordinate systems in dynamics are defined using only the 'technical' markers, which are markers placed on body segments but which do not correspond to anatomical landmarks. However, in some cases it is useful to get the displacement of anatomical landmarks in dynamics without attaching markers on them. In order to do this, the "solidification" procedure is used, but in this case is the point is 'moved' from static to the dynamic trial. In detail, this step has been done for medial bony prominences, like medial femoral epicondyle, medial malleolus, for the hip joint centre and for other markers removed during the dynamic trial, such as the marker put medially on the prosthetic knee.

Afterwards, a new *.c3d* file is created containing all markers trajectories, including the ones just "solidified", the resultant Ground Reaction Force and resultant torque, which are obtained as sum of the contributions from the force platforms, when available. Before the creation of a new file, both marker coordinates, forces and torques are arranged column-wise following Vicon convention (X medio-lateral, Y antero-posterior, Z vertical) and their units of measurements are set to millimetres, Newton and Newton*millimetres respectively.

Joint Angles calculation

Once the definition of reference frames is concluded, one gets to the core of kinematic analysis, namely the description of relative motion between two adjacent body segments, also known as joint kinematics. To this purpose, for each pair of contiguous segments, the rotation matrix and position vector of the joint are required, which describe orientation and the location of the distal segment with respect to the proximal one. Joint rotation matrix (R_{joint}) is obtained as product of the orientation matrices of the segments (R_{prox} , R_{dist}) with the matrix of the proximal segment transposed.

$$R_{joint} = {R_{prox}}^{T} * R_{dist} \qquad (5.4)$$

Joint position vector O_j can be obtained by multiplication of the transpose of the proximal rotation matrix and the distance between the origin points of the CS of each segment, but in this analysis it is not calculated.

R_{joint} is interpreted as the matrix resulting from the multiplication of three elementary rotation matrices describing rotation about moving axes. It is crucial to establish the order of rotations, because different orders lead to different results. In this case, the order chosen for the description of the orientation of hip and knee joint is the Cardan sequence $Z - x' - y''$, meaning that the first rotation takes place around the Z axis of the proximal segment, the second around the once rotated x axis of the distal segment and the third around the twice rotated y axis of the distal segment. Conversely, the order chosen for the description of ankle joint orientation is $Z - y' - x''$, because the movement about the vertical axis is greater than the movement about the frontal axis.

The calculation of Cardan angles from rotation matrix is implemented in the functions `R2zxy`, `R2zyx`, which compute the inverse trigonometric operations and gives in output a matrix containing the three-dimensional rotation angles, frame-by-frame. The order of angles in the column reflects the order used in the formula.

According to ISB recommendations, joint angles should be represented using the following sign conventions [7].

Table 5.1. Joint angles sign convention

HIP	Flexion (+)	Extension (-)
	Adduction (+)	Abduction (-)
	Internal rotation (+)	External rotation (-)
KNEE	Flexion (+)	Extension (-)
	Adduction (+)	Abduction (-)
	Internal rotation (+)	External rotation (-)
ANKLE	Dorsiflexion (+)	Plantarflexion (-)
	Internal rotation (+)	External rotation (-)
	Inversion (+)	Eversion (-)

To be consistent with these conventions, some adaptations are necessary after the calculation of joint angles. For example, having all medio-lateral axes pointing rightward, the flexion movement for the knee angle is clockwise and therefore negative, but its sign is inverted to make flexion positive. Analog changes are made for the internal rotation and adduction of the left limbs, which occur in clockwise direction with respect to their longitudinal and frontal axes, but they have to be considered as positive.

Neutral positions, in the sagittal place, are the condition in which the longitudinal axes of the segments are aligned, that is they form a 0° angle, but for the ankle is considered the 90° position of the plantar aspect foot relative to the frontal plane of the shank.

Function `R2zxy` is used also to obtain the angles describing the three-dimensional orientation of the pelvis with respect to ground. The terminology used for pelvis is different: pelvic tilt is the orientation of pelvis in the sagittal plane, pelvic obliquity is the orientation in the frontal plane and pelvic rotation is the orientation in the transverse plane [50], [51]. Sign conventions adopted for pelvis are the following.

Table 5.2. Pelvic absolute angles sign convention

PELVIS	Anterior tilt (+)	Posterior tilt (-)
	Upward obliquity (+)	Downward obliquity (-)
	Internal rotation (+)	External rotation (-)

Each triplet of angles, e.g. `hip_angles_R`, is then used to calculate joint angular velocities, obtained as first derivative of joint angles.

The last steps of the kinematic analysis pipeline are necessary mainly for results visualization. In particular, the events 'Foot Contact' and 'Toe Off' have to be identified in order to describe the variation of angles during the gait cycle. These events instants are detected by the custom function `getEvents` from the GRF signal and it will be described in the following section. Moreover, mid-stance instants are identified as the instant in which the vertical projection of the Greater Trochanter (GT) on the ground overlaps the 5th metatarsal head (VMH) for the unaffected limb and as the instant in which the vertical projection of GT passes through the prosthetic knee centre (KJC) for the affected limb. In other words, it is the instant in which a selected pair of markers have the same antero-posterior coordinate except for a variable small offset.

Joint angles and joint angular velocities are segmented using gait cycle events and then normalized over stride time, so that their average and standard deviation can be calculated and represented.

Eventually, a MATLAB structure `outKine<Subj><#trial>` is created to save the variables needed for the dynamic analysis, in particular the rototranslation matrices relative to each body segments, the resultant GRF vector, joint angles and joint angular velocities.

The entire pipeline of commands and functions can be summarized in the following flowchart.

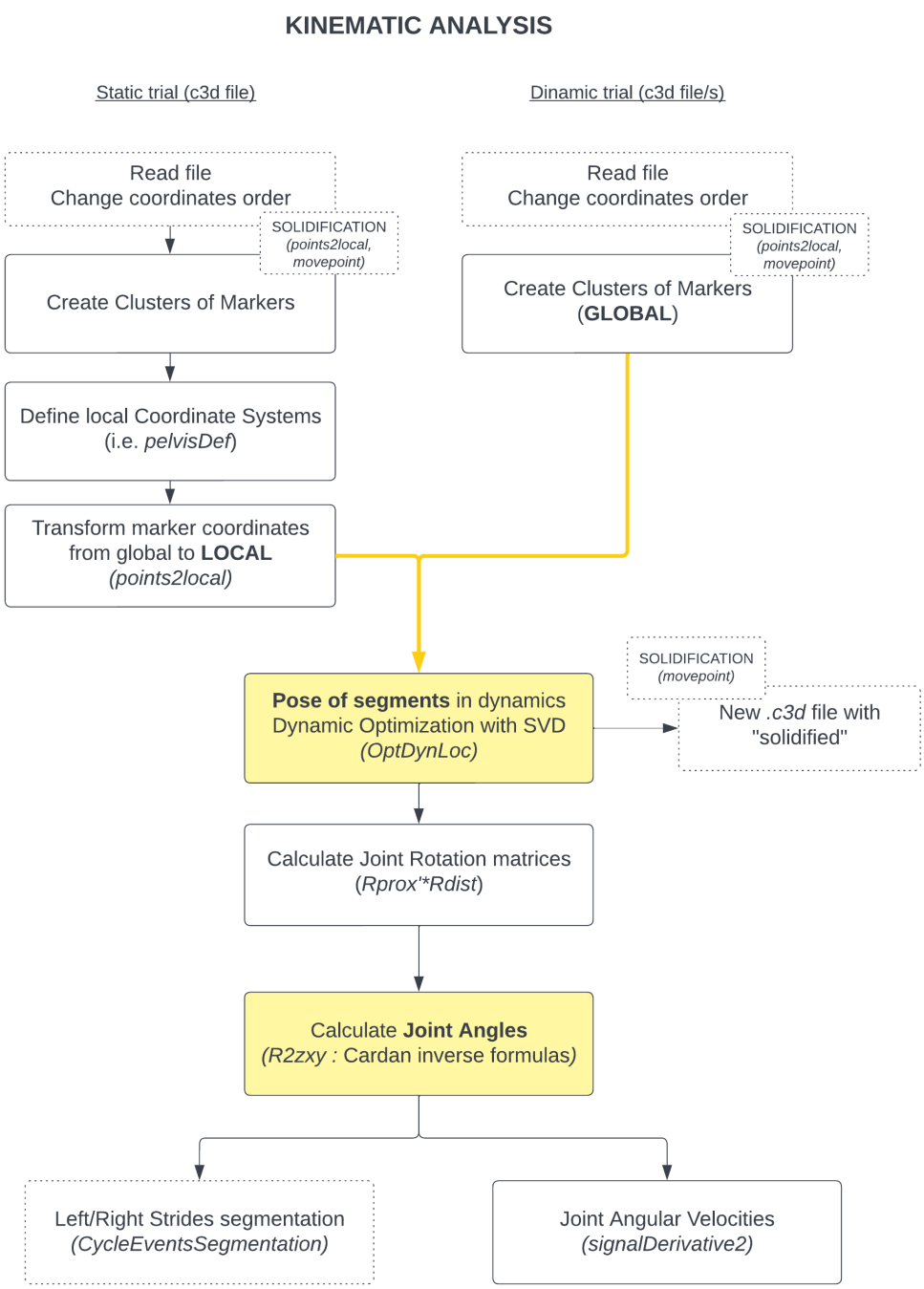

Figure 5.8. Workflow Kinematic Analysis

Dynamic analysis

The purpose of dynamic analysis is the study of the Ground Reaction Forces produced by the athlete while running and the calculation of joint reaction forces and joint moments caused by external forces. During OS1 and OS2, forces were measured using force platforms placed below the treadmill, therefore data are relative both to affected and unaffected limb. Conversely, during OS3 forces data are relative only to the affected limb, since they were measured through

the load cell mounted in the prosthesis.
Regardless of the source of the data, magnitude, direction and point of application of the Ground Reaction Force are required in order to compute the proper kinetic analysis.

Ground Reaction Forces analysis

The data acquired through the force platforms during OS1 and OS2 and the data acquired through the wearable load cell during OS3 have been analysed to obtain the Ground Reaction Forces, which are one of the substantial outputs of the biomechanical analysis. Data have been processed in two different ways, depending on their source.

Treadmill tests

Force platforms data are contained in the same *.c3d* file used for the kinematic analysis and are extracted using the function `btkGetAnalogsValues`.
The preliminary step of the processing consists in filtering the signals, which are affected by noise due to the vibrations of the treadmill frame and of its motor when the treadmill is switched on. As for SSR tests, after spectral analysis, two filters in cascade are applied. First, a band-stop Butterworth 2nd order filter, which rejects frequencies that lie between 15 and 35 Hz, and then a 2nd order Butterworth filter with 43 Hz cut-off frequency. Conversely, for RAR tests, only one 4th order15 Hz cut-off lowpass filter has been applied.

Subsequently, the analysis of force data is quite similar for both types of tests, except for the representation of the results since the calculation and representation of average values among steps is suitable only for SSR tests, while in RAR test each step has been treated separately.

- The first step is the identification of Foot Contact (FC) and Foot Off (FO) events, which is achieved by setting a 100 N threshold on the signal relative to the vertical force. Despite this threshold is quite high, with respect to other lower values found in literature, still some errors occur in the detection of correct time instants. For example, it may happen that there are peaks above 100 N which do not correspond to real steps, because their duration is shorter than 0,01 seconds or longer than 0,2 seconds. Therefore, if the intervals between events do not respect the minimum (10 frames) or maximum (200 frames) values, the wrong events are discarded.
- Once obtained all FC and FO events, they are split according to whether they belong to the unaffected or affected foot. The vertical force peak relative to the first step is compared to the peak of the second step: if the first is greater than the second, then the sequence of steps begins with UL, otherwise it begins with AL. In fact, it has been

observed that AL generates less vertical force than UL. This is consistent with literature, therefore the method can be considered reliable.

- The following step consists in the calculation of net vertical and horizontal impulses for each limb. Horizontal force is here considered as the anterior-posterior component only, while medial-lateral force has been neglected at the moment.

  Impulse in each step is the integral of the force, vertical or horizontal respectively considering both positive and negative values, over the duration (in seconds) of the stance, calculated using the MATLAB function `trapz`, which performs the trapezoidal numerical integration. Body weight has been subtracted from the vertical GRF before computing the impulse.
- In addition to net impulses, the horizontal braking and propulsive impulses have been calculated separately. Braking impulse is the area under the negative part of the F_x curve, while propulsive impulse is the area under the positive part of the F_x curve, obtained with the function `trapz`.
- The multiplication of contact time (difference between FC and FO instant) by the velocity gives the contact length. In SSR tests, velocity is a constant value which has to be entered by the user depending on the speed set on the treadmill during the trial under analysis, while in RAR tests speed is obtained by calculation of the first derivative of the AP trajectory of a marker sticked to the treadmill on this purpose. In detail, the trajectory consists in the iteration of small displacements corresponding to the length of the treadmill, so its derivative only shows a series of peaks. In order to obtain a continuous speed curve, the signal has been filtered using the moving median and then fitted with an eighth order polynomial.

The final output of the GRF analysis in SSR tests is the representation of the mean and standard deviation of F_x and F_y forces over the last six steps (per leg) of the trial..

The analysis of GRF in RAR tests gives is output the representation of the force (F_x or F_y) in each step, so one can note how force vary while the subject accelerates. The representation of the horizontal impulses, either net or divided into breaking and propulsive in each step is also given in output.

Moreover, during the Resisted Accelerated Running tests performed in the laboratory, force data have been acquired also through the mono-axial load cell. These data have been briefly processed to estimate the horizontal force applied at the centre of mass of the athlete, which has then been plotted together the horizontal component of GRF and the velocity.

The load cell measures the instantaneous resistance applied at the harness worn by the athlete and it should be equal to the horizontal force measured by the force platforms, except for an offset representing the frictional force of the treadmill. Such frictional force has been estimated through an experimental test, in which the treadmill – put in passive mode – has been accelerated by the triride of a wheelchair, which was in turn connected through a rope to the monoaxial load cell. During the test, the triride accelerated in multiple speed stages until reaching 15 km/h and each speed has been maintained for a about 5 seconds, so that the force measured by the load cell corresponds to the frictional force exerted by the treadmill when acceleration is zero. The average frictional force among all speed stages has been calculated and it is equal to about 87 N, which can be considered as a constant and speed-independent value.

$$F_{friction} - F_{cell} = m * a = 0$$
$$F_{friction} = F_{cell}$$

(5.5)

In addition, another experimental test has been carried out with the same wheelchair, in order to estimate the equivalent inertial mass of the treadmill. This time the triride accelerated continuously from 0 to 15 km/h. The force measured by the load cell is equal to the frictional force plus the acceleration of the equivalent mass of the treadmill.

$$F_{cell} = F_{friction} + \boldsymbol{m_e} * \ a(t)$$

(5.6)

In the equation above, the only unknown term is the equivalent mass ($\boldsymbol{m_e}$), which has been calculated as the average of $\frac{F_{cell}(t_0) - F_{friction}}{a(t_0)}$ in each time instant t_0, which is approximately 70 Kg. This value is one of the essential parameters for the design of an inertial treadmill, which is also included among the goals of Olimpia project, but its validity has yet to be assessed.

The computation pipeline describing the GRF analysis is represented in Figure 5.9.

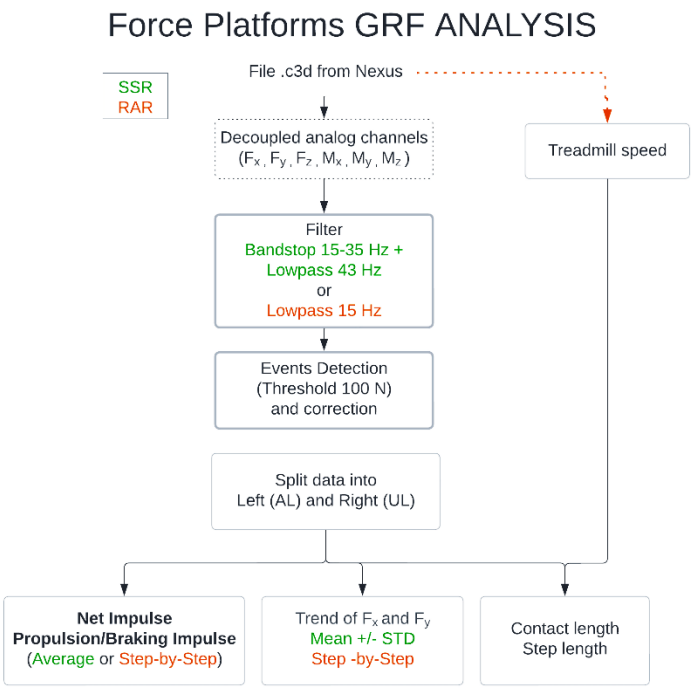

Figure 5.9.Worflow of GRF analysis

Track tests

In the second case (OS3), raw data from the 6-axis load cell consist in six signals with 2000 samples per second. The preliminary steps required for the subsequent data processing are:

- Decoupling of forces and torques components. In order to extract them from the raw signals, a calibration matrix is required. It has been given by the load cell manufacturer, however the results obtained using this matrix only were not accurate. Therefore, thanks to an additional experimental test, some correction factors have been estimated and added to the calibration matrix, in order to obtain a more correct decoupling of the signals.
- 'Zeroing' forces and toques. The 'zero' has been set using the values measured when the athlete had her leg lifted at the beginning or at the end of the trial as reference values. Such instants are clearly discernible in force data because they are preceded or followed by three peaks, which correspond to the three kicks done by the athlete with the prosthetic leg. In practice, the offset removed from each channel has been calculated as the mean signal in the time window in which the variance of the signal itself is minimum.

- Changing the reference system of the load cell. The sensor has been mounted with its sagittal axis pointing backward and named 'Y' and its vertical axis pointing upward, but named 'Z'. To be consistent with all reference systems used in the kinematic and kinetic analysis, forces and moments signs and labels have been changed consequently, so that:
  - X components are relative to the sagittal axis pointing forward;
  - Y components are relative to the vertical axis pointing upward;
  - Z components are relative to the frontal axis pointing rightward.

Afterwards, since the acquisition system *DTS* and the motion capture system *Vicon* were not synchronized, force signals have been manually aligned with stereophotogrammetry. In order to do this, first they have been downsampled, from 2000 Hz to 300 Hz, then for the estimation of the correct time shift, the data from the inertial sensor - also downsampled - have been used. In detail, the cross-correlation between the angular velocity ω_z measured by the sensor and the angular velocity obtained as derivative of the orientation matrix relative to the proximal foot reference system has been calculated with one signal sliding over the other. Maximum correlation indicates that the two signals are representing the same steps, so the time shift corresponding to that correlation value is the offset to be added or removed from the *DTS* signals, depending on whether this shift is positive or negative.

The following step consists in the identification of gait cycle events by the application of a threshold on the vertical force F_y. Prior to this, the signal needs to be filtered to eliminate some noise relative to the oscillation of the prosthesis. The spectral analysis of the signal revealed that the prosthetic foot has a proper resonance frequency equal to 66 Hz. Various attempts have been to individuate the best cut-off frequency and in the end 52 Hz has been chosen. The threshold which best allows the correct detection of Foot Contact and Foot Off events is equal to 5 N, which has also been selected empirically. At this point, force signals can be segmented stride-by-stride. Despite force signals are available for the whole running duration, the window of interest is the one where the athlete runs across the volume of acquisition of the motion capture system.

As for the TSSR tests, force values relative to vertical (F_y) and antero-posterior (F_x) axes have been averaged over 5 steps, while for the START test each step has been treated separately. The ratio $\rho = \frac{F_x}{F_y}$ has also been calculated, which is an important mechanical parameter for the estimation of the stiffness of the prosthetic foot.

Figure 5.10 summarizes the steps in the analysis of forces coming from the wearable load cell.

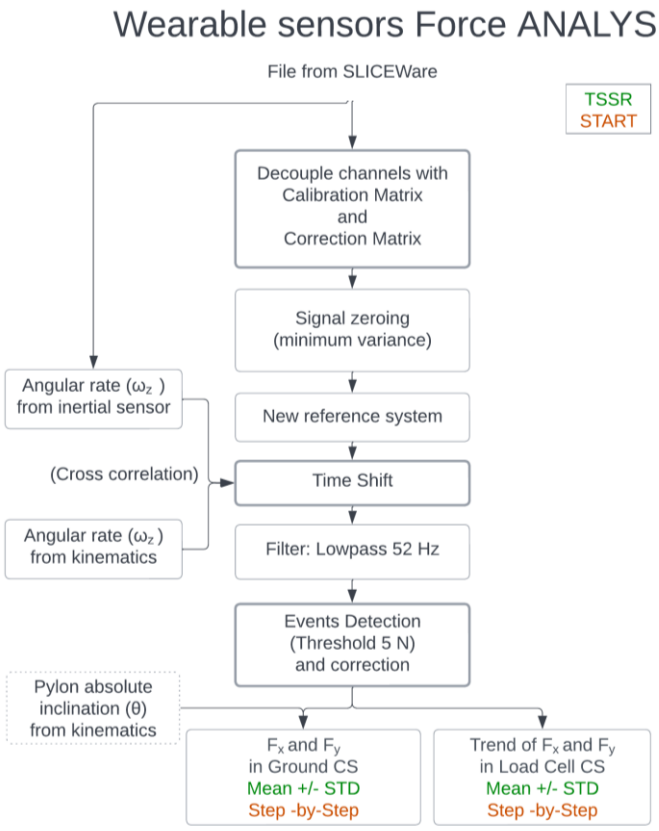

Figure 5.10. Workflow of analysis of Reaction Forces from load cell

Centre Of Pressure

This section describes the methods used to calculate the bidimensional trajectory of the COP, starting from the data relative to forces and moments.

For what concerns data coming from force plates (OS1 and OS2), the goal was to create a fifth "virtual" platform, which lies at the same height of the treadmill belt and covers the entire surface of the treadmill. The creation of this "virtual" platform, allows the visualization of the resultant GRF vector.

- First, the file relative to the dynamic trial is loaded in MATLAB using the *BTK* function `btkReadAcquisition`, which returns a handle to the file. Such handle is used as input for the other *BTK* functions, which return a structure containing data from the force platforms or a matrix having in each column the values corresponding to analog channels. Each platform has six analog channels, three for forces and three for torques. By plotting the signal of whatever channel, one can notice that the signal is quite noisy. To remove such noise, the power spectrum of the signal is computed and plotted to

visualize in which frequency range the main content of the signal concentrates. This way, a proper cut-off frequency to be used in the low-pass filter can be selected.

- Next step is the calculation of the resultant GRF by summation of the three components from each platform. The addition cannot be performed straightaway, because the reference systems of the platforms are not consistent among each other nor consistent with the global one. All platforms have the z-axis pointing downward, so the opposite of F_z has to be considered to obtain a vector pointing upward; platforms #1 and #4 have the transverse axis pointing leftward and the frontal axis pointing backward, while platforms #2 and #3 have these axes pointing rightward and forward. The force components of platforms #1 and #4 need to have their sign inverted to make all forces homogeneous. In the end, F_x and F_y components have to be swapped to be homogeneous with the global reference system used in Vicon (X= ML, Y = AP, Z = V).

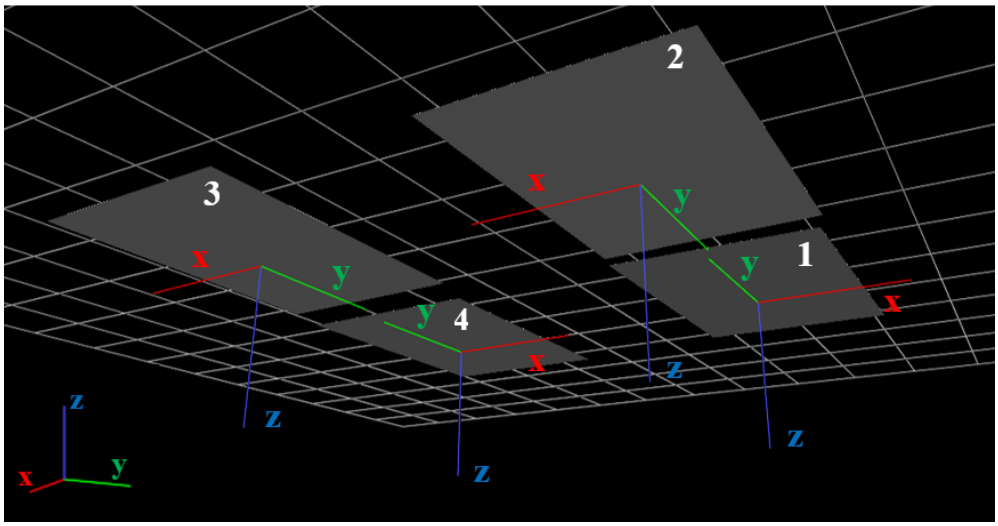

Figure 5.11. Force platforms (bottom view) in Vicon Nexus

The same adjustments are applied to torque components.

The sum of the modified forces, component by components, gives the total GRF.

- In order to define the position of the "virtual" platform, the coordinates of its corners and of its centre must be calculated. Each corner corresponds to an external corner of the four individual platforms and the centre is the mathematical average of the centres of the platforms. The figure below shows how platforms are located in the plane XY (Vicon global CS).

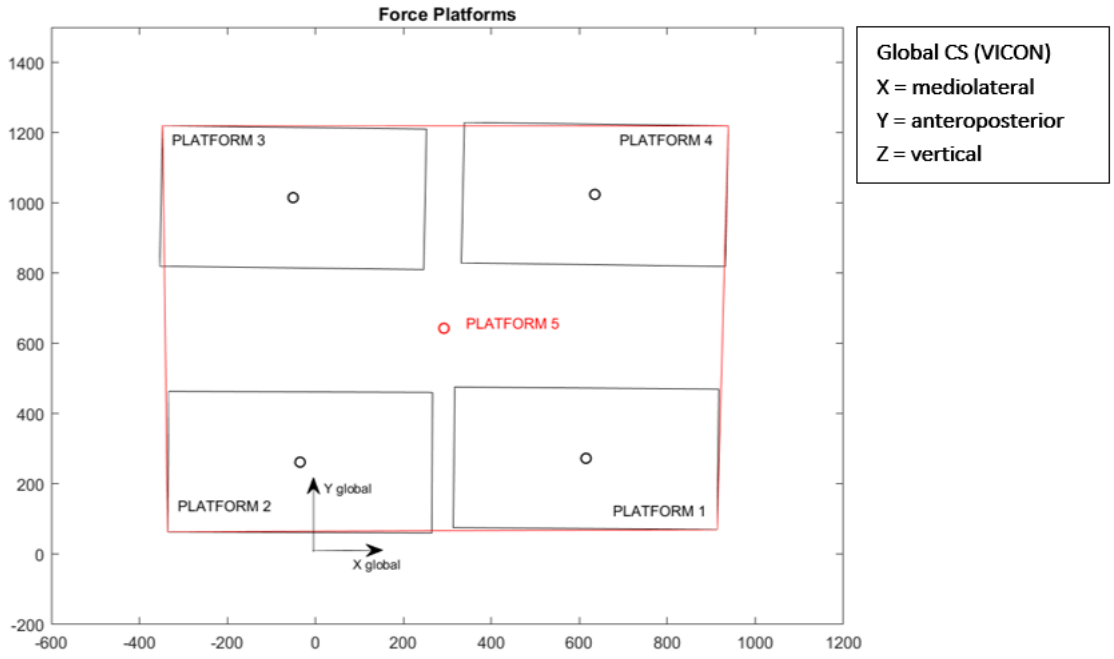

Figure 5.12. Force platforms transverse view

The total torque about x-axis has been calculated as the sum of two parts. The first part is the contribution of the four forces F_z, which have a moment arm equal to the distance along y-direction from the centre of the single platform to the centre of the "virtual" platform, which is about 375 mm; the second part is the contribution of F_y forces of each platform, which has a lever arm equal to the vertical distance between the centre of the "virtual platform" and the centre of each platform, which is about 348 mm. The total moment about y-axis is computed in the same way, but this time forces F_z have been multiplied by their lever arm along x-direction (about 335 mm) and the second contribution is given by F_x, multiplied by the moment arm along z-axis.

Once obtained total forces and moments the formula shown below can be applied.

$$COP_x = \frac{-M_{TOT,y}}{F_{TOT,z}} \qquad COP_y = \frac{M_{TOT,x}}{F_{TOT,z}}$$

The "virtual" platform is added to the *.c3d* file, which can be the visualized in software *Vicon Nexus* (Figure 5.13*)*.

To sum up, the mathematical process which has led to the trajectory of the Centre Of Pressure is just the linear combination of forces and moments contributions with respect to a reduction point located in the middle of the force platforms.

Figure 5.14 shows the flowchart with all the steps implemented for COP calculation.

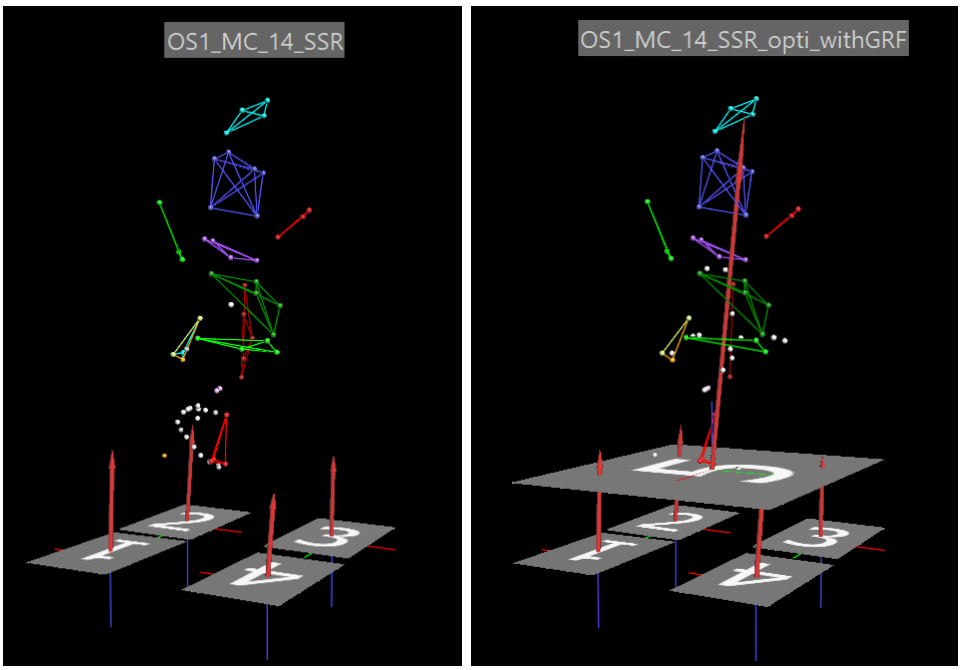

Figure 5.13.Visualization of "virtual" platform in Vicon Nexus

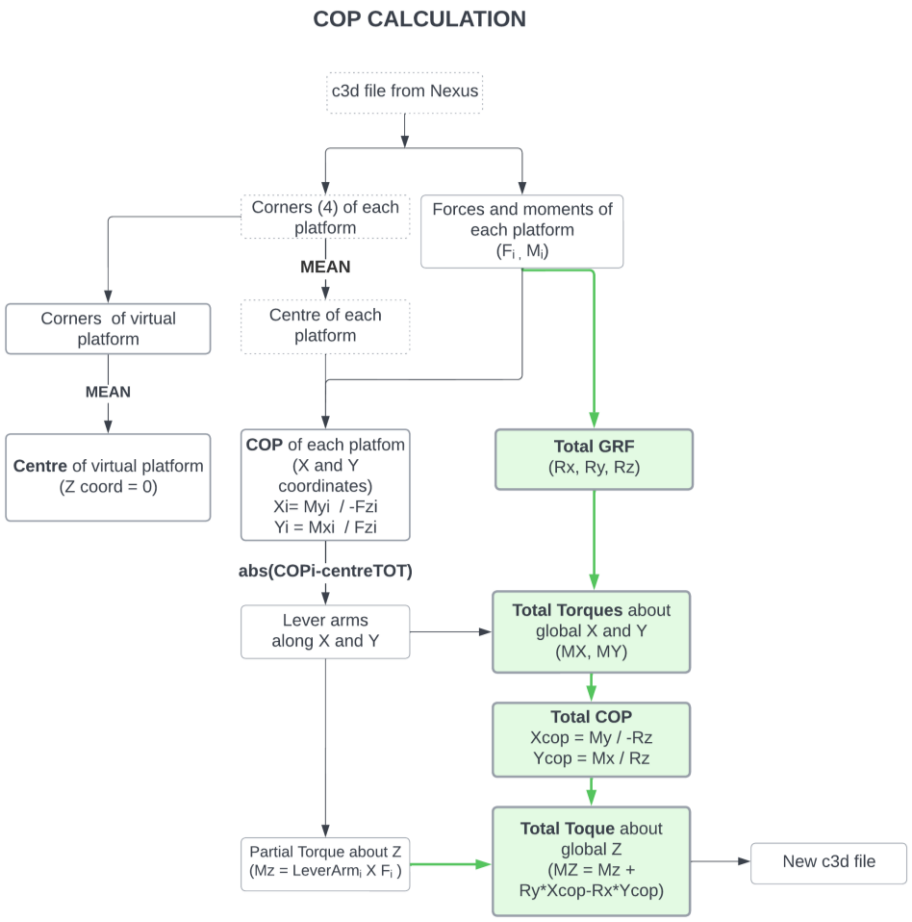

Figure 5.14. Workflow for COP calculation

Unfortunately, this procedure does not give the desired result. While in the central part of stance phase the trajectory of COP results very close to that of markers placed on the foot, at foot contact and foot off the estimated COP is far from the foot, so it cannot be considered correct. Errors may be due to residual noise in the force signals or mistakes in the calculation. Due to time lack, and due to difficulties in visualising the precise location of the COP in a *.c3d* file, this approach has not been further investigated.

Another possibility to get the COP trajectory could be using the software *BTS Smart Analyzer*, which allows to graphically create a computation scheme, called protocol, and apply them to force plates data force. The calculation performed by the software takes in input the three force components and the three moment components for each platform and gives in output the resultant GRF and the resultant moment of the four platforms. In addition, it calculates the position of the overall centre of pressure. However, this method presented some weak points.

- The format of the file to be loaded in the software cannot be a *.c3d* file. Therefore, the file containing the information about the three-dimensional trajectories of all markers could not be used. Moreover, *BTS Smart Analyzer* do not produce *.c3d* files, but only files in formats like *.tdf, .emt* and *.mdx,* which are not suitable to be loaded in *Nexus* to proceed with the labelling of the markers. Therefore, they need to be converted manually. Regarding *.tdf* format, these files can be opened with *BTS Smart Tracker* and export them as *c3d,* but some errors occurred during the export procedure and the system was unable to save the files or when it succeed in saving them, the resultant GRF was not visible or its application point remained fixed. Another option is to use the functions *btkReadAcquisition* or *btkTransformTDFToViconC3DFile* implemented in the *BTK* library, but in this way the resultant force was not present. As for the *.emt* files, they could be converted into text files with *.txt* extension, but the conversion required opening the file in a text editor and re-save it in the new format. In the end, the *.mdx* file could be converted into a *.mat* file through a custom function implemented in MATLAB, which basically extracts information from the first file and organizes them in a structure array.
- The time axis of the force data is not consistent with the time axis of the markers data. Besides the different acquisition frequency (1000 Hz vs 250 Hz), it happened that some samples in force, moments and therefore COP data were missing, but instead of replacing them with a NaN, they were simply skipped. Therefore, in a hypothetical trial of 5 seconds there could be less than 5000 samples in force data, while in markers data

there were exactly 1250. As a consequence, when trying to align the two series of data, after interpolation and downsampling, some shift errors occurred.

- The COP calculated by *BTS* resulted in a very noisy signal. Despite the attempts to apply filters and delete noise, the signal was still different from the trajectory of the markers placed on the feet of the subject, either the intact foot or the RSP, which are reasonably close to the real COP.

In the end, the trajectory of COP has not been determined with neither of the two explained methods. For the sound foot, it has been assumed that the Centre of Pressure corresponds to the projection on the ground of the marker placed on the second metatarsal head, while for the prosthetic foot it has been assumed that COP varies linearly from the midpoint of markers FD2-FD3 and the foot tip FD1.

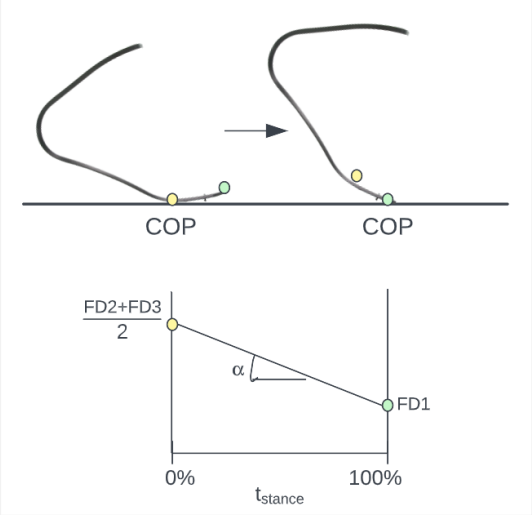

Figure 5.15. Schematic representation of COP displacement

For what concerns OS3, the identification of the coordinates of the COP from force and torque signals measured through the load cell has been implemented as follows.

Given the matrix describing the orientation of the load cell with respect to ground, forces can be projected from the local (load cell) reference system onto the global reference system. Next, given the coordinates of the origin of the local CS (OL) and thus the vertical distance of the load cell from the ground (y_{OL}), and given the torque about z, M_z measured by the load cell, the relative horizontal distance between the load cell and the point of application of the force ($\overline{OL_x - OG_x}$) can be easily calculated.

$$M_{z_L} = GRF_y * (\overline{OL_x - OG_x}) + GRF_x * y_{OL}$$

(5.7)

The absolute x-coordinate of the COP can be then obtained by subtracting the just computed relative horizontal distance to the absolute horizontal distance of the origin OL.

$$x_{COP} = x_{OL} - (\overline{OL_x - OG_x})$$

(5.8)

The y-coordinate of the COP is zero and the z-coordinate has not been estimated yet. Due to the fact that in the inverse dynamics the three dimensional trajectory of the COP is required, also for OS3 the COP is calculated from the markers.

Roll Over Shape

The calculation of the Centre Of Pressure is the preliminary step necessary to compute the Roll Over Shape (ROS), which is a biomechanical parameter useful to study the physiological behaviour of the ankle-foot complex and to compare different prosthetic feet.

ROS is the projection of the COP onto a reference system consistent with the lower limb, that corresponds to the estimation of the instant rotation centre in a proximal reference system. It describes the rolling of the ankle-foot complex on the ground. It can be characterized in terms of length and radius of curvature, which can then be correlated with the metabolic consumption, which is in turn estimated as the external work of GRF on the centre of mass, according to the Step-to-Step transition model. The power relative to this work is calculated as the product of the GRF and the velocity of COM. The calculation and discussion of metabolic consumption will not be addressed in this work.

For the sound limb, three different specific reference systems can be defined for the ROS calculation: Foot (F); Ankle-Foot (AF) and Knee-Ankle-Foot (KAF). The system chosen in the present work is AF and it is built as follows:

- centre (O) is the midpoint between lateral and medial malleoli (AJC);
- longitudinal axis (y) connects O to the midpoint between lateral and medial femoral epicondyles;
- temporary axis ($temp$) joins the centre to the lateral malleolus;
- sagittal axis (x) is obtained as cross product of y and $temp$ so that it points forward;
- frontal axis (z) is obtained as cross product of x and y

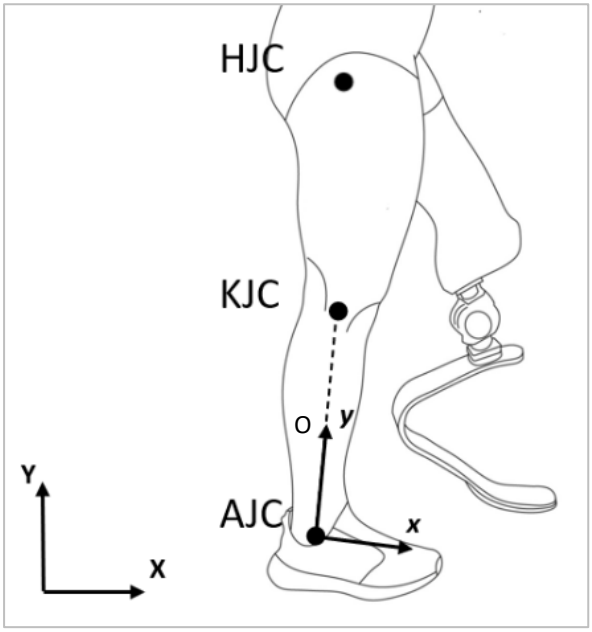

Figure 5.16. Coordinate systems defining Ankle-Foot roll-over shape (AFROS) for right side

For the prosthetic limb, a custom reference system has been defined:

- centre (O) is the midpoint between lateral and medial clamp markers;
- longitudinal axis (y) connects O to the midpoint between lateral and medial prosthetic knee markers;
- temporary axis ($temp$) joins the centre to the lateral clamp marker;
- sagittal axis (x) is obtained as cross product of y and $temp$ so that it points forward;
- frontal axis (z) is obtained as cross product of x and y

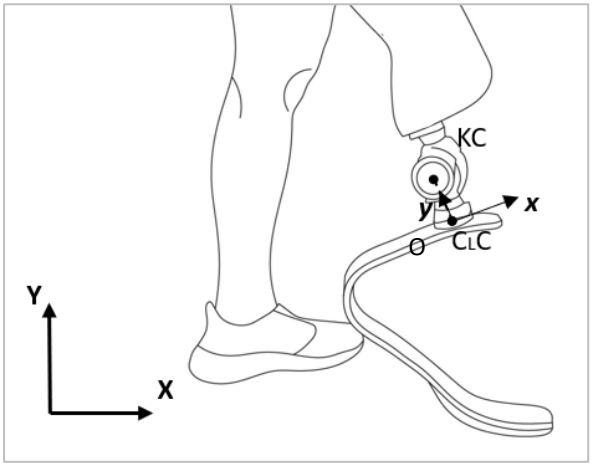

Figure 5.17. Coordinate systems defining Ankle-Foot roll-over shape (AFROS) for right side

Either in the case of three-dimensional ROS 'AFROS 3D' or bi-dimensional ROS 'AFROS 2D', the projection of the COP from the global onto the local coordinate system is obtained

through the multiplication of the matrix describing the pose of the local CS with respect to the global (frame-by-frame) and the position vector describing the trajectory of the COP (frame-by-frame) in the global CS. In the case of 'AFROS 2D' the rotation matrix is sized 2 x 2, so the pose matrix is 3 x 3, while for 'AFROS 3D' rotation matrix is 3 x 3 and pose matrix is 4 x 4.

$$ROS = {}^{loc}COP = {}^{loc}T_{glo} * {}^{glo}COP \quad (5.9)$$

In order to make the computation faster, it is usually computed the three-dimensional ROS and then only the coordinates on the sagittal plane (x and y) are represented.

ROS trajectory is then used to calculate the power produced by the ankle, either in the right limb or in the left limb, where the ankle is substituted by the clamp of the RPF.
Power is obtained as scalar product of the velocity of ROS and the GRF expressed in the local AFROS reference system.

$$Power = {}^{loc}GRF \cdot v_{ROS} \quad (5.10)$$

Velocity of ROS is calculated as first derivative of the bidimensional trajectory and local GRF is obtained by pre-multiplication of GRF three-dimensional components by the rotation matrix describing the AFROS reference system and then considering only the x and y components.

Kinetic analysis implementation

As described in Chapter 1, there are two possible approaches to obtain joint forces and joint moments, which are the inverse dynamics method and the simplified method. In this section the implantation of both methods is explained, starting from the inverse dynamics method.

Anthropometric parameters like body mass (BM), height (H), and sex must be entered (hard coded) and saved in a MATLAB structure. The side of the body (left/right) for which the computation of dynamic analysis has to be executed must also be provided. In both athletes, AS and MC, the left leg is the prosthetic one.

The *.c3d* file relative to a static acquisition has to be loaded and the markers trajectories are extracted. Then, the custom function `inertialParam` calculates the inertial properties of body segments. In detail, the function preliminarily converts the markers coordinates from millimetres to meters, and swaps their order, so that the order of the columns of the matrix containing marker trajectories corresponds to the x, y, and z coordinates respectively, which in

turn correspond to the antero-posterior, vertical and medio-lateral direction. Afterwards, it calculates the mass of thigh, shank and foot segments as percentage of the total body mass. Length of the body segment is obtained as the distance between proximal and distal joint centres. Given the segment length, the location of the Centre of Mass (COM) of that segment is obtained as percentage of its length and is intended to be measured along the vector joining the proximal to the distal joint. The following step is the calculation of the radius of gyration, which is also obtained as percentage of body segment length, but in this case three different percentages are used for the three components x – y – z of the radius. The square of each radius component multiplied by the segment mass gives the moments of inertia relative to the principal axes. Such components, usually called Ixx, Iyy and Izz are saved as diagonal elements of a 3 x 3 matrix. All coefficients employed to calculate mass, COM location and radius of gyration are different depending on whether the subject is male or female and the function implements both cases. The final output of the function is a structure containing all just calculated inertial parameters.

Back to the main script, markers trajectories from the dynamic trial are loaded, converted from millimetres to metres and the order of the coordinates swapped. In order to reduce noise in the signals of the trajectories, they are filtered using a low-bass Butterworth filter with 10 Hz cut-off frequency.

Next, the MATLAB structure containing the outputs from kinematic analysis (poses of body segments, joint angles, joint angular velocities and forces) is loaded. From the structure, the total force from the force platforms is extracted and downsampled from 1000 Hz to 250 Hz, while the force from the load cell is already downsampled. The origin of each local CS is moved to the centre of mass of the segment, obtained using the coefficients saved in `inertialParam`.

When using the data from force platforms, since they contain information for both right and left leg, they have to be adjusted so that the vector GRF is zero when the selected limb is in swing phase. In order to do this, a logical vector containing ‘1’ in the positions corresponding to the frames of stance and ‘0’ or otherwise. The boolean vector is then also used to multiply the trajectory of the of the centre of pressure. In the end, the vector `g` containing the components of gravitational acceleration is defined.

At this point, one can proceed with the calculation of joint forces and moments. In order to implement the inverse dynamics approach, the custom function `DistDynCalc` has been developed. For each joint, in the order ankle, knee and hip, the function is given the following inputs:

- force and the moment applied at the distal end of the body segment, foot, shank and thigh respectively;
- rototranslation matrix of the segment;
- mass of the segment;
- tensor of the moments of inertia of the segment;
- point of application of the distal force, that is the distal joint centre or the COP;
- point of application of the proximal force, that is the proximal joint centre;
- reduction point for the calculation of torques;
- vector of gravitational acceleration;
- acquisition frequency of the stereophotogrammetry data.

The core of the function `DistDynCalc` consists in solving the equilibrium equation of forces and moments.

$$\sum \overrightarrow{F_d} + \overrightarrow{F_p} + m * \vec{g} = m * \overrightarrow{a_{com}} \quad (5.11)$$

$$\sum \left(\overrightarrow{b_d^{LOC}} \times \overrightarrow{F_d^{LOC}}\right) + \left(\overrightarrow{b_p^{LOC}} \times \overrightarrow{F_p^{LOC}}\right) + \overrightarrow{M_d} + \overrightarrow{M_p} = (I_{com}) * \overrightarrow{\alpha^{LOC}} + (\overrightarrow{\omega^{LOC}} \times \left(I_{com} * \overrightarrow{\omega^{LOC}}\right) \quad (5.12)$$

The proximal joint force $\overrightarrow{F_p}$ is the force exerted by the proximal segment on the distal one and it is calculated by solving the equation (5.11), where the linear acceleration $\overrightarrow{a_{com}}$ is the second derivative of the position of the COM obtained with the custom function `signalDerivative2`. It is expressed in the global CS.

The proximal joint moment $\overrightarrow{M_p}$ is the moment that the proximal segment exerts on the distal one. In the case of the foot, it is the moment at the ankle that the shank exerts on the foot; in the case of the shank, it is the moment exerted at the knee by the thigh and for the thigh it is the moment exerted at the hip by the pelvis.
It is calculated from the equation (5.12) and is expressed in the local CS of the distal segment to be homogenous with the Moment of Inertia, which must be expressed in the local CS to be time and space invariant. All the terms involved in the calculation must also be expressed in the same cs, therefore forces $\left(\overrightarrow{F_d}, \overrightarrow{F_p}\right)$, lever arms $(\vec{b}_d, \vec{b}_p)$ and distal moment $(\overrightarrow{M_d})$ have to be projected onto the local reference system.
Angular velocity $\overrightarrow{\omega^{LOC}}$ and acceleration $\overrightarrow{\alpha^{LOC}}$ of the target need to be calculated.

- Angular velocity is obtained from the orientation matrix of the segment. Each component of the orientation matrix is derived (first derivative) and assigned to a new

3 x 3 matrix, $\dot{R}$. This matrix is then pre-multiplied by the transpose of the original orientation matrix R^T . Such product gives an antisymmetric matrix, $S(\omega) = R^T\dot{R}$, from which the three components of angular velocity $\omega_x, \omega_y, \omega_z$ are extracted. They are already expressed in the local CS.

- Angular acceleration is the first derivative of the angular velocity, calculated with `signalDerivative2`.

The computation of forces and moments is iterated for the three joints, starting from ankle, then knee and eventually hip. Forces and moments obtained from the linear equation are expressed in the local coordinate system of the distal segment, therefore, prior to give them in input to the function `DistDynCalc` which calculates the reactions in the more proximal segment, they must be referred to the global CS and their sign must be inverted.

The second possible approach to compute the kinetic analysis is the simplified method, which consists in calculating, for each joint, the moment arm from the joint centre to the point of application of the Ground Reaction Force. Three lever arms are calculated for the unaffected limb, while for the affected limb only the lever arms relative to hip and knee. Moments are then calculated as the cross product of the lever arm and the GRF vector. Such moments are external, because they represent the effect of the external force GRF on the joints, but since the interest is on the internal moments, their opposite has to be computed.

All moments obtained up to this point are referred to global reference system. However, to give them a physiological meaning, they have to be projected onto a local coordinate system, close to the joint they refer to.
In literature there is little agreement on the reference system to be used to represent joint moments (and powers).
One possible solution is to define a new coordinate system for each body joint (JCS), according to the method by Grood and Suntay [52], which was originally proposed for the knee joint only, but here extended to all joints. It consists in the definition of a coordinate system composed of three axes. Two axes are embedded with the segments whose relative motion is to be described, they are called 'body fixed' axes and have unit base vectors `e1` and `e3`, which are not mutually orthogonal. The third axis is the common perpendicular axis to both 'body fixed' axes. It is also called 'floating' axis and it has unit base vector `e2`.
For each JCS, the mediolateral axis, called `e1`, corresponds to the z-axis of the proximal segment, pointing rightward, the vertical axis, called `e3`, is the y-axis of the distal segment and it points upward, and the anteroposterior axis, called `e2`, is obtained as cross product of `e3` and

`e1`, so that it points forward. For what concerns the ankle, some adjustments are required. JCS are represented in Figure 5.18.

The three vectors are arranged row-wise in a matrix, which is then multiplied by the Moment vector of each joint. This way, the projection of the moment onto the three non-orthogonal axes `e1, e2, e3` is easily obtained. The new local moment vector will have the flexor/extensor moment (or dorsiflexor/plantarflexor for the ankle) as first component, the adductor/abductor moment (or invertor/evertor) as second component and the intra-rotator/extra-rotator moment as third component.

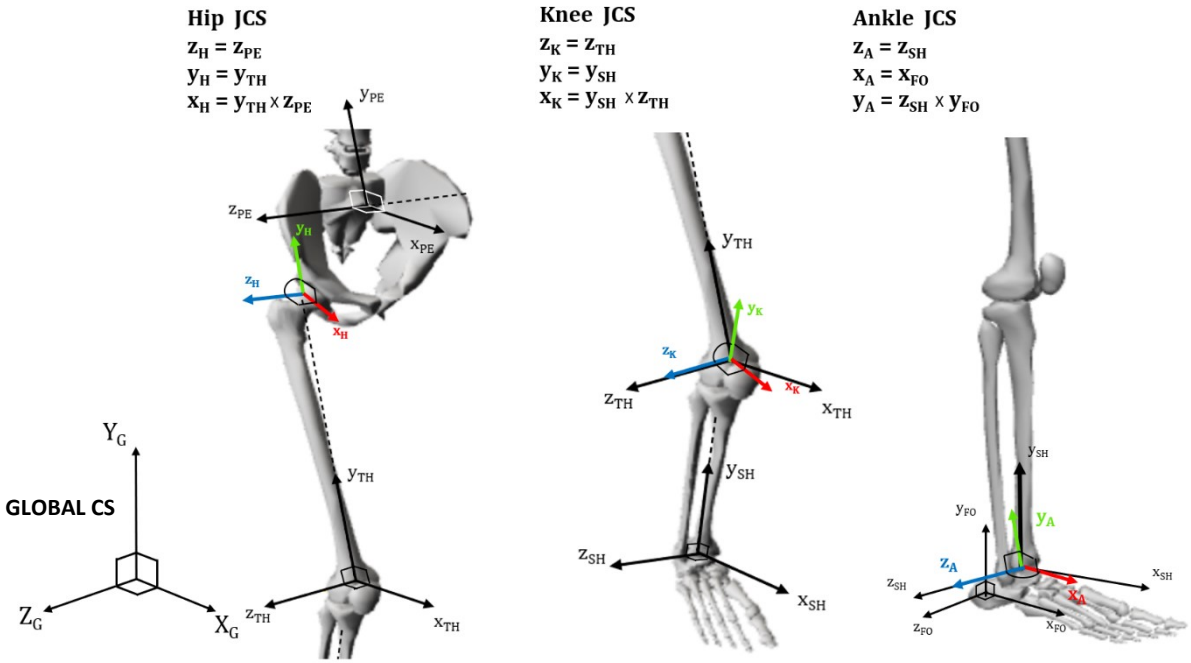

Figure 5.18. Joint Coordinate Systems for right limb

Looking at the sagittal plane, internal moments are considered positive if they act against gravity, that is if they act to extend the joint. Consequently, if a sagittal view from the right is adopted, hip and ankle torque have to be considered positive if they are clockwise about the z-axis looking from the positive direction, while knee torques are considered positive if they act counterclockwise. This notation is consistent with the one adopted by Novacheck [5] .

Torque calculation gives the correct sign only in the case of the knee, whereas for hip and ankle a swap is needed. For what concerns the frontal and the transverse plane, it has been decided to consider positive the clockwise moments, therefore signs are inverted for all joint torques.

The sign conventions chosen for the interpretation of joint moments are presented in Table 5.3

Table 5.3. Joint Moments sign conventions

HIP / KNEE	Extensor (+)	Flexor (-)
	Abductor (+)	Adductor (-)
	External rotator (+)	Internal rotator (-)
ANKLE	Plantarflexor (+)	Dorsiflexor (-)
	External rotator (+)	Internal rotator (-)
	Evertor (+)	Invertor (-)

The last step required to complete the kinetic analysis is the computation of power, which expresses whether the muscles crossing the joint are doing a concentric or an eccentric work. In the former case, power is generated, while in the latter case power is absorbed.
Power (P) is obtained as the scalar product of joint moment (M_{joint}) and joint angular velocity ($\dot{\varphi}_{joint}$), which can be extracted from the structure containing the output of kinematic analysis.

$$P_{joint} = (-)M_{joint} * \dot{\varphi}_{joint}$$

(5.13)

Due to the sign conventions adopted for joint moments, the calculation of joint power requires the inversion of the sign of the moment. In this way, power is positive when moment and angular velocity describe the same movement, e.g. flexor moment and flexion angle, whereas it is negative when they describe opposite movements, e.g. flexor moment and extension angle.

For the calculation of power, joint moments and joint angles should be expressed in the same reference system. In particular, if joint moments are referred to the JCS, joint angles should be calculated from the same JCS rotation matrix through Euler or Cardan inverse formulas. Due to time lack, this step has to be implemented yet. Therefore, to be consistent with the reference system in which joint angles and joint angular velocities are calculated, joint moments have been projected from global CS to local CS of the proximal segment. For what concerns the z-axis it is completely equivalent to the projection of the moment onto z-axis of the Joint Coordinate System, while for the other axes there are small differences, but they do not affect the result much.

A schematic representation of the kinetic analysis pipeline is given in the Figure 5.19.

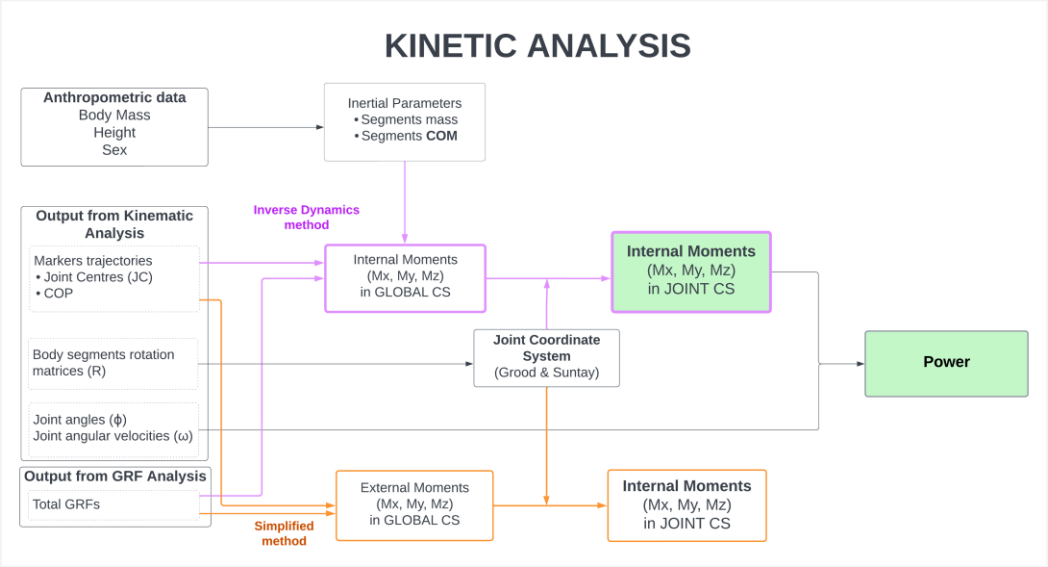

Figure 5.19. Workflow of kinetic analysis

Starting from left, the elements required for the kinetic analysis are enclosed in the black boxes. They are the anthropometric data (hardcoded or manually inserted), results coming from the kinematic analysis (joint centres and COP location, orientation matrices of the body segments, joint angles and joint angular velocities) and results from the GRF analysis (filtered and summed/projected GRF).

The purple path describes the inverse dynamics method, which needs the anthropometric data to get the inertial parameters, the three-dimensional coordinates of the joint centres and the GRFs. Internal joints moments are calculated at first in the local CS of the distal segment and then projected into the global CS.

The orange path depicts the simplified method, for which only three-dimensional coordinates of joint centres and GRFs are necessary. External joint moments in the global CS are computed and then transformed into internal moments.

Thanks to the joint orientation matrices obtained from the body segments matrices, internal joint moments are projected onto the JCS (up to now, moments are projected onto the local CS of the proximal segment and not onto the JCS).

In the end, joint moments and joint angular velocities are scalarly multiplied to obtain joint power.

Chapter 6

Results

The Biomechanical Analysis tool has been used to process the data acquired during the three Olimpia sessions. In particular, four tests relative to OS1, six tests relative to OS2 and three tests relative to OS3 have been analysed so far. In the results, the following abbreviation will be used: OS#_<SBJ>#_<test type> (A#). For example, OS1_MC_14_SSR (A2) stands for 'Olimpia session 1, Martina Caironi, Steady State Running, Alignment 2'.

Kinematic analysis results

For what concerns the kinematic analysis, the main outputs are the three-dimensional joint angles, calculated with the inverse Cardan formulas. They are represented according to the sequence chosen for their calculation, that is $Z - x' - y''$, so the first column in the following figures is relative to flexion/extension angle, the second column to the adduction/abduction angle and the third to the intra/extra rotation. Regarding ankle joint, the sequence adopted for the calculation of angles was $Z - y' - x''$, so the order of display is different from the other joints.

Thanks to the great repeatability of curves during SSR tests, as can be noted in the figure below relative to hip flexion/extension angle, it was possible to calculate the average of the biomechanical variables across strides.

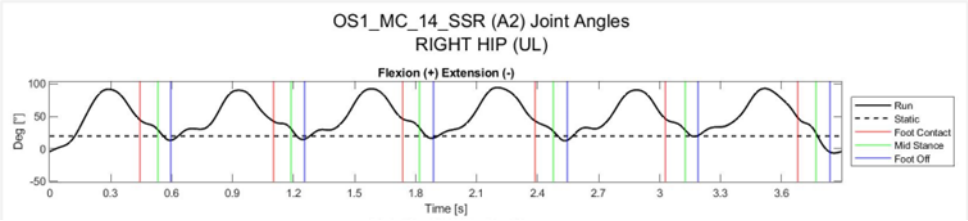

Figure 6.1.Right hip angles in the sagittal planes in SSR test for athlete MC

Figure 6.2 to 6.7 show the joint angles and joint angular velocity calculated for one SSR test of the athlete Martina Caironi wearing the prosthesis with the alignment A2.

The black dashed line represents the mean value of the same angle calculated in the static trial. This information is useful to better understand the oscillations in dynamics.

Vertical green and blue lines correspond to Mid Stance and Foot Off events respectively, while Foot Strike is not represented because it corresponds to the 0% of stride. The second row displays angular velocities. They are obtained as first derivative of corresponding joint angle.

Hip Angles

As expected, the greatest range of motion takes place in the sagittal plane, while in the other planes there are only small vibrations. During stance phase, right hip (Figure 6.2) extends and reaches its maximum extension at the toe off, but it remains about 10°-13° flexed. During initial and mid swing, right hip flexes up to 90° and then starts extending in the terminal part of swing, to prevent excessive deceleration at initial contact. Considering the static hip angle in the sagittal plane, which is nearly 20°, the position of the hip at toe off can be considered extended. The hip angle in static is far from zero because the coordinate system of the pelvis is titled anteriorly, since markers on posterior iliac spines have been positioned about 10 cm higher than the level of markers on the anterior iliac spines.

Angular velocity along z-axis is negative in stance because angle is decreasing to extension and crosses the zero when joint angle reaches its minimum. Angular velocities along x- and y- axes are close to zero, because the respective angles do not show significant oscillations.

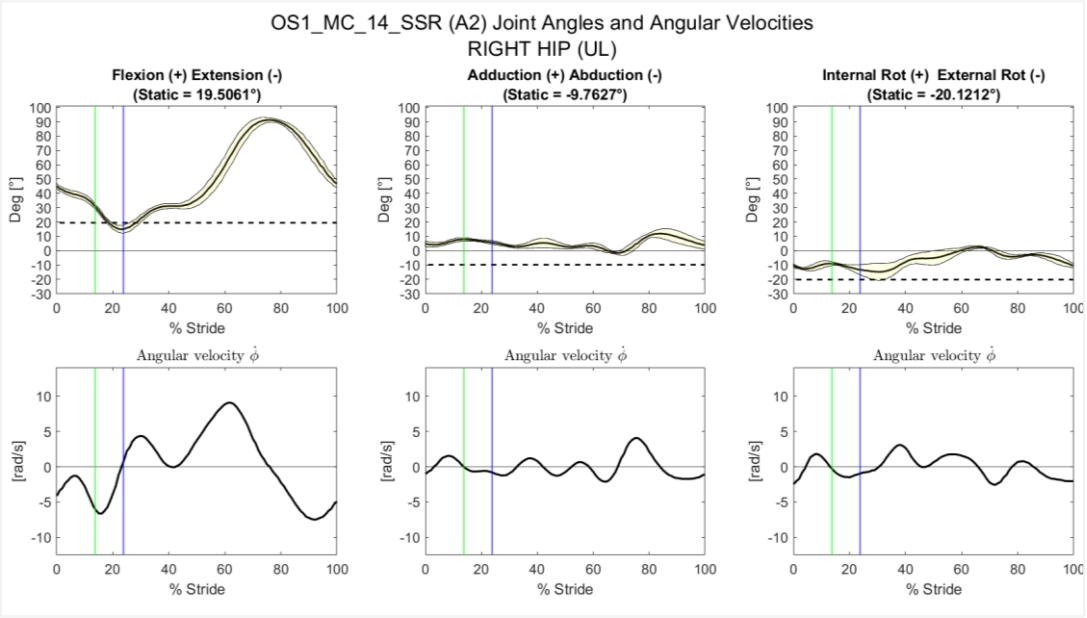

Figure 6.2. Right hip angles and angular velocities in the three planes during a SSR test. Black solid line: average trend over 6 steps; yellow band: 1 SD range; green vertical line: midstance; blue vertical line: foot off.

The behaviour of left hip (Figure 6.3) is similar to right hip in terms of range of motion, but the maximum flexion angle is higher than right hip, exceeding 95°, and the minimum hip flexion angle - at toe off - is 20°. In this case, the static angle is nearly 50°, possibly due to the posture of the athlete during the static acquisition, in addition to the incorrect positioning of the markers mentioned above. Given that the prosthetic leg is longer than the sound one, the athlete moved the prosthetic foot further forward than the healthy foot, resulting in a greater angle between pelvis and socket than between pelvis and right thigh.

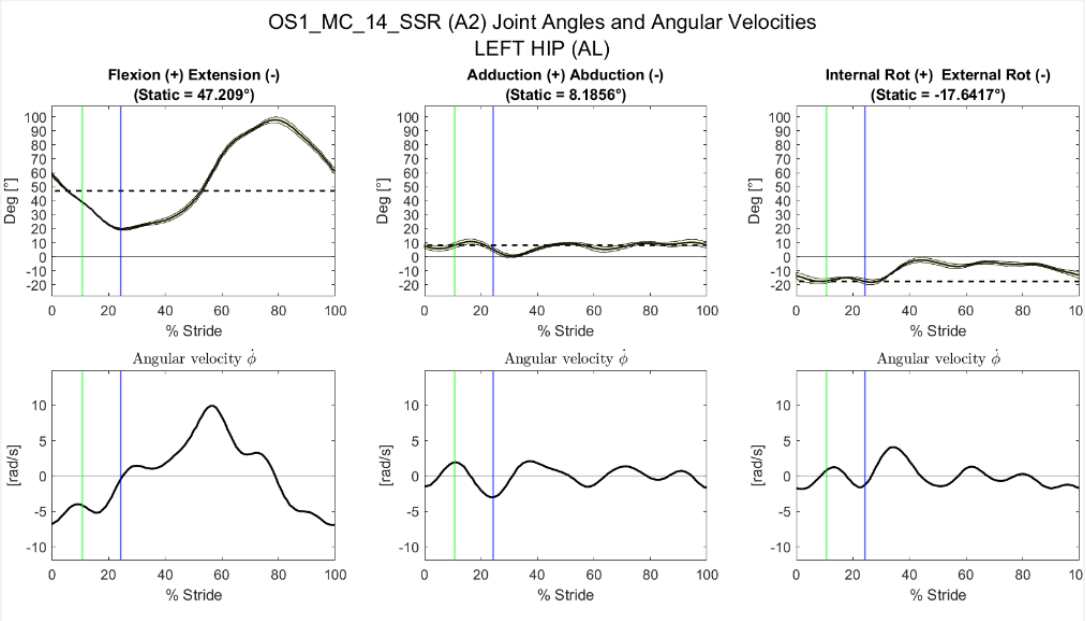

Figure 6.3. Left hip angles and angular velocities in the three planes during a SSR test. Black solid line: average trend over 6 steps; yellow band: 1 SD range; green vertical line: midstance; blue vertical line: foot off.

Knee Angles

Knee has been analysed as a 3-degree-of-freedom joint, although its main degree of motion is in the sagittal plane.

Healthy knee shows two periods of flexion, one during support and the other one during swing. In stance phase, knee first flexes to approximately 30° and then extends to 20°- 25°during the propulsion period of stance. During swing phase, flexion is maximum, with peak values reaching 150°.

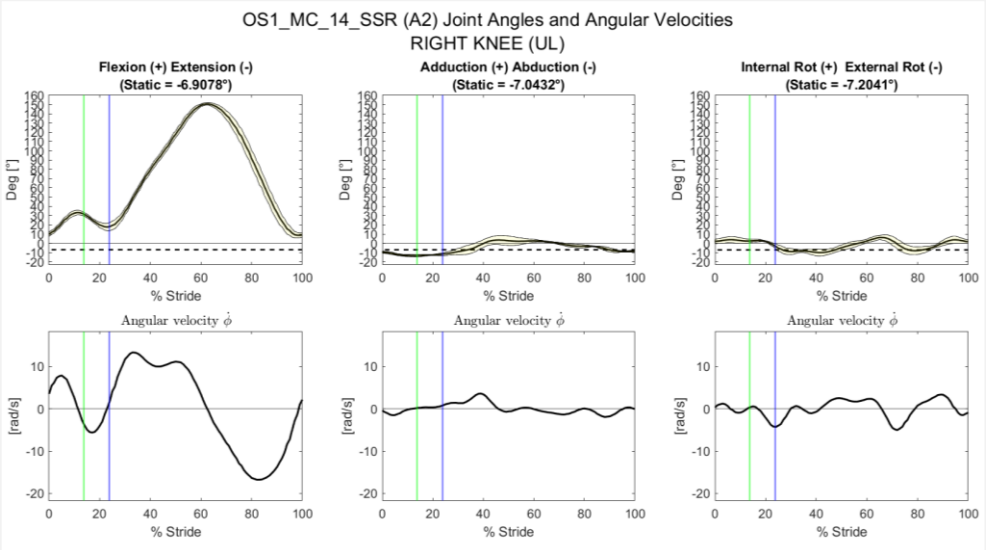

Figure 6.4. Right knee angles and angular velocities in the three planes during a SSR test. Black solid line: average trend over 6 steps; yellow band: 1 SD range; green vertical line: midstance; blue vertical line: foot off.

Prosthetic knee behaves differently. During stance it is completely extended (flexion angle is equal to 0°), except for some oscillation due to noise in the signal. This happens because prosthetic knees are designed so that, when weight is placed on the prosthesis, they do not bend until the weight is released. At toe off, knee starts flexing and reaches a maximum of 80° flexion, then it extends and in the terminal part of the swing it is already completely extended, so it is prepared for the next foot contact.

Since the prosthetic knee is monocentric and has a single axis of rotation, the only possible motion is around the z-axis. In fact, angles measured in the non-sagittal planes are always zero, and so the angular velocity. This result is useful to assess the accuracy of the Motion Capture system and computational procedure.

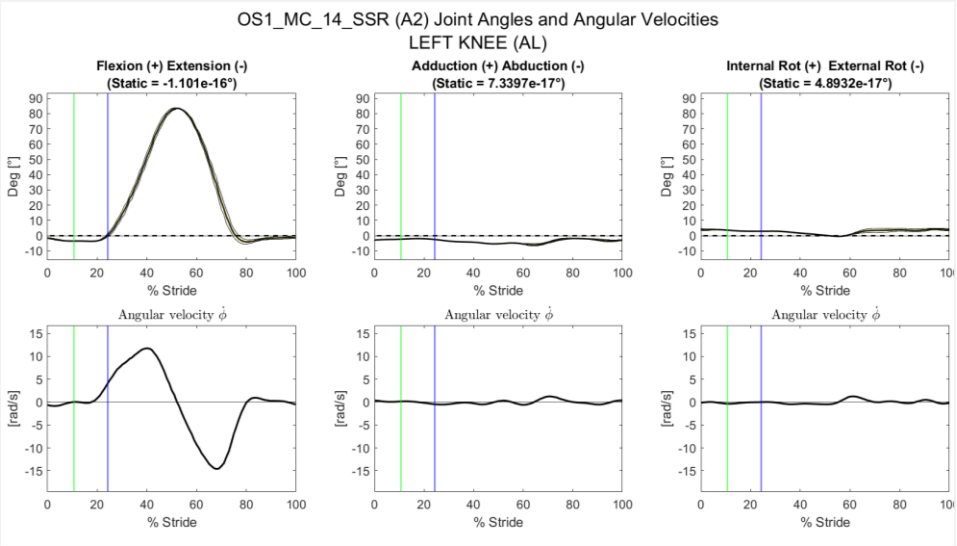

Figure 6.5. Left knee angles and angular velocities in the three planes during a SSR test. Black solid line: average trend over 6 steps; yellow band: 1 SD range; green vertical line: midstance; blue vertical line: foot off.

Ankle Angles

Ankle joint has been analysed only for the unaffected limb, since in the prosthetic limb the relative movement between mechanical components is not comparable to that of a biological ankle. As the subject is a forefoot striker, her ankle begins to dorsiflex as soon as initial contact occurs and does not make the rapid plantarflexion movement typical of rearfoot runners. Ankle continues to dorsiflex until about 10° in midstance, when the weight of the body is completely transferred to the leg in stance. Then the propulsion phase begins and ankle plantarflexes, reaching maximum extension just after toe off, which is about -50°. During the swing phase, plantarflexion reduces, first slowly and then rapidly, and eventually ankle extends again to -30° prior to next foot contact.

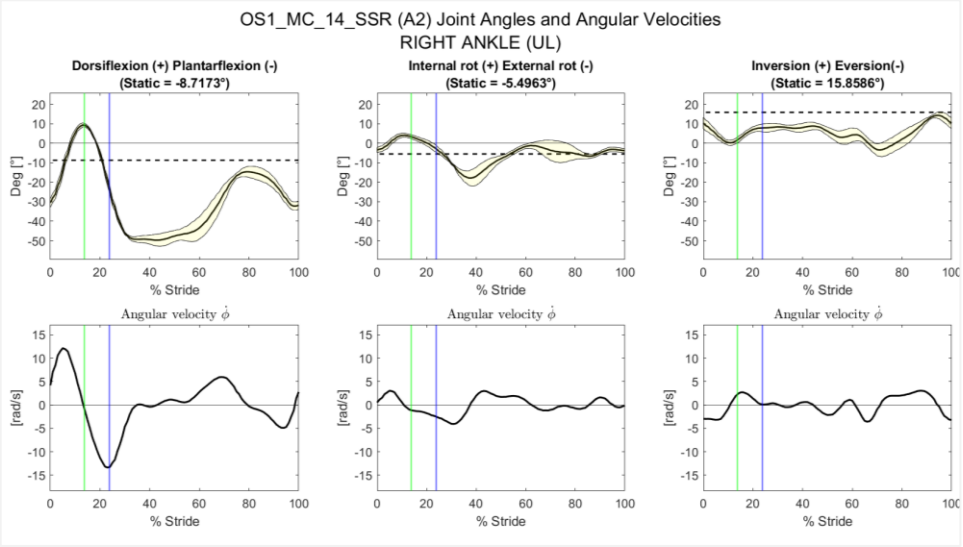

Figure 6.6. Right ankle angles and angular velocities in the three planes during a SSR test. Black solid line: average trend over 6 steps; yellow band: 1 SD range; green vertical line: midstance; blue vertical line: foot off.

Pelvic orientation

Pelvic orientation has been calculated with the Cardan inverse formulas using the pelvis as proximal segment and the ground as distal segment. In the graphic, only the events relative to right gait cycle are represented.

Oscillations of the pelvis in the three planes are relatively small with respect to the angles measured in static. Moreover, unlike other segments, pelvic motion is minimised in sprinting, thus saving energy.

The first column, tilt, is the rotation around z-axis, second column, obliquity, is the rotation about x-axis and third column is the rotation about y-axis. Sign conventions are the same adopted by Mandalidis et. al [50]

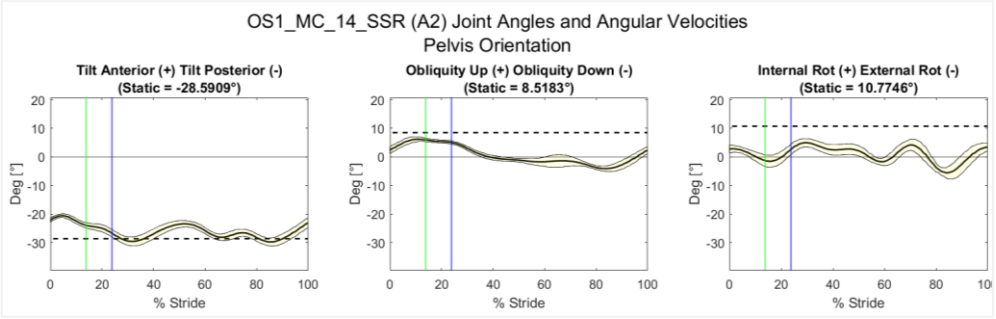

Figure 6.7. Pelvic orientation angles in the three planes during a SSR test. Black solid line: average trend over 6 steps; yellow band: 1 SD range; green vertical line: midstance; blue vertical line: foot off.

GRF analysis results

One of the outputs of the analysis of Ground Reaction Forces from steady state running tests is the average ($\pm$ SD) of the vertical and anteroposterior components of the GRF over six steps. For the tests carried out in the laboratory, results are available for both legs, while for tests carried out on track results are available for the prosthetic limb only.

Figure 6.8, relative to a treadmill test, shows the vertical force in blue and horizontal force is represented in red. For both left (AL) and right (UL) leg, the vertical GRF lacks the initial posterior impact peak and shows only the propulsive peak, which reaches about 2.7 BW and 3.5 BW for the two limbs respectively.
The AP force shows an initial braking phase, with minimum values equal to -0.3 BW (AL) and -0.5 BW (UL), and a second propulsive phase, when anteroposterior GRF turns positive up to 0.5 BW for both limbs.

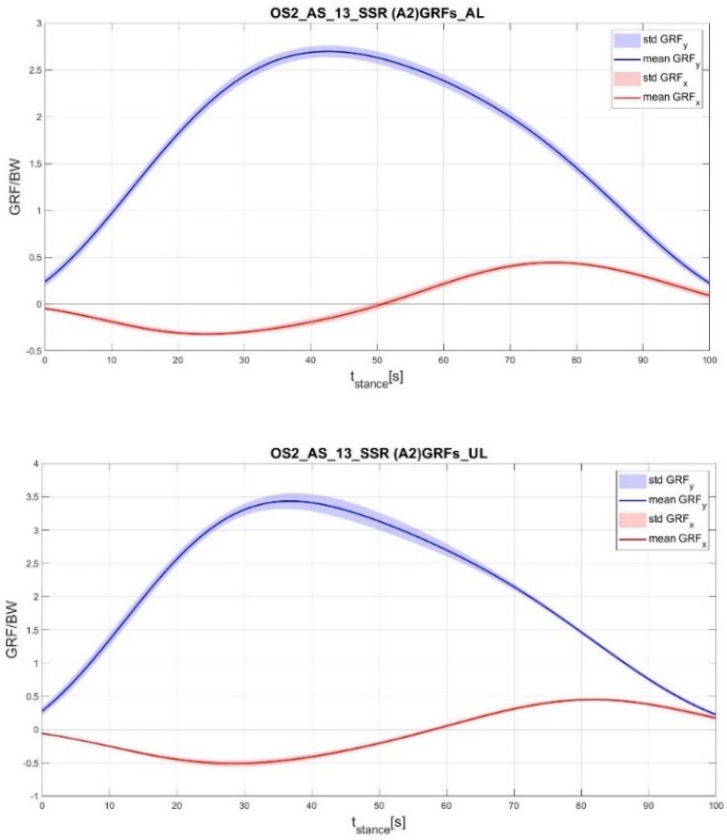

Figure 6.8. Vertical (blue) and Anteroposterior (red) average GRF (ground CS) over 6 steps in SSR test. Affected (top) and unaffected (bottom)

In addition to vertical and horizontal forces, for the prosthetic foot the ratio $\rho_L = Fx_L/Fy_L$ has been calculated for each step and represented together with the force components (Fx_L, Fy_L) and the inclination of the pylon with respect to the global vertical axis. Such angle has been

called ‘Theta Shank’ (θ_s), in analogy to the healthy limb. These parameters are crucial for reproducing the running movement in the test bench.

Figure 6.9 shows the forces measured by the wearable loadcell and expressed in the reference system of the load cell, so they are indicated with the subscript ‘L’.

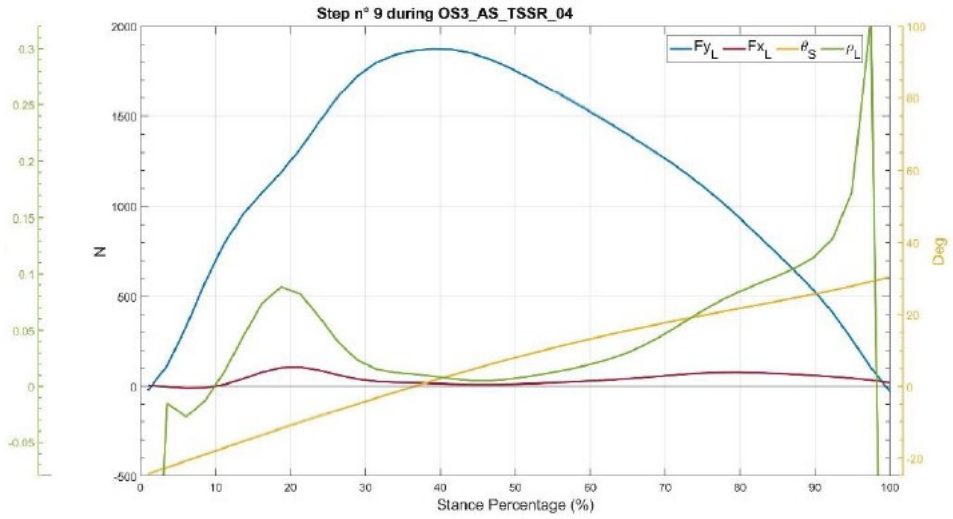

Figure 6.9. Vertical and Anteroposterior Reaction Forces (load cell CS), ρ_L and Theta Shank for a single step in TSSR test.

Figure 6.10, concerning impulses, shows that the vertical impulse is greater in the right limb (UL), but the horizontal impulse is greater in the left limb (AL) and the net horizontal impulse is positive for this limb and negative for the other limb, denoting the reduced braking effect of the affected limb if compared to the sound limb. Impulses shown in the chart are the averages of the individual impulses over six steps for each limb.

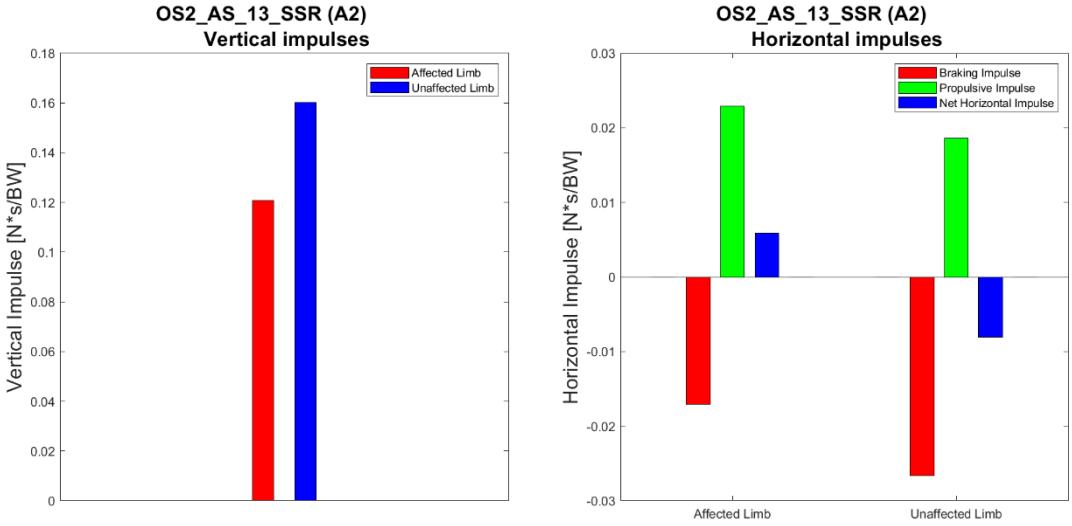

Figure 6.10. Vertical (left) and horizontal (right) impulses of GRF in treadmill SSR test

The force measured by the uniaxial load cell, anchored through an elastic rope to the subject's waist during RAR tests, has been represented together with the horizontal (AP) GRF and the speed of running, so it is possible to observe that as the athlete accelerates, so the force measured by both cell and force platforms increases.

In the figure, GRF relative to affected and unaffected limb are shown using two different colours, red and blue respectively, the black line represents speed and the green line represents the force from the uniaxial load cell.

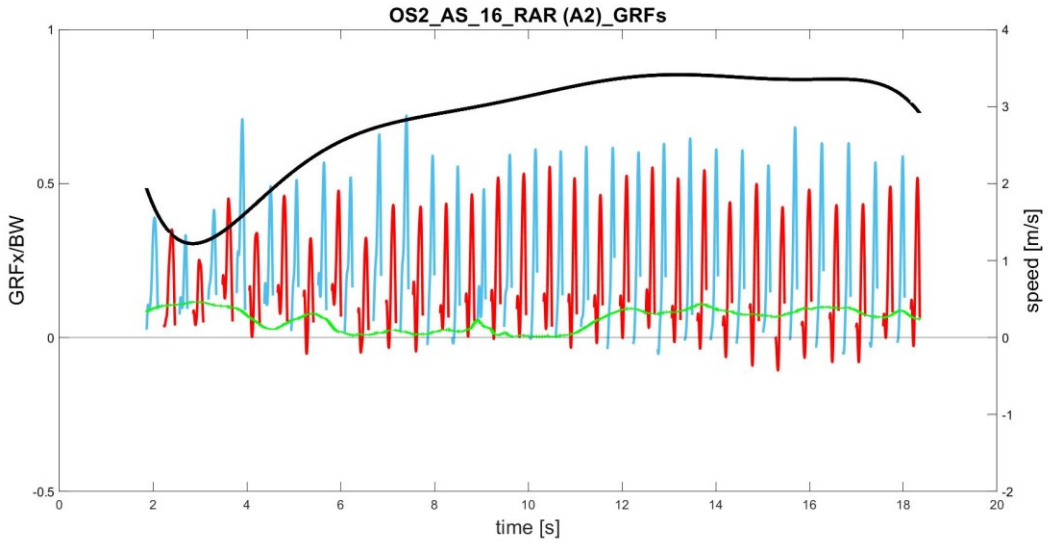

Figure 6.11. GRF in x-direction for affected (red) and unaffected (blue) limb, overlapped with force from load cell (green) and treadmill speed (black) in RAR test

ROS results

Despite the various attempts to estimate the COP through the analytic equations involving forces and moments measured by the force platforms, results were very uncertain. Therefore, the projection of specific markers (IIMHR and FD1-FD2-FD3) on the ground has been provisionally used as COP trajectory. The same choice has been adopted also for track tests, to be consistent with the calculations. As a consequence, the Roll over Shape consists basically in the projection of the position of those markers into another coordinate system.

Errore. L'origine riferimento non è stata trovata. shows the results obtained during a SSR tests. The blue curve represents the ROS in the unaffected limb, while red the ROS in the affected limb during the stance phase only, from foot strike (full dot) to foot off (blank dot). The coordinate (0;0) stands for the origin of the reference system AFROS, which is centred in the right Ankle Joint Centre or in the Clamp Centre, and has y-axis aligned with the tibia or the pylon respectively.

The movement in X-direction in the case of the right foot is very limited, since the horizontal

distance between ankle and second metatarsal head remains almost fixed. On the contrary, ROS displacement is bigger for the left foot, because the prosthesis has a larger deformation range in AP direction than the healthy foot.

Looking at the Y-coordinate, it can be noted that it is always negative, since the COP is located below the origin of the reference system. The distance from origin reduces from foot strike to midstance, which is the point in which the curve reverses, because the heel lowers and the prosthetic foot is deformed by the load. In the second half of the stance, COP moves again away from CS origin, because the ankle plantarflexes and the prosthetic foot extends.

In the case of the prosthetic foot, ROS has a negative X-coordinate because the local reference system is slightly backward rotated with respect to the vertical line passing from clamp to foot tip.

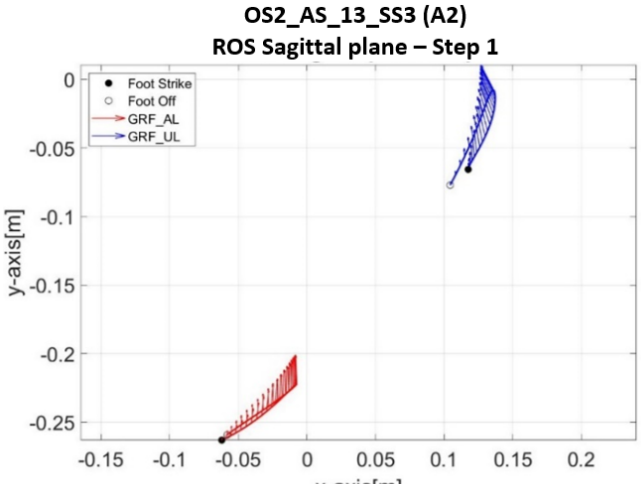

Figure 6.12. Roll Over Shape for one step in a SSR test

Kinetic analysis results

Kinetic analysis has been carried out using both the simplified method and the inverse dynamics method. The former is considered as a benchmark, because it describes the simple but realistic pattern of joint moments. Therefore, when the moment obtained with the inverse dynamic approach is similar to the moment obtained with the GRF vector approach, it can be considered in magnitude correct.

In Figure 6.13 to Figure 6.17, internal joint torques and joint powers in the three planes are represented. Different colours stand for the methods employed (green: Inverse Dynamics, black: GRF vector). Up to now, results obtained with both methods are available for the right limb only, because inertial properties of the prosthetic components have not been calculated yet.

In general, main torque is the one acting in the sagittal plane M_z, while in frontal and transverse plane smaller angular velocities, accelerations and smaller lever arms imply reduced M_x and M_y torques, except for the hip, whose moment in the frontal plane is not negligible.

Hip extensor muscles contract concentrically to extend the hip prior to and just after initial contact, then they act towards flexion until midstance to resist the extension caused by the external forces. Last part of stance is characterized again by extension, while in swing, flexor moment is predominant.

Looking at power, in the first part of stance, hip muscles perform a fast concentric contraction and then work eccentrically, so they absorb power, while in the propulsive phase of stance and in the second part of swing they contract concentrically, thus producing power. For what concerns torques in the frontal plane, during stance phase the gluteus medius contracts eccentrically to abduct the hip and absorbs power to counteract the adduction moment caused by gravitational and acceleration loads. Afterwards, during the propulsion phase, the gluteus medius contracts concentrically, abducting the hip and generating power.

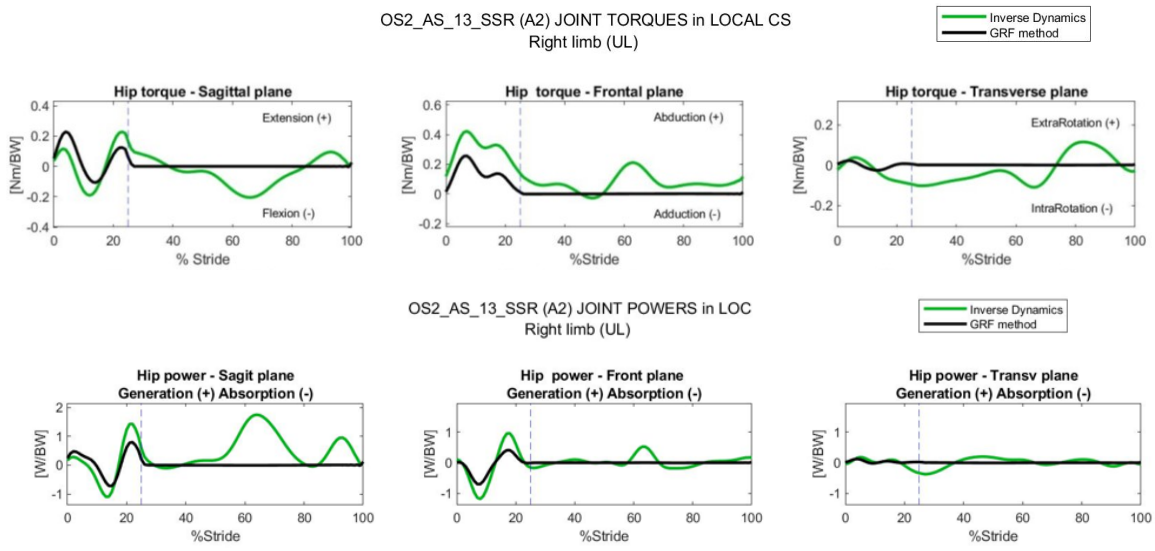

Figure 6.13. Internal joint torques (top) and joint powers (bottom) in the three planes for the right hip. Average over 6 steps in a SSR test.

At the knee, a brief flexor moment is produced at initial contact, with the quadriceps contracting eccentrically to absorb the shock of the impact. At the same time, muscles crossing the knee act to abduct the knee. Afterwards, quadriceps muscles produce an extensor moment, which contrasts the flexing moment produced by the Ground Reaction Force and in the second half of stance they act for propulsion of the limb. In the first half of swing, there is no significative sagittal moment, while in the second half of swing, hamstrings produce a flexor moment to

control the knee rapid extension and prevent hyperextension prior to foot contact.

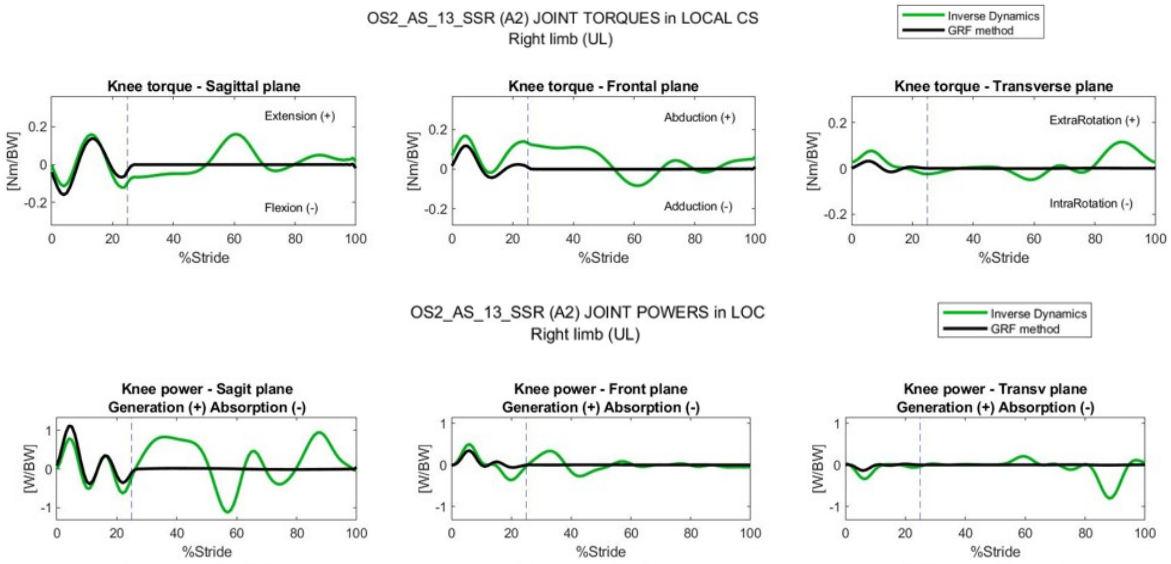

Figure 6.14. Internal joint torques (top) and joint powers (bottom) in the three planes for the right knee. Average over 6 steps in a SSR test.

Ankle torques present the greatest similarity between the Inverse Dynamics and the simplified method, because the effect of inertia in the foot is very small. Muscles crossing the ankle, mainly the gastrocnemius, exert an extensor moment for most of the support period. The absence of an initial dorsiflexion moment means that the athlete completely avoids the rearfoot striking and lands with the foot extended.

Power is negative in the first part of stance, when muscles contract eccentrically to absorb the impact. After midstance it turns positive because muscles are generating energy required for the forward propulsion. During swing phase, power production and absorption is almost null.

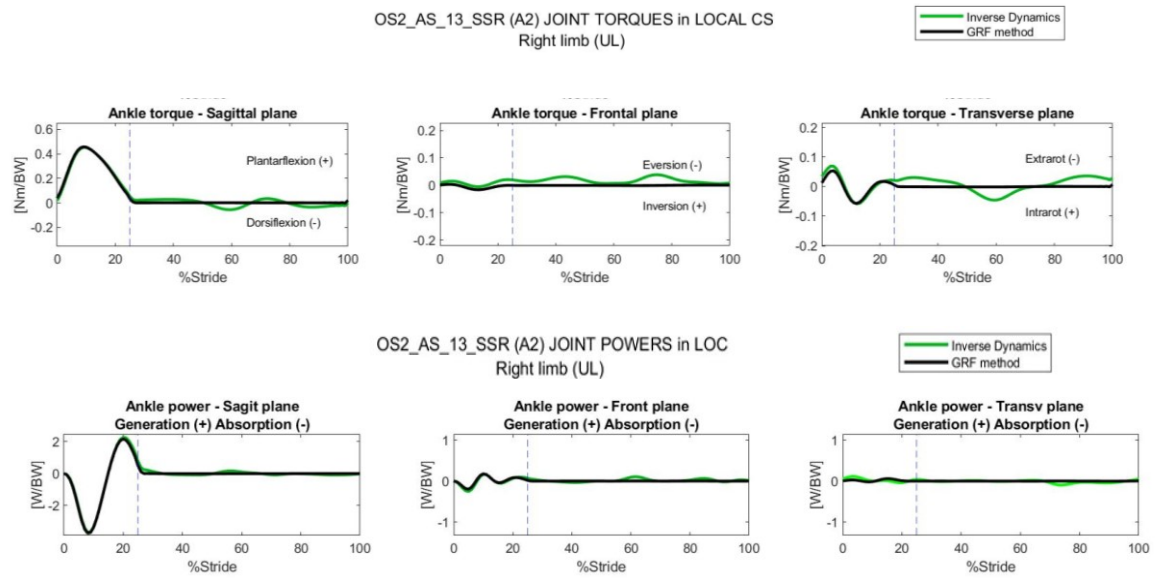

Figure 6.15. Internal joint torques (top) and joint powers (bottom) in the three planes for the right ankle. Average over 6 steps in a SSR test.

In the case of the prosthetic limb, hip moments and powers – calculated with simplified method only- follow the same patterns described for the sound limb, but in this case peak values are lower and the abduction moment is almost zero.

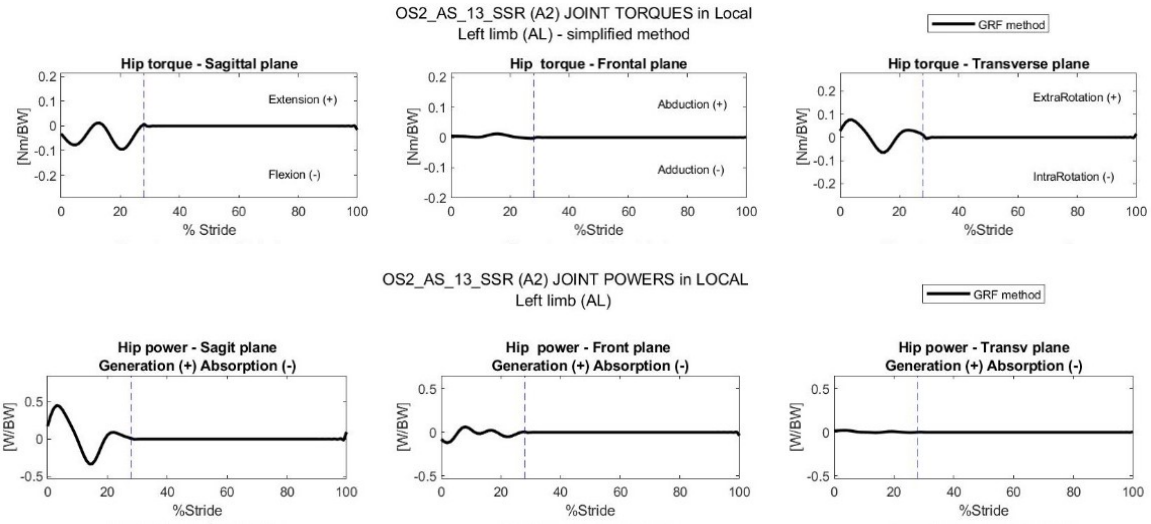

Figure 6.16. Internal joint torques (top) and joint powers (bottom) in the three planes for the left hip. Average over 6 steps in a SSR test.

With regard to the prosthetic knee, it must be noted that in the sagittal plane the moment is much smaller than that of the right limb and it is always flexor throughout the stance phase, which means that the external moment received acts in extension. This situation is fundamental for the knee to be intrinsically safe. If the external moment were flexing the knee, the knee would close and the athlete would fall.

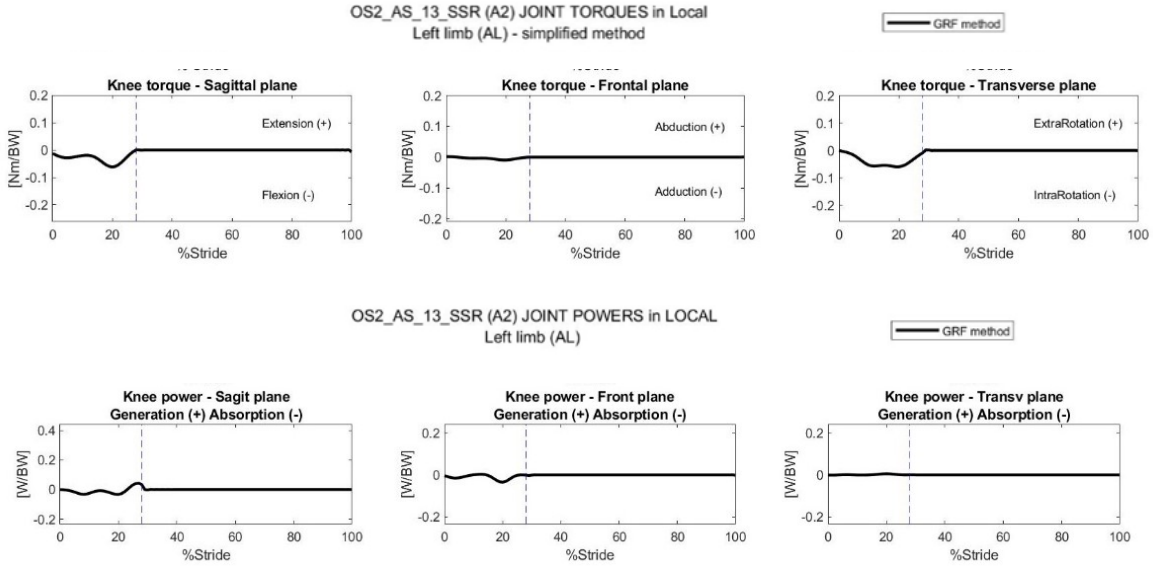

Figure 6.17. Internal joint torques (top) and joint powers (bottom) in the three planes for the left knee

Regarding the prosthetic limb, although there is not a mechanical component which reproduces the movement of a biological ankle, it has been possible to estimate the power at the Running Prosthetic Foot. In this case, since no moments nor angular velocities can be used, power can be related to the force exerted by the RPF, that is the opposite of GRF, to induce a relative displacement of the COP with respect to the clamp, that is the velocity of the ROS. Therefore, power is calculated as dot product of the GRF (with its sign inverted) and velocity of the ROS (first derivative of the ROS trajectory).

In order to validate this method, the calculation has been performed first for the right ankle (UL), for which both ROS and power obtained from joint moment and angular velocities are available. Results have been compared and found to be to a great extent overlapping. Therefore, this method for power estimation has been used for the left side.

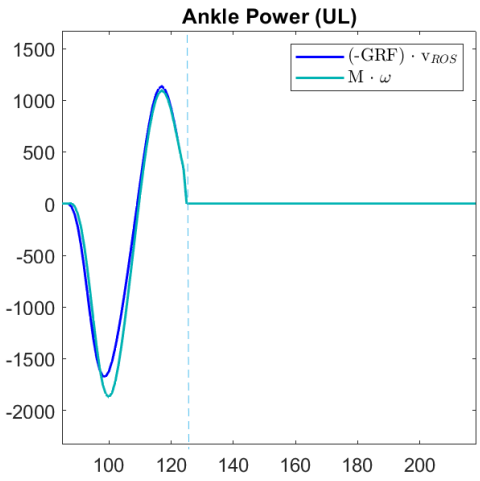

Figure 6.18. Comparison of power calculation methods for right ankle

The following plot summarizes the main outputs of the kinematic and kinetic analysis. Each column represents a body joint, starting from the left there are hip, knee and ankle joints. Each row represents one category of results, starting from the top: joint angles, joint angular velocities, joint moments and joint powers (they all refer to the sagittal plane only). Colour red stands for the affected limb and colour blue stands for the unaffected limb. The trial represented is a SSR test, so the curves correspond to the average values over six steps.

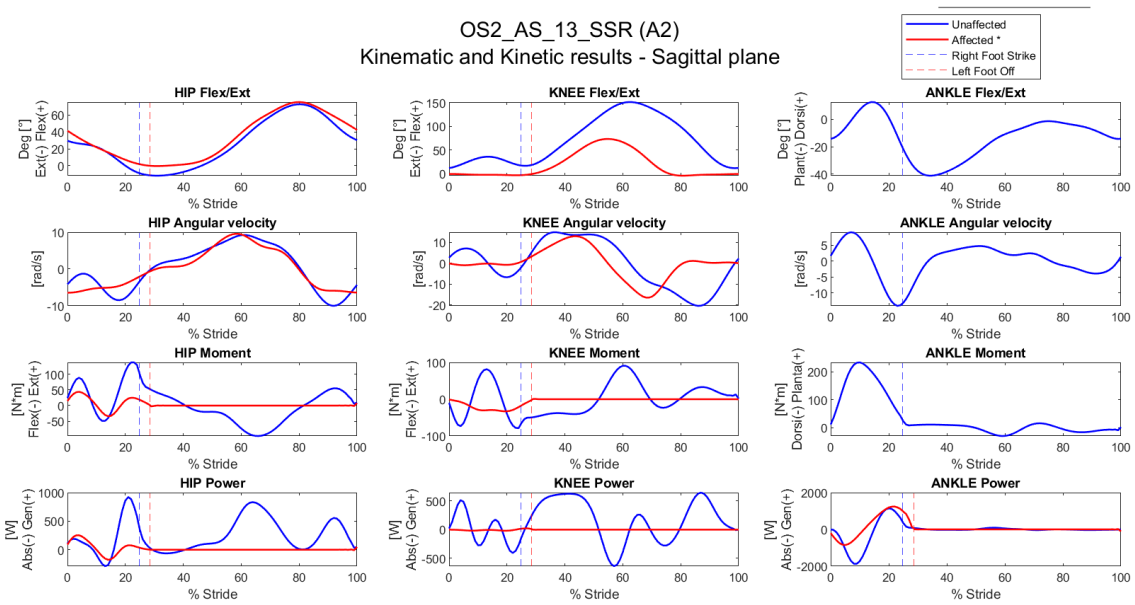

Figure 6.19. Joint Kinematics and Kinetics in the sagittal plane. Average values over 6 steps in a SSR test.

To sum up, the main differences between affected and unaffected limb lie in the knee angle and angular velocity, with the prosthetic knee fully extended during stance phase while the biological knee performs a short flexion movement. Further differences relate to joint moments and powers. In this case, the lower values reached by red lines are in part due to the absence of inertial components and in part to the inability of passive mechanical components to produce energy.

All diagrams presented in this Chapter are examples of the outputs provided by the biomechanical analysis software. Similar figures were produced for each analysed trial of those listed above and can be found in the official document *Deliverable 2.12* of OLIMPIA project.

Chapter 7

Discussion

Results obtained from the biomechanical analysis are here compared in order to answer to the research questions (RQs) at the basis of this work.

Differences between types of running tests

The RQ1 focuses on the differences between Steady State Running (SSR) and Resisted Accelerated Running (RAR), considering only treadmill tests.
The results described in Chapter 6 as examples of the outputs of the biomechanical analysis software are relative to SSR tests only. Since the athlete maintained a constant speed, either set in the treadmill or self-imposed, the shape of the curves relative to joint angles, joint moments and the value of the impulses are almost identical for the whole test duration.

On the contrary, in RAR tests is not possible to compute the average, since in each step speed varies. To analyse these tests, the temporal variation of each parameter for the whole test duration can be used instead. In treadmill tests, athletes never reached a constant speed as high as the one adopted in the steady state running tests, therefore it is hard to compare steps between the two types of tests.

From the plots relative to OS2_AS_16_RAR (A2) (Figure 7.1) it can be observed that as velocity increases, so the hip flexion becomes greater, in particular for the hip of the unaffected limb, which moves with a maximum Range of Motion (ROM) of 100°, from -5° (at toe off) up to 95° (in mid swing).
Left hip has a smaller ROM and during the terminal phase of stance it extends less than it does in SSR.

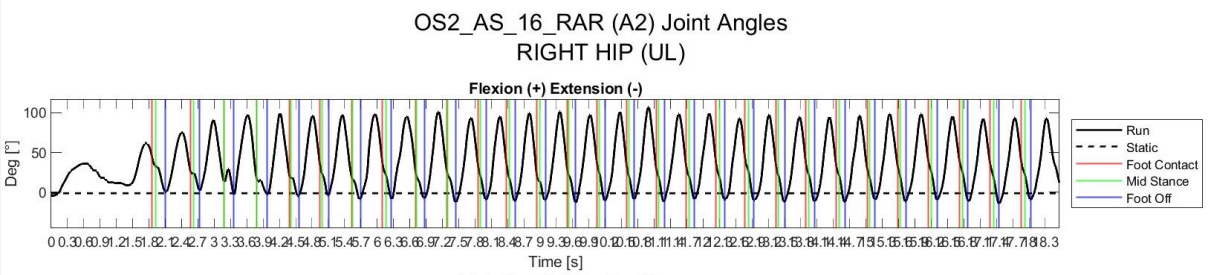

Figure 7.1. A) Right hip angles in the sagittal plane during a RAR test for athlete AS

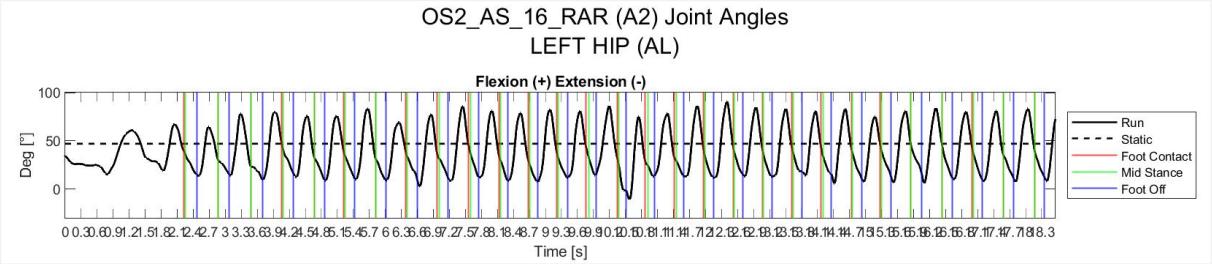

Figure 7.1. B) Left hip angles in the sagittal plane during a RAR test for athlete AS

During RAR tests, the maximum flexion angle in swing does not vary neither for the unaffected knee nor the prosthetic knee. However, the movement of the healthy knee differs from the pattern characterizing SSR tests. The two periods of flexion are no more clearly discernible, because during terminal swing the knee does not fully extend. At foot contact, knee is 25° to 40° flexed, with values changing according to increasing speed.

Left knee do not show appreciable changes.

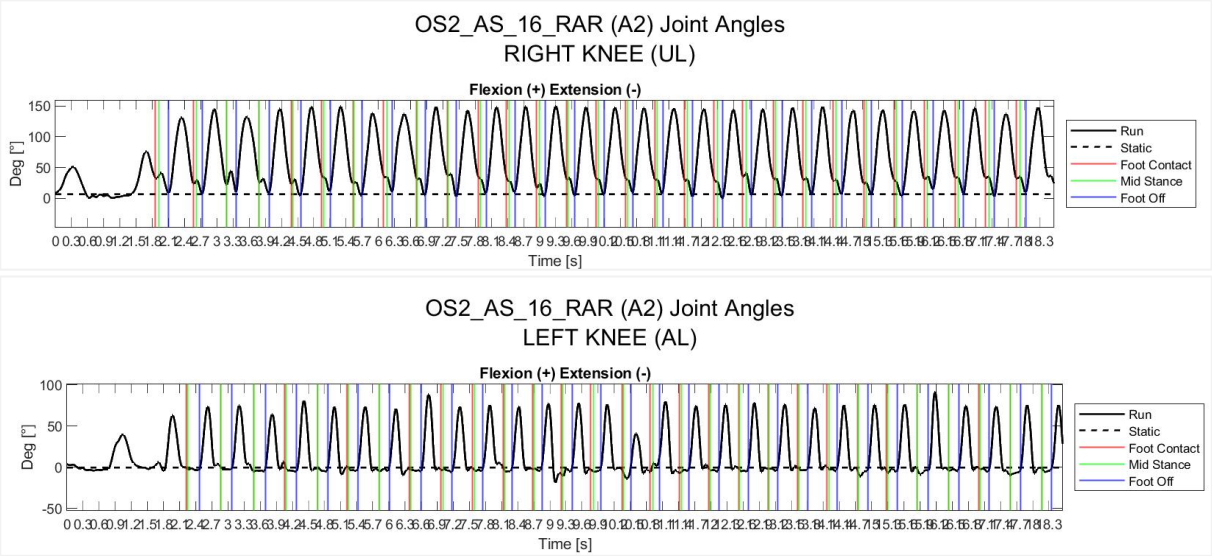

Figure 7.2. Right and left knee angles in the sagittal plane during a RAR test for athlete AS

Concerning right ankle, in the acceleration tests, range of motion maintains similar to SSR tests, but shifted 5° upwards and the flexion movement after toe off is more rapid.

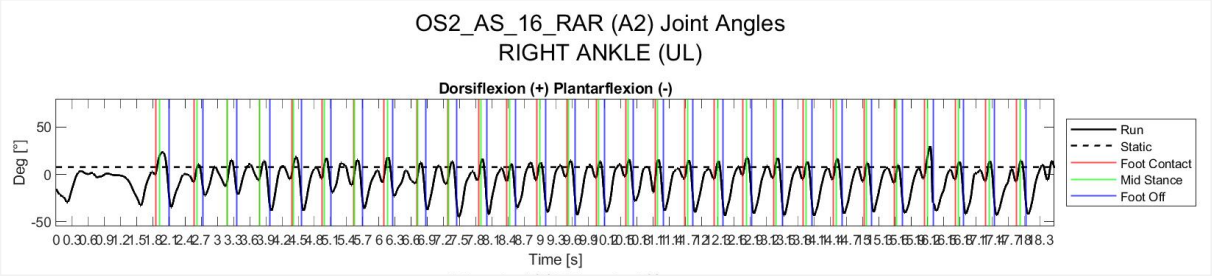

Figure 7.3. Right ankle angles in the sagittal plane during a RAR test for athlete AS

In constant speed tests, trunk inclination with respect to vertical slightly increases from foot contact to mid-stance of the unaffected limb and then decreases from mid-stance to toe-off from 7° to 2° on average. For the affected limb, the trunk inclination increases during stance, but its maximum leaning angle equal to 4° (with alignment A2).

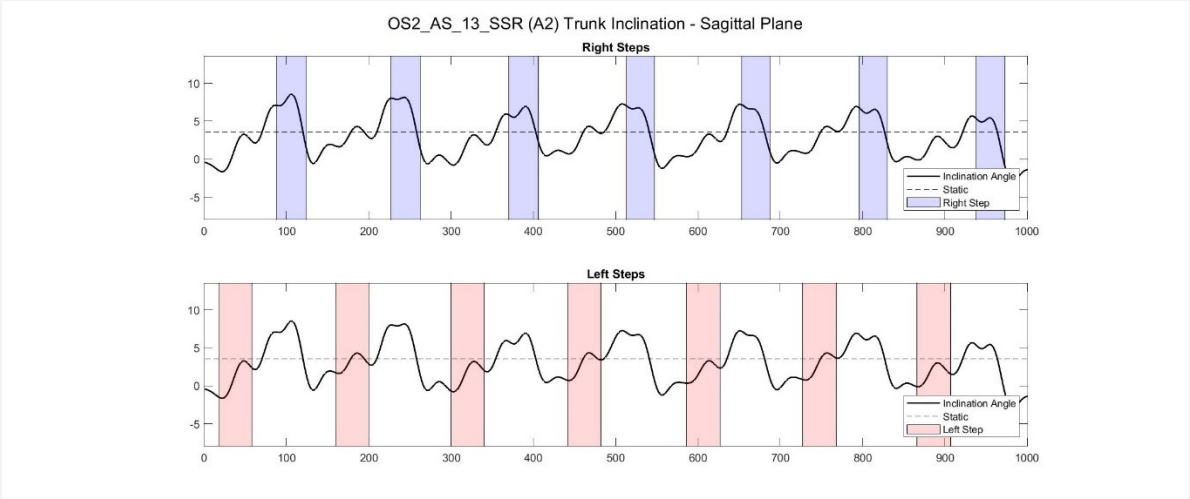

Figure 7.4. Trunk inclination angle during a SSR test for athlete AS

In acceleration tests, as speed increases, trunk leans more forward with values ranging from 25° to 35°, whereas the differences in the trunk movement between the unaffected and affected limb stance time remains unchanged.

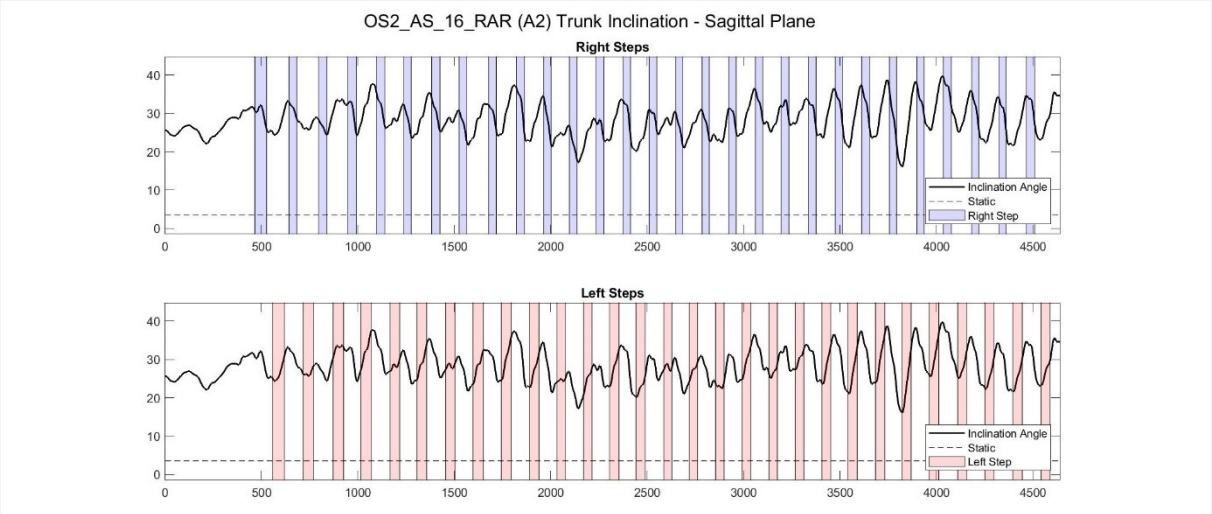

Figure 7.5. Trunk inclination angle during a RAR test for athlete AS

Differences in joint angles between SSR and RAR tests are subtle, but more evident contrasts arise from the comparison of GRFs.

In Figure 7.6, in the picture left, average GRF and standard deviation for the affected limb are represented with red lines and shades respectively. In the picture right, the same parameters are represented for the unaffected limb. For what concerns RAR tests, the first 10 steps for each limb have been used to compute the mean.

First of all, it can be observed that vertical GRF reaches higher values in the SSR tests than in RAR tests. For the unaffected limb, maximum vertical GRF in SSR is about 3.8 BW, while in RAR it is just above 3 BW. In the affected limb this gap is bigger, with 3 BW for SSR and 2.1 BW for RAR. This difference can be attributed to the fact that in SSR test the athlete is running at 5 m/s, while in RAR test, the maximum speed reached in 10 steps is lower, nearly 3 m/s. Moreover, it can be noted that the standard deviation in curves belonging to the RAR test are wider than the ones relative to the SSR test. This is indicative of the great variability between steps in an accelerated running test.

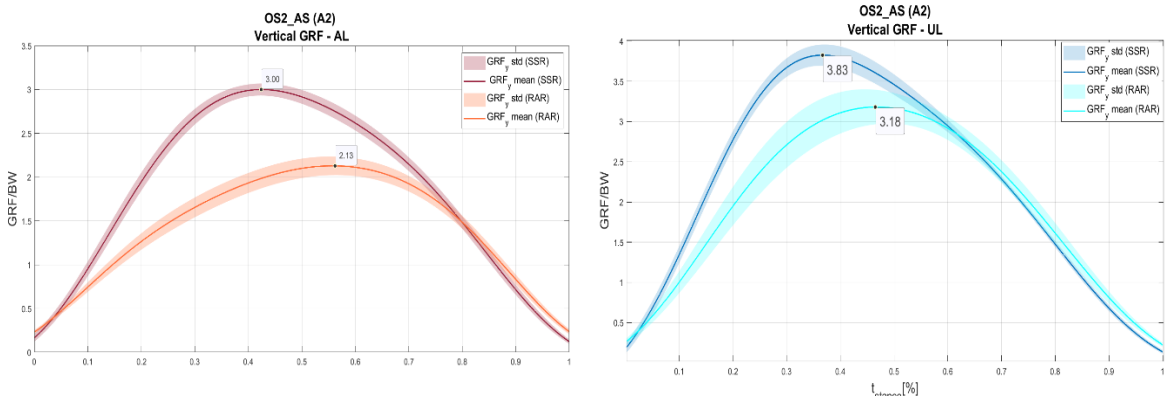

Figure 7.6. Vertical GRFs in affected (left) and unaffected (right) limb for SSR (dark red and dark blue) and RAR (light red and light blue) tests for athlete AS

Horizontal GRFs (Figure 7.7) also present some dissimilarities between the two types of tests, which are at most visible for the unaffected limb. When the athlete runs at constant speed, the sound limb exerts a braking force for more than half of stance phase, whereas during the acceleration test it produces only propulsive force. The affected limb behaves in a similar way, but in the SSR test, the negative peak is of smaller magnitude than in the sound limb.

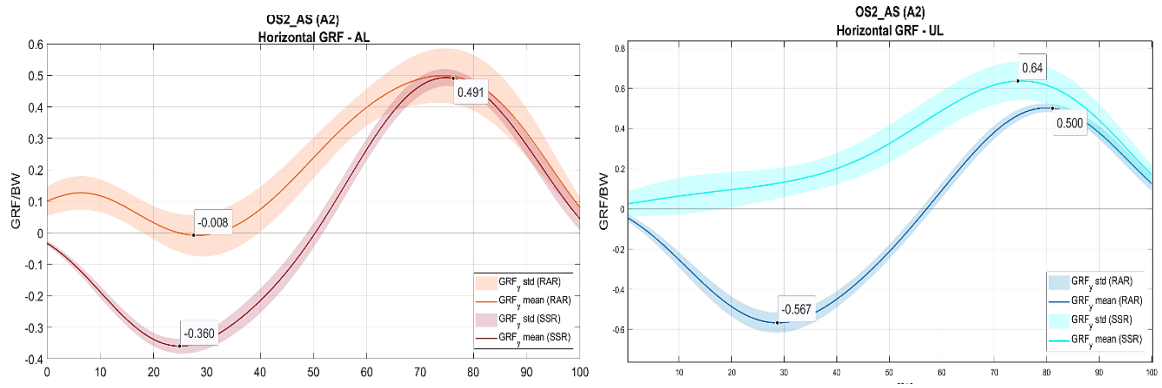

Figure 7.7. Horizontal GRFs in affected (left) and unaffected (right) limb for SSR (dark red and dark blue) and RAR (light red and light blue) tests for athlete AS

The great variability of GRFs in RAR tests is further explained in the figures below, relative to the affected limb. Each step is represented with a different colour, from blue to red, in ascending

order.

It can be pointed out that, in each step, the horizontal GRF has a different trend, but it is always positive, except for some small negative deflections in the first part of steps 7 to 10.

In the graphic at the bottom, it can be clearly observed that stance time decreases going from step 1 to step 7 and then it maintains in an intermediate range close to 0.2 s.

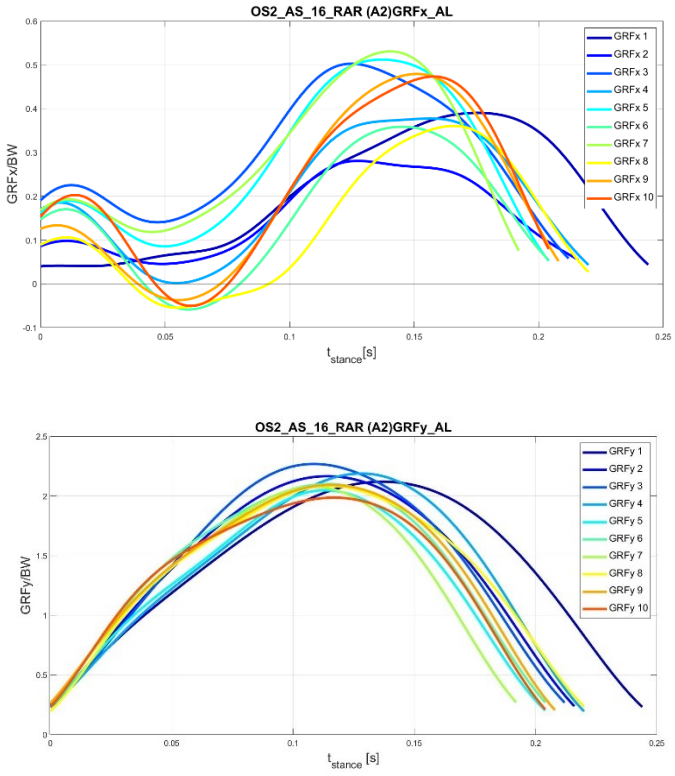

Figure 7.8. Horizontal (top) and vertical (bottom) GRFs for the affected limb in a RAR test for athlete AS.

Decrease in stance time during RAR tests is accompanied by an increment in contact length, which can be noticed in Figure 7.9 . More precisely, since the athlete is running on a treadmill, her centre of mass stays always in the same position, except for some small oscillations forwards and backwards. Therefore, contact length has been calculated as step length plus the horizontal displacement of the centroid of the pelvis, which approximates the COM.

The greater hip flexion angle as velocity increases contributes to the increment in contact length, but once the athlete reaches a constant speed, contact length also plateaus. In addition, it can be observed that the affected limb has a greater step length and a greater contact time than the unaffected one.

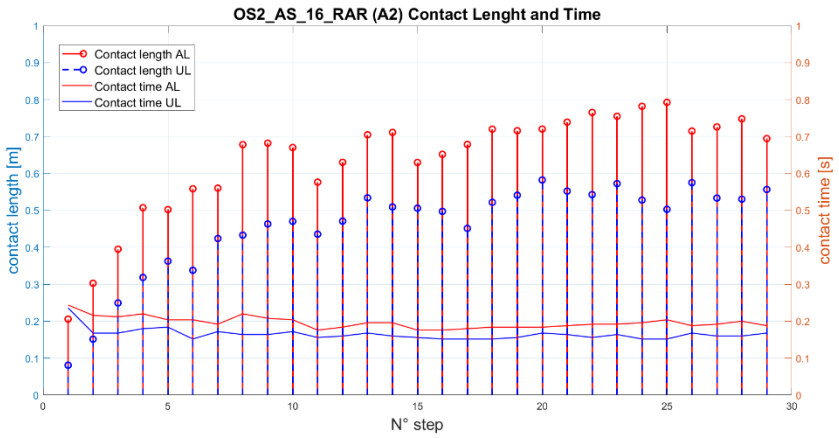

Figure 7.9. Contact time and contact length in a RAR test for athlete AS

Looking at impulses of GRF_x in RAR tests, they are only positive, either for the prosthetic (left) and the sound limb (right), meaning that forces are only propulsive and there is no braking effect, which in turn could be observed in SSR tests (Figure 6.10).

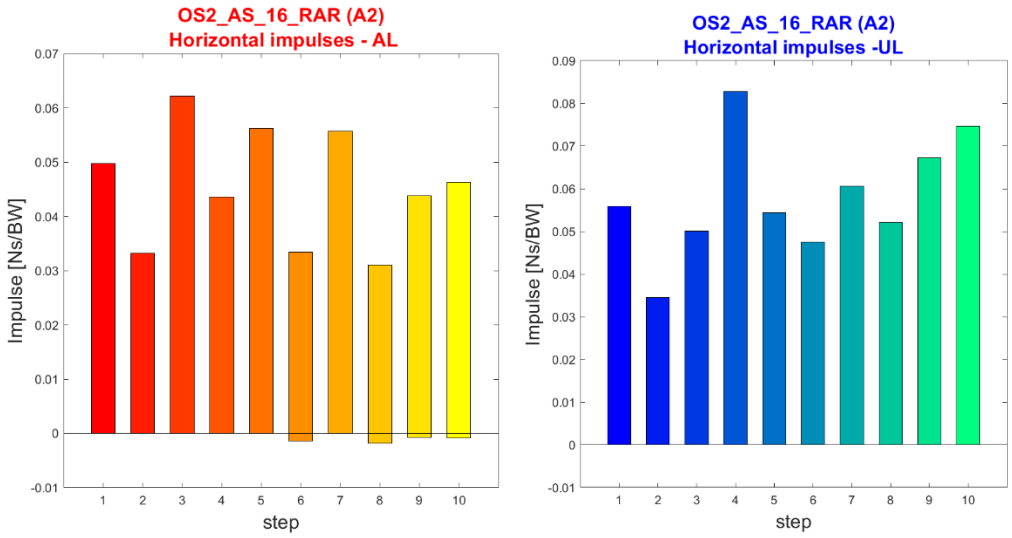

Figure 7.10. Horizontal impulses of GRF for affected (left) and unaffected (right) limb in treadmill RAR test for athlete AS.

To answer the RQ1, there is evidence of differences between SSR and RAR. The main differences lie in the GRFs. In the case of RAR, the horizontal force is propulsion-only, whereas in the case of SSR there is first a braking phase and then a propulsion phase. This is also proven by the comparison of the horizontal impulses. Steps of RAR exhibit much greater variability than the steps of SSR, as seen by the greater dispersion in the averaged graphs.

Regarding the kinematics, appreciable differences concern the behaviour of the sound knee, for which in RAR the double flexion curve is much attenuated or absent, and also the trunk, which is much more vertical in SSR than in RAR.

Differences between running surfaces

The topic of the second RQ is the running surface, and the goal is to show if tests performed on track are comparable to those performed on treadmill by athlete AS.
In order to reduce the number of independent variables, test on treadmill with alignment A3 is the only one considered, because A3 is the same alignment used by the athlete for running on track. Comparison focuses on the steady state running (SSR and TSSR) only, and it must be remarked that in the first case the athlete ran at 5 m/s, while in the second one the average speed maintained in the central part of the run was 6.7 m/s.

The average peak values (minimum and maximum) of joint angles and ROM are listed in the Table 7.1., which summarizes the joint angles in the sagittal plane for the three joints in two test conditions. For what concerns hip, knee and ankle, both left and right (in the case of the ankle only right), they are reach greater flexion angles – in swing phase – during the track tests than during the more flexed during the track test than during the treadmill test, with maximum flexion always occurring in swing phase.

Table 7.1. Joint Angles (Hip, Knee, Ankle) in treadmill (TRD) and track (TRK) tests for athlete AS

	L HIP		R HIP		L KNEE		R KNEE		R ANKLE	
(avg)	TRD	TRK	TRD	TRK	TRD	TRK	TRD	TRK	TRD	TRK
MIN	-6.07°	12.78°	-24.18°	-10.06°	-7.79°	8.98°	8.09°	24.51°	-24.96°	-26.06°
MAX	61.34°	102.03°	57.07°	93.02°	93.37°	100.34°	137.35°	146.77°	12.24°	31.65°
ROM	86.34°	93.79°	101.79°	106.85°	144.67°	110.36°	153.37°	127.25°	46.37°	61.33°

Looking at the hip of the affected limb, it has a greater range of motion in the TSSR than in the SSR, but the values are still smaller than ROM of the unaffected limb (Figure 7.11).

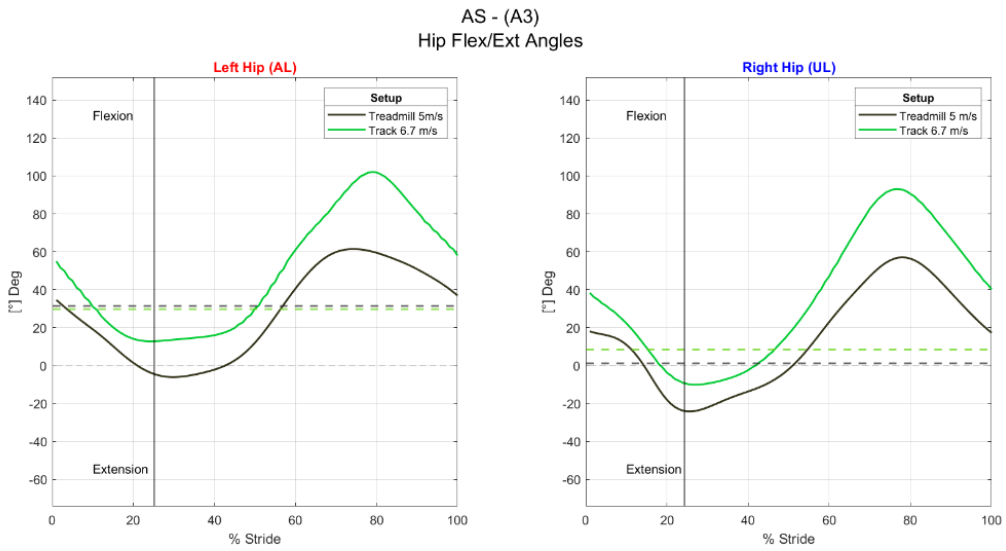

Figure 7.11. Average left and right hip angles in treadmill (black) and track (green) tests for athlete AS

Left knee seems quite flexed during stance time in the track test and a slightly hyperextended during treadmill test. These values are affected by a bias, since the prosthetic knee must have 0° flexion during stance phase, to ensure the stability of the athlete. These shifts may be due a wrong definition of coordinate systems of the prosthetic knee, maybe because of the choice of a time frame in which the knee was not perfectly extended has been selected.

As shown above in the Table 7.1, both left and right knee, despite reaching higher flexion angles in track tests, have a greater ROM during treadmill tests.

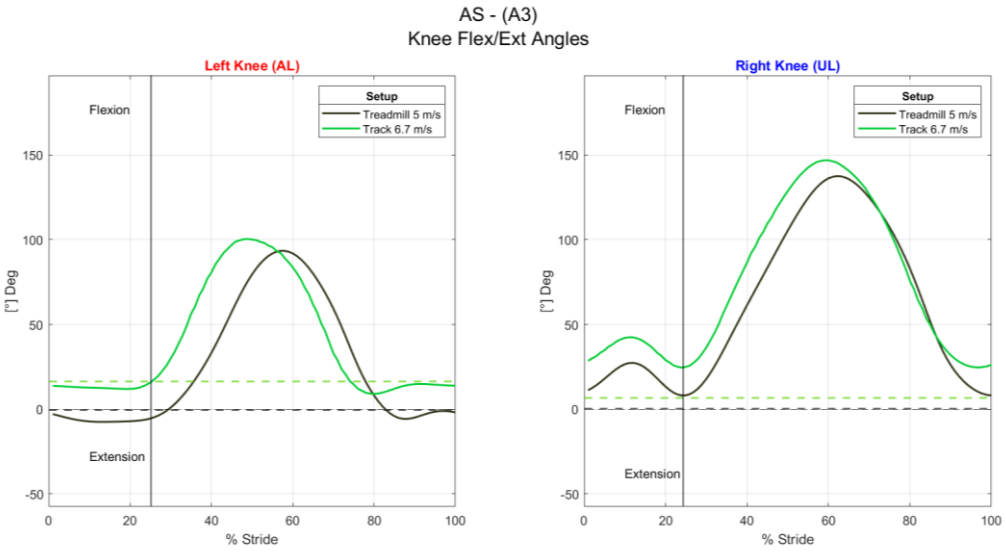

Figure 7.12. Average left and right knee angles in treadmill (black) and track (green) tests for athlete AS

Interesting observations arise from the comparison of Ground Reaction Forces. Since for tests on track no forces have been measured for the unaffected limb, the focus will be on affected limb only.

Reaction Forces measured by the load cell during track tests have then been projected onto the global reference system, so they are comparable with the GRF measured in treadmill tests. In the following figures, the average (±1SD) forces from a track and a treadmill test are displayed overlapped.

Vertical GRF peaks at about 3.6 BW, which is 34% higher than the peak value of AL in the treadmill test. Loading rate is also higher in track test than in treadmill test.

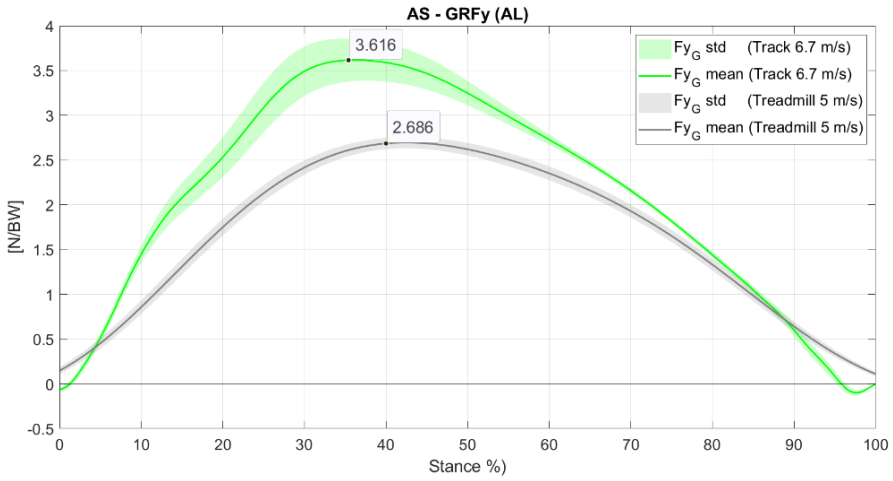

Figure 7.13. Vertical GRFs for affected limb in SSR and TSSR test for athlete AS

Regarding horizontal GRFs, it can be observed that during track test the athlete exerts a greater propulsion force: positive peak value in track almost doubles the positive peak value measured on treadmill. Nevertheless, the negative braking peak is also higher in track tests.

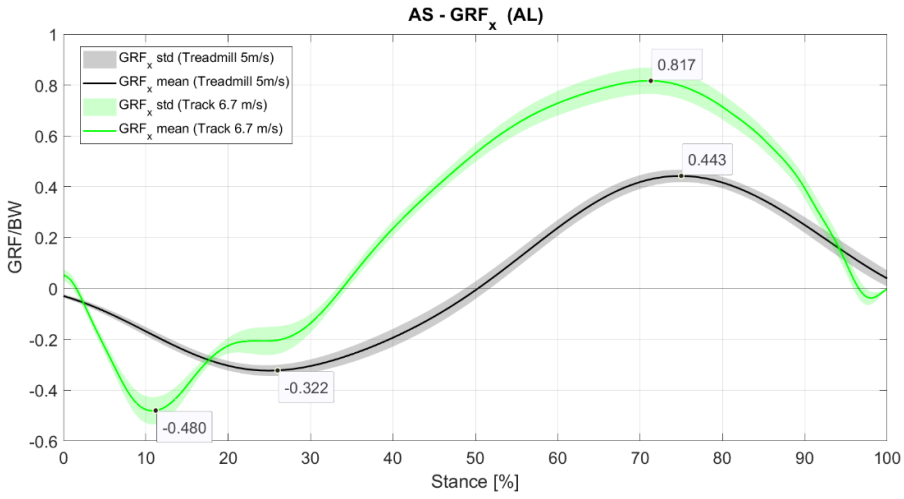

Figure 7.14. Horizontal GRFs for affected limb in SSR and TSSR test for athlete AS

The same conclusions can be drawn by observing the impulses of horizontal GRFs. During track tests, the propulsive impulse is two times bigger than in treadmill tests, while breaking impulses are comparable. Therefore, the net impulse is definitively higher in track tests.

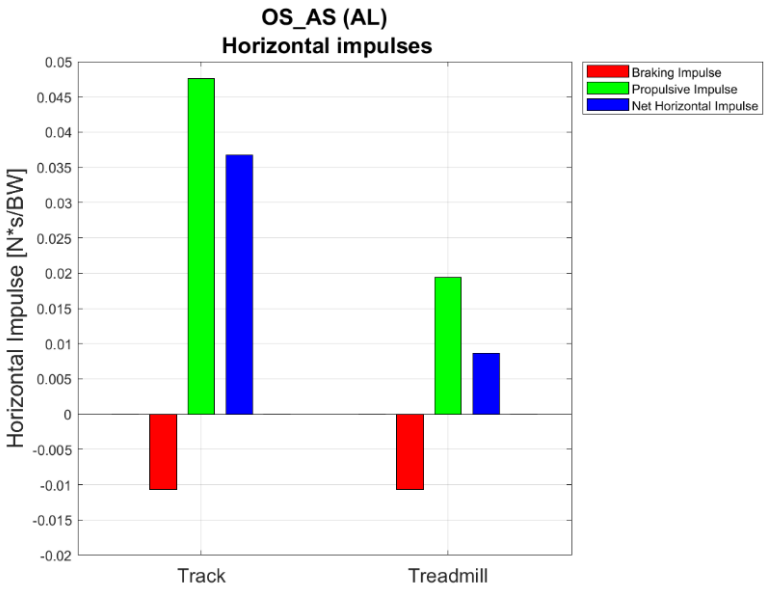

Figure 7.15. Horizontal impulses of GRF in TSSR and SSR test for athlete AS

Joint moments, calculated with the GRF vector method, are considerably greater in the track tests, possibly due to the greater force magnitude and the greater lever arm produced by the greater flexion angle either at hip and at knee.

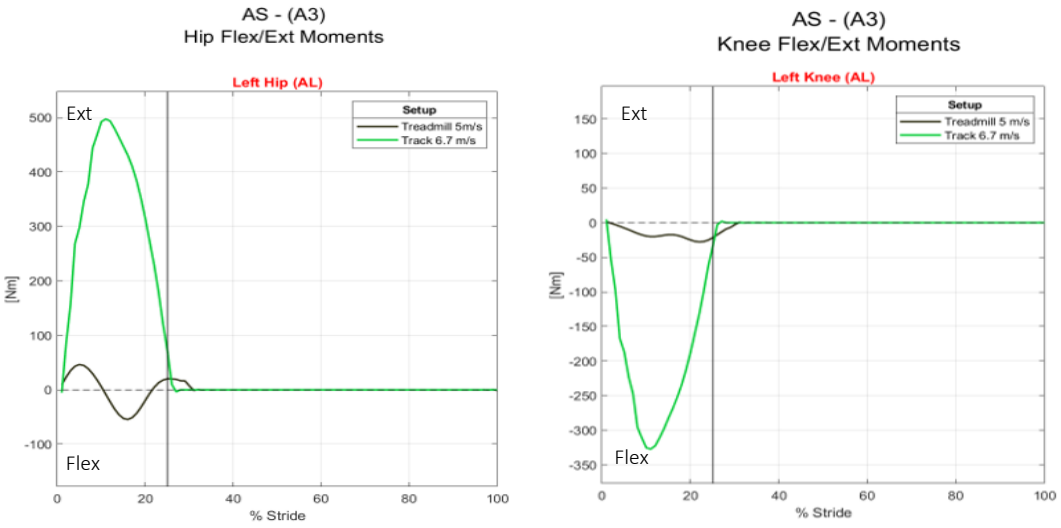

Figure 7.16. Average left hip and left knee moments in treadmill (black) and track (green) tests for athlete AS

Hip moment represented in green (TSSR) acts in extension for the whole stance phase, while the black line (SSR) is positive in the first half of stance and negative in the second half, meaning that when the athlete runs on the treadmill hip muscles counteract the external moment first with extension and then with flexion. Knee moment is always negative, that is flexor, because it is the opposite of the external moment, which acts to extend the knee.

Differences can be observed also in the power values. In TSSR test, hip is generating much more power than in SSR, thus possibly because on track the athlete relies more on the hip for the propulsion than she does on the treadmill.

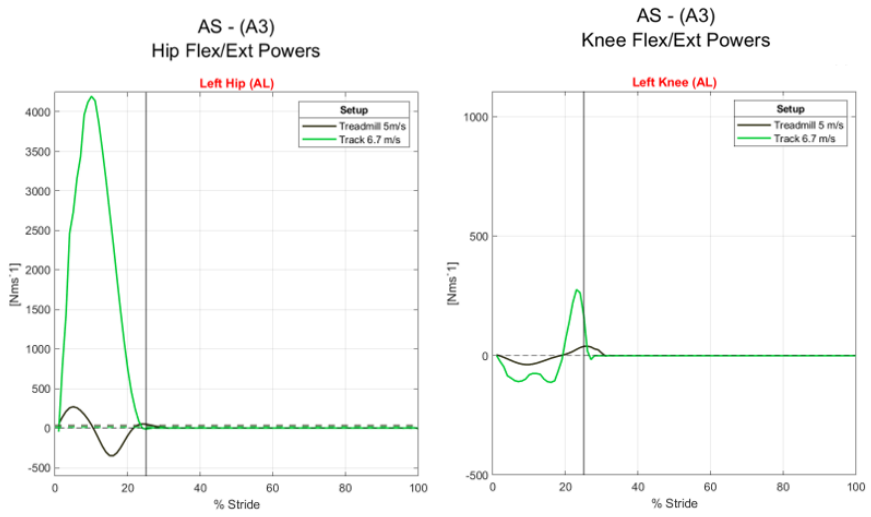

Figure 7.17. Average left hip (left) and left knee (right) power in treadmill (black) and track (green) tests for athlete AS

Hip power is always positive in TSSR because the moment is aways extensor and hip angular velocity is negative, meaning that the joint is doing and extensor movement.

Knee power in the two tests shows an initial period of absorption and then a brief period of generation, just before toe off. This is not caused by a change in the moment, but rather in a change in the angular velocity, which turns from negative to positive. The graphic below shows the angular velocities for hip and knee, for both limbs (red is affected, blue is unaffected).

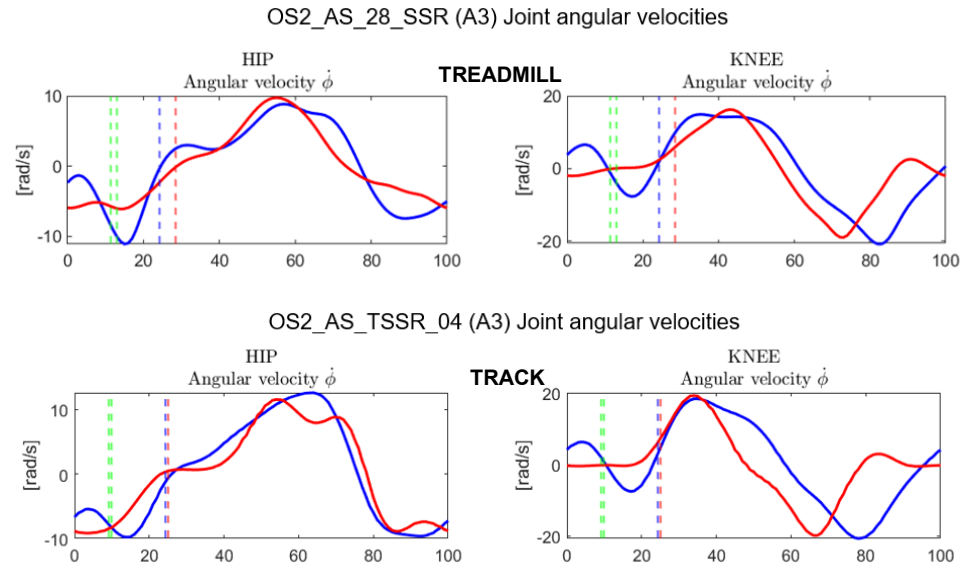

Figure 7.18. Average hip and knee angular velocity in treadmill (top) and track (bottom) tests for athlete AS.
Red : affected limb; blue: unaffected limb.
Green vertical dashed line: mid-stance; red and blue vertical dashed lines: toe off of AL and UL respectively.

Either in TSSR or in SSR, RPF power is at first negative, meaning that the spring-like foot is storing energy, and then positive, when the foot elongates and releases energy. This is the same behaviour of the healthy ankle. They are represented in the figure below.

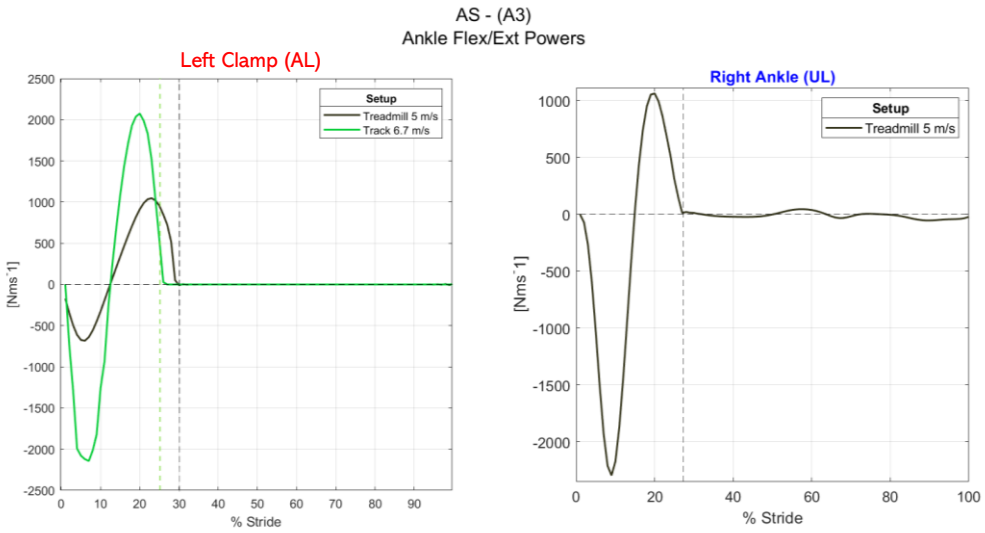

Figure 7.19. Average left and right ankle power in treadmill (black) and track (green) tests for athlete AS

On the whole, to answer RQ2, the biggest differences between treadmill and track running tests are still in the GRFs. When the athlete runs on the track, she exerts more force, both in the vertical direction and even more so in the horizontal direction, where the peak propulsive force is twice as high as the peak recorded on treadmill. The net impulse is therefore greater for track running.

Furthermore, both the hip and knee of the affected limb are more flexed at the moment of foot contact.

The combination of the two conditions is probably the cause of the almost 10 times higher joint moments during track tests than during laboratory tests.

Differences between socket alignments

The third research question addressed in this work is whether there are differences between socket alignments. Both athletes, MC and AS tested four different socket alignments. However, in the case of AS, results are available for three alignments only, up to this moment.
Alignments are characterized by the angle between the lateral axis of the socket and the vertical axis passing from GT and KJC. This angle, called γ, has been set to 5°, 9°, 12° and 15° for A0, A1, A2 and A3 respectively during the alignment procedure performed before the tests.
Socket Tilt, $\widehat{ST}$,is defined as the socket absolute orientation with respect to the vertical axis, and in midstance it should corresponds to the alignment angle γ.

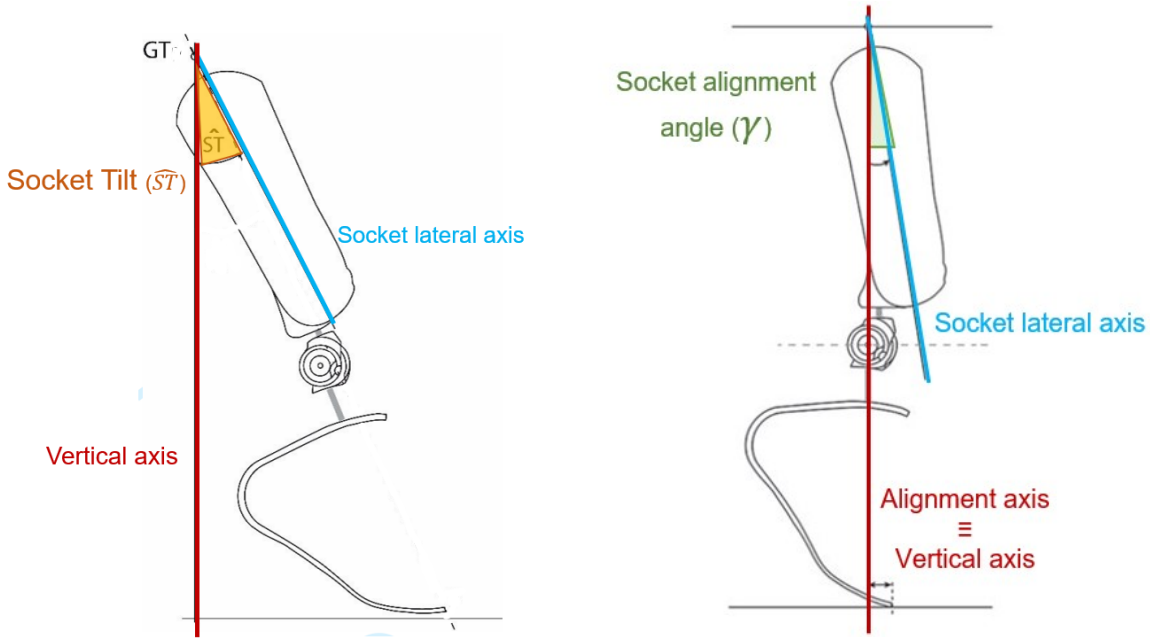

Figure 7.20. Socket tilt (left) and reference socket alignment angle (right)

Angles $\hat{\gamma}$ measured in dynamic tests in OS1 (Table 7.3) and OS2 (Table 7.4) slightly differ from the reference values, but still preserve the incremental trend. Discrepancies in the values may be due to errors in the identification of midstance, which has been estimated as the instant of time in which the horizontal distance between GT and KJC is minimum. This distance was hardly less than 5 mm and this may have led to a distortion in the calculation of the angle. For athlete MC, angles relative to trials performed with alignment A3 have been not calculated yet.
Angles $\widehat{ST}$ have been calculated for the whole duration of the test. The values of $\widehat{ST}$ at Foot Strike and at Foot Off and the differences between these two values (ROM) are reported in the table.

Results relative to trials performed by MC during OS1, shown in Table 7.3. Socket tilt angles at midstance, foot strike and foot off for athlete MC running on treadmill at 4.4 m/s, can be compared with the results obtained in a previous experimental session [32], in which the same athlete ran on an instrumented treadmill, at 5.5 m/s (results in Table 7.2). Angles obtained from that test session have been calculated from bi-dimensional video analysis (using the software Kinovea), while in OS1 and OS2 from the three-dimensional analysis of the trajectory of the markers placed on the socket. Thereby, some differences in the results can also be attributed to the different data collection systems. In both studies, as $\hat{\gamma}$ increases, so $\widehat{ST}$ results more tilted at foot strike and less extended at foot off but with a similar range of motion in all alignments.

Table 7.2. Socket tilt angles at foot strike and foot off for athlete MC running on treadmill at 5.5 m/s. Angles in midstance reported as the range of values obtained with video measurements [Migliore et.al., 2020 [32]]

Athlete MC (Tokyo, 2019) [32]				
Alignment	Midstance $\hat{\gamma}$ [°]	Foot Strike $\widehat{ST}$ [°]	Foot Off $\widehat{ST}$ [°]	ROM (FS-FO) [°]
A0 ($\gamma = 5°$)	5 (± 1)	27	-17	44
A1 ($\gamma = 9°$)	9 (± 1)	30	-12	42
A2 ($\gamma = 12°$)	12 (± 1)	35	-9	44

Table 7.3. Socket tilt angles at midstance, foot strike and foot off for athlete MC running on treadmill at 4.4 m/s

Athlete MC (OS1)				
Alignment	Midstance $\hat{\gamma}$ [°]	Foot Strike $\widehat{ST}$ [°]	Foot Off $\widehat{ST}$ [°]	ROM (FS-FO) [°]
A0 ($\gamma = 5°$)	7.8	27.1	-16.9	44.0°
A1 ($\gamma = 9°$)	11.5	33.6	-9.0	42.6°
A2 ($\gamma = 12°$)	13.3	36.6	-6.4	43°

Results relative to athlete AS are consistent with results of MC for what concerns the increment in $\hat{\gamma}$ in midstance, but values also differ from the reference ones. The causes can be the same cited above, which are primarily errors in the identification of midstance instant.

Table 7.4. Socket Tilt angles at midstance, foot strike, foot off for athlete AS running on treadmill at 5 m/s

Athlete AS (OS2)				
Alignment	Midstance $\hat{\gamma}$ [°]	Foot Strike $\widehat{ST}$ [°]	Foot Off $\widehat{ST}$ [°]	ROM (FS-FO) [°]
A1 ($\gamma = 9°$)	9.9	30.9	-16.9	46.9
A2 ($\gamma = 12°$)	11.9	37.6	-12.7	50.3
A3 ($\gamma = 15°$)	12.9	36.3	-11.2	47.5

In terms of joint angles, different alignments do not produce macroscopic differences, or at least do not show differences as evident as the ones arising from comparisons in RQ2.
The parameter which at first glance most varies among the alignments is the moment at the prosthetic knee. For athlete MC, results relative to Tokyo session are shown in the graphic below (Figure 7.21) and results relative to OS1 are shown in Figure 7.22.

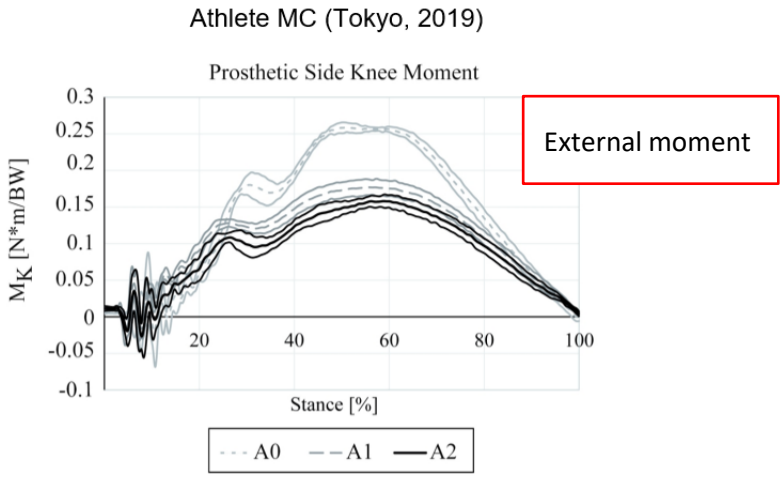

*Figure 7.21. **External** moment acting at the prosthetic knee joint for each alignment (mean ± 1 std) for athlete MC running on treadmill at 5.5 m/s. Positive: moment acting in extension, negative: moment acting in flexion [Migliore et.al., 2020]*

The moment exerted by GRF at the knee decreases with alignment. In Figure 7.21 the external moment - normalized for body weight - is represented, and since it acts in counterclockwise direction, its sign is positive.

The joint moment represented below is relative to OS1. Its sign is negative because is the opposite of the external moment: it acts in flexion throughout stance phase, thus avoiding knee from buckling. A reduced moment could mean less effort to counterbalance the external moment. These results are consistent with what was obtained in the Tokyo session.

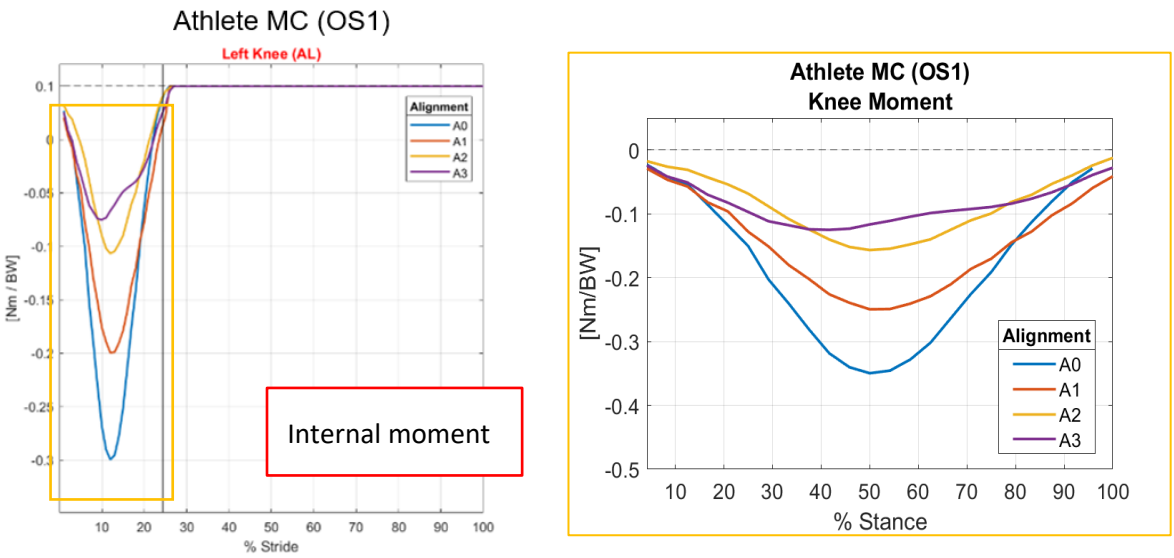

Figure 7.22. ***Internal*** *moments acting at left knee (AL) for athlete MC running on treadmill at 4.4 m/s. Colours correspond to different alignments*

In Tokyo only three alignments were compared, with A0 producing the greatest knee moment (0.25 Nm/BW) and A2 the smallest (0.15 Nm/BW). During OS1 in Padua, a similar trend has been observed, but the gap between A0 and A2 is bigger, about 0.2 Nm/BW. Alignment A3, characterized by an even higher degree of pre-flexion, further reduces the moment at knee, but the difference compared with A2 is minimal.

Similar trends can be observed in the results of OS2 relative to athlete AS. Alignment A1 produces the biggest knee moment, which reaches -0.15 Nm/BW, that is 15% less than the peak of MC with the same alignment.

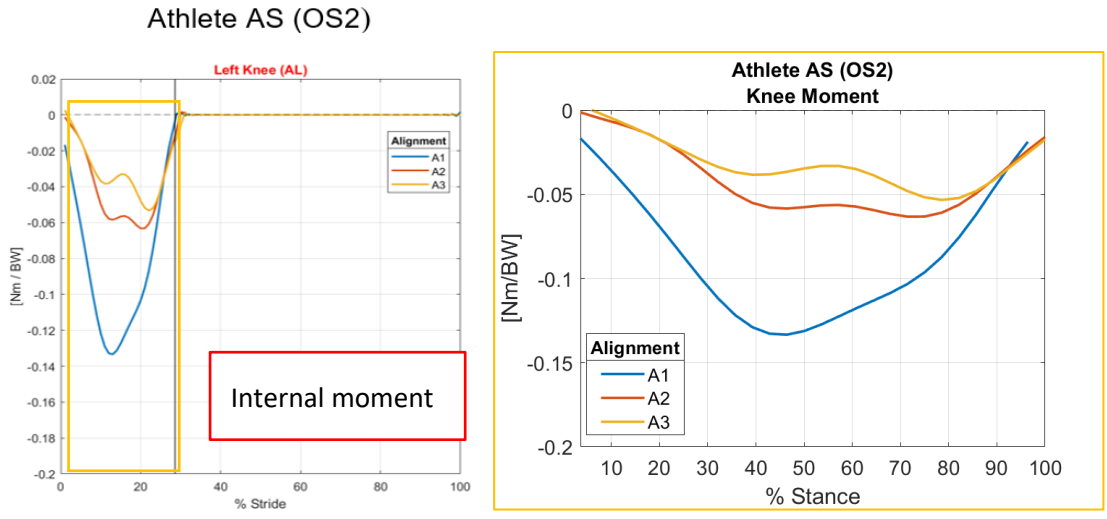

Figure 7.23.Internal moments at knee for athlete AS running on treadmill at 5 m/s. Colours correspond to different alignments

For what concerns Ground Reaction Forces in the affected limb, it can be noted that in athlete MC the propulsive impulse increases from A0 to A2 (from 0.022 to 0.024 Ns/BW), while it slightly decreases from A0 to A1 (from 0.022 to 0.021 Ns/BW) and from A2 to A3 (from 0.024

to 0.023 Ns/BW). At the same time, braking impulses decrease constantly from A0 to A3, therefore net impulses increase from A0 to A3 (Figure 7.25).

The increment in propulsive impulse and the decrease in the impulse from A0 to A2 has been observed also in the Tokyo test session, with positive impulse reaching higher values, possibly due to the more sustained running speed (Figure 7.24).

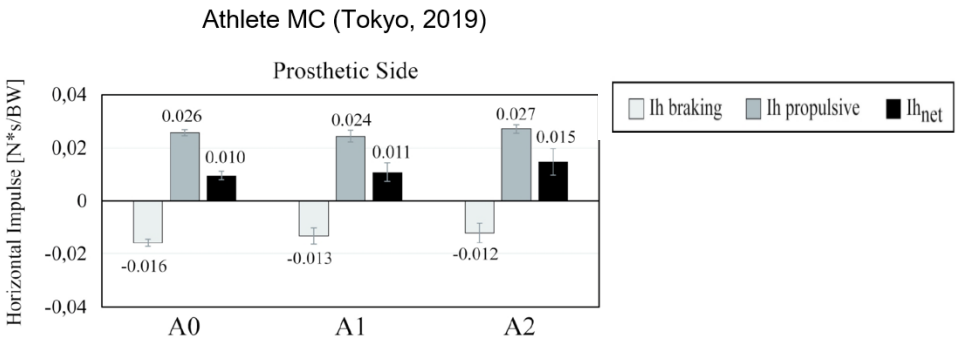

Figure 7.24. Horizontal braking, propulsive and net impulses of the GRF for athlete MC running on treadmill at 5.5 m/s. Affected limb only [Migliore et.al, 2020]

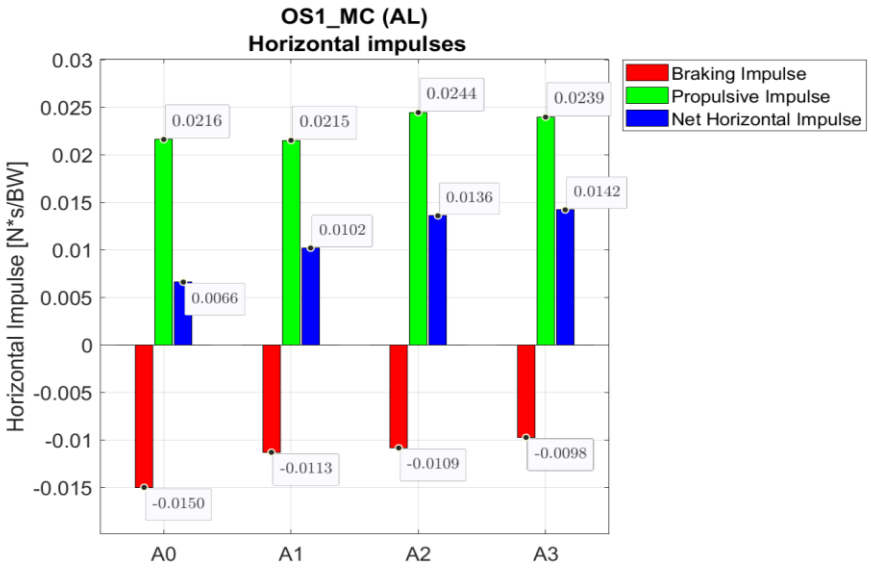

Figure 7.25. Horizontal braking, propulsive and net impulses of the GRF for athlete MC running on treadmill at 4.4 m/s. Affected limb only

Outcomes relative to vertical impulses of GRF during OS1 are partly consistent with the results obtained in Tokyo. Both in OS1 and in Tokyo, vertical impulse of GRF in the affected limb decreases from A0 to A2, but in OS1 (Figure 7.27) the difference between A1 and A2 is in the order of 10^{-4} Ns/BW, which correspond to 0.09 Ns, while in Tokyo (Figure 7.26) the difference

between A1 and A2 is in the order of 10^{-2} Ns/BW, that is 9.8 Ns. From A2 to A3 the vertical impulse slightly increases, but it is still smaller than the impulse in A0.

As far as the sound limb is concerned, the minimum vertical impulse is recorded when the athlete (in OS1) runs with the alignment A3, followed by A1, A2 and in the end A0, while in the previous experimental session the minimum vertical impulse was relative to alignment A2, which is smaller than A1 and also smaller than A0.

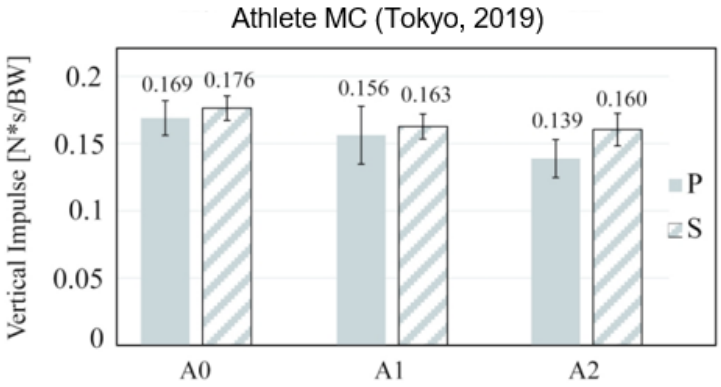

Figure 7.26. Vertical impulses of the GRF for athlete MC running on treadmill at 5.5 m/s. Affected (plain grey) and unaffected (striped grey) limb [Migliore et al., 2020]

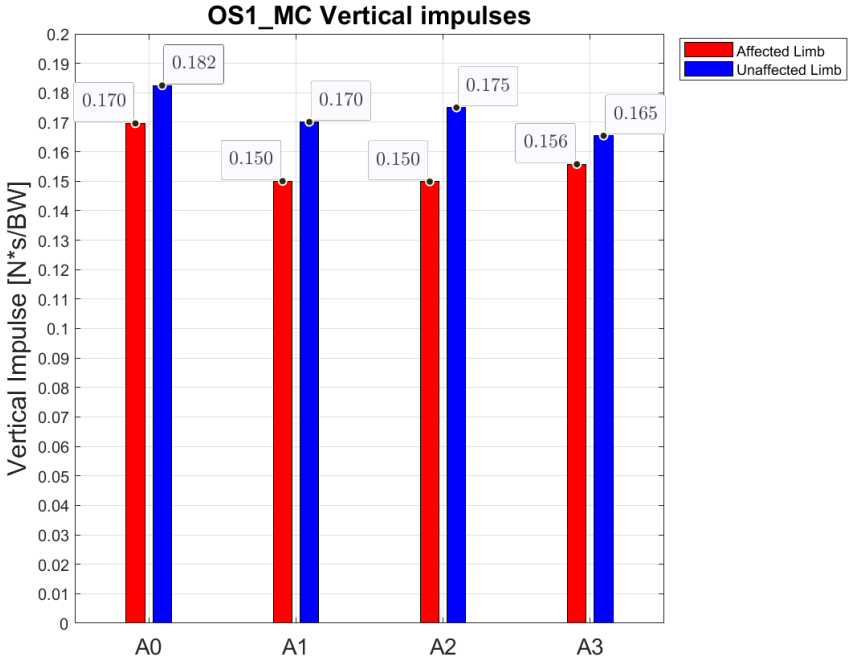

Figure 7.27. Vertical impulses of the GRF for athlete MC running on treadmill at 4.4 m/s. Affected (red) and unaffected (blue) limb.

It can be concluded that despite some differences in the horizontal propulsive impulse values and in the vertical impulse values (for UL), results from the two sessions are consistent, and

therefore the instrumental setup adopted in OS1, which is treadmill on force platforms, provides kinetic quantities comparable to the ones obtained with an instrumented treadmill.

In the paper describing the results obtained in Tokyo, the impulse of the moment at the left hip has also been calculated. However, hip joint moments calculated for athlete MC from data acquired in OS1 are not directly comparable with those results, since the reference system of the pelvis is anteriorly rotated with respect to the ground plane and this probably causes some issues in the values of hip moments, which are always flexor throughout the stance phase.

Data relative to OS2, in which athlete AS ran of the at 5 m/s, are represented in Figure 7.28 . The trial in which the athlete used alignment A0 has not been processed yet, but the moment at hip joint calculated when she used alignment A1, A2 and A3 can be analysed.

Contrary to what resulted from the data of MC in Tokyo, A2 is the alignment producing the highest impulse of moment, calculated as the integral of moment over stance time, while A1 is the alignment producing the smallest impulse of moments. Results reported in the graphic below are not normalized for bodyweight.

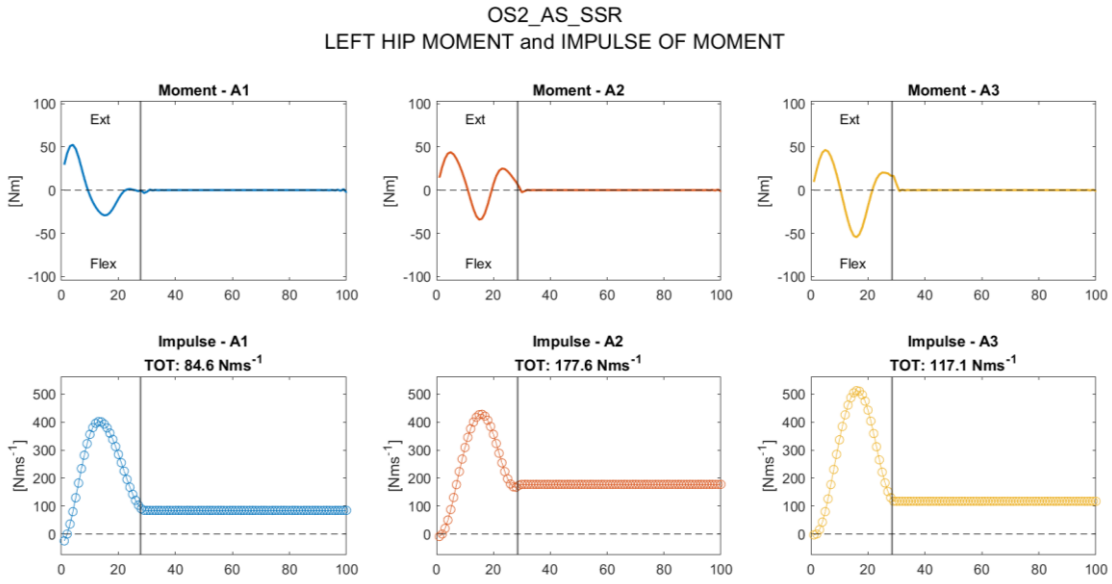

Figure 7.28. Left hip moment and impulse of moment (sagittal plane) for athlete AS running on treadmill at 5 m/s with three alignments

To conclude, the answer to RQ3 is that socket alignment affects running biomechanics, especially in terms of prosthetic knee joint moment and vertical impulse, which decrease as alignment angle increases, while the horizontal impulse increases. Results obtained during OS1 largely confirm the results obtained in a previous experimental session, however there are

discrepancies when it comes to socket tilt dynamic measurements. Nevertheless, in OS1 they still preserve the expected trend.

Limitations

The present work has several limitations, partly due to the experimental procedure itself but partly also due to residual weak points in the software implemented in MATLAB.

One limitation is relative to marker placement, which influences the pose of the reference system of the segments and the location of the centre of mass. Indeed, marker placement and trajectory reconstruction play a crucial role in the evaluation of joint angles and moments.
For example, in the trials conducted with the athlete MC, markers on the posterior iliac spines were placed too high with respect to their real anatomical position, possibly due to the presence of the safety harness and of the elastic rope used in RAR, which limited the space available for markers on the pelvis. As a consequence, pelvis tilt, hip angles and hip moments resulted in not accurate values.
During the second test session, with athlete AS, as the athlete changed socket alignment, static trials have been performed without placing the whole markerset on the subject. While for the unaffected limb this problem has been easily solved through the "solidification" procedure, for the affected limb it was difficult to reconstruct the location of the marker placed medially on the socket. This marker is essential to define the socket local CS, which is then employed in the calculation of hip angle and influences also knee angle.
Moreover, static trials have not been performed with the athlete having the prosthetic limb completely extended, therefore some angles show an offset which could be misleading in the interpretation of the results.

Another limitation is related to the instrumentation setup. Athletes were not used to run on a treadmill, so their running speed was lower than the speed they usually reach during overground running and their acceleration style was completely different from what they usually do in sprinting. This is a common problem in many research works, which are based on biomechanics measurements collected in a controlled environment, such as a laboratory, where the conditions are quite different from a real competition. For this reason, the direct association of biomechanical parameters with performance are difficult to obtain.
In the case of this work, differences observed with varying socket alignment cannot be directly attributed to better or worse performance, but perhaps rather to a training effect. The more athletes get used to running on the treadmill, the more their kinematic and kinetic parameters may improve, even regardless of the prosthesis alignment.

Additional constraint to an extended results discussion is related to the reduced amount of trials data processed. This is mainly due to the very time-consuming pre-processing step, consisting in the markers labelling. In the acquisitions relative to the first and second test sessions, markers trajectories resulted very discontinuous and vibrating, possibly due to the limited number of MoCap cameras or to the presence of the external frame of the treadmill, which impaired the view of some markers. Therefore, the time required to prepare data has been longer than expected. For instance, to complete the labelling procedure of a RAR test, it takes about 3-4 days.

Due to time lack, the inertial properties of the prosthesis components have not been estimated and included in the calculation of joint moments. For this reason, joint moments of the left side are obtained with the simplified method only.

Future Developments

Uncertainties in the calculation of the Centre of Pressure have been solved with the assumption that the COP corresponds to a marker on the foot. However, this way the oscillations of the real centre of pressure in the foot area are neglected, which means that the results for Roll over Shape and joint moments cannot be considered fully correct.
For what concerns treadmill tests, a revised calculation method could bring to more accurate results and for the track tests, the estimation the bidimensional trajectory of the COP from load cell force data can be implemented.

Calibration matrix and correction factors used to decouple the signals from the wearable load cell still needs some revising. Definitive validation of the data acquired through wearable sensors could be done once the athlete will run with the same equipment over a force platform placed on the ground. Data from platforms and from load cell should then match.

Once the moment of inertia of the socket, pylon, knee and prosthetic foot are known, calculation of moments through the Inverse Dynamics method can be then carried out. The calculation will also consider the different thigh mass and length of the affected limb compared to that of the unaffected limb, because atrophy resulting from amputation makes the residual thigh weigh less than the healthy thigh. In addition to joint moments, also joint power can be calculated. Power of the prosthetic knee in swing phase can be a useful parameter which could enable better adjustments of the level of friction of the mechanical components.

The mechanics of maximum constant speed running are different from those in the acceleration phase. While for steady state running average value across a set of steps can be considered representative of the whole performance, in accelerated running, either on treadmill or on track, each step has to be considered independently, therefore it is difficult to compare trials, either of the same athlete or of different athletes. It would be useful to find a statistical index or a parameter representative of the kinematic quantities in such tests, which could be easily used for comparisons.

Regarding RAR tests, the results obtained in treadmill tests are not applicable to actual sprinting in a competitive setting. To fill this gap, the design of an inertial treadmill has already begun, which consists in a system of modular elements allowing the adjustments of the inertia of the treadmill depending on the mass of the athlete running on it. This way, the treadmill could better simulate the actual force generated on track and, if placed on force platforms, it could be used as a test bench to evaluate performance.

Additional research ideas, which would complete the kinematic analysis implemented up to now, include the investigation of the movement of the arms to assess their role in optimizing energy expenditure and in acting as a counterbalance for the rotating lower extremities. Moreover, data collected by the instrumented starting blocks could be processed and the resulting information coupled with the outcomes of the analysis of Reaction Forces from load cell.

In the end, the study of differences between TF and TT athlete can be carried out. Using the available data, it will be possible to compare kinematic quantities only, as the MM athlete had no wearable sensors during the test session at Palaindoor.

Conclusions

The aim of this work was the analysis of the biomechanics of running in elite Paralympic sprinters, in order to investigate the differences between the types of tests performed, the running surface and the socket alignment.

The study is based on two indoor test sessions and on one outdoor test session, which were carried out in collaboration with INAIL, in the context of the OLIMPIA project.

During the indoor sessions, two Paralympic medallists Martina Caironi (T63) and Ambra Sabatini (T63) performed running trials on a treadmill placed on four force platforms and surrounded by Motion Capture cameras. They used four different socket alignments and for each alignment they performed two types of tests: steady state running, with the treadmill set at a constant target speed, and resisted accelerated running, with the treadmill put in passive mode and the athletes running from still condition.

During the outdoor test, athlete Ambra Sabatini ran overground in an indoor athletics track. She performed two types of tests: steady state running, with the athlete self-regulating her running speed, and sprint starts from blocks. Measurement systems consisted in Motion Capture cameras place all along the running lane, a wearable loadcell and an inertial sensor mounted on the prosthesis and connected to a portable data logger placed in a running backpack worn by the athlete. During the same test session, athlete Maxcell Amo Manu (T64) also participated, but analysis of data relative to his trials has yet to be carried out.

Kinematic and kinetic data have been collected and then processed through the custom-made software tool implemented in MATLAB.

Regarding types of running tests, it was observed that in acceleration tests Ground Reaction Forces are lower in magnitude if compared to constant speed tests, but the horizontal impulses are always positive, thus meaning that there is no braking effect. In both tests, the unaffected limb generated higher vertical GRFs than the affected limb, in agreement with several similar results in the literature. In SSR tests the sound limb produced greater braking horizontal forces than the prosthetic limb, which in turn had a positive net horizontal impulse.

Comparisons between kinematic results obtained from the treadmill and track tests show that when athlete runs overground, limbs have wider range of motion and therefore greater peaks in joint angles. Furthermore, joint moments in the prosthetic limb are more than 10 times higher in the track tests than in treadmill tests, possibly due to the higher force generated, but more in-depth analyses are needed in order to validate these results.

Different socket alignments induced variations in the impulses of the GRF, either vertical or horizontal. The increment in the horizontal propulsive impulse from A0 to A2 and the

decrement of the vertical impulse from A0 to A2 confirm what has been found in previous research works. There is also consistency with respect to knee moment values, which decrease as alignment increases.

Among the limitations of this work there is the quantity of trials data elaborated, which is too scarce to enable a significant statistical analysis. Moreover, errors in the experimental procedure and in the data processing may have introduced bias in the results, which will need to be revised. Once the errors of the analysis tool have been corrected, further data can be processed, which will allow further comparisons and the extraction of concise and effective descriptive parameters of running performance.

BIBLIOGRAPHY

[1] 'Inail.it'. https://www.inail.it/cs/internet/home.html

[2] 'Inail Centro Protesi'. https://www.inail.it/cs/internet/attivita/prestazioni/centro-protesi-vigorso-di-budrio/ricerca-e-sperimentazione.html (accessed Jul. 01, 2022).

[3] Y. Namiki, S. Hashizume, A. Murai, Y. Kobayashi, H. Takemura, and H. Hobara, 'Joint moments during sprinting in unilateral transfemoral amputees wearing running-specific prostheses', *Biol. Open*, vol. 8, no. 2, 2019, doi: 10.1242/bio.039206.

[4] R. Williams, K, 'The Dynamics of Running', in *Biomechanics in Sport*, V. M. Zatsiorsky, Ed. Oxford, UK: Blackwell Science Ltd, 2000, pp. 161–183. doi: 10.1002/9780470693797.

[5] T. F. Novacheck, 'The biomechanics of running', *Gait Posture*, vol. 7, no. 1, pp. 77–95, Jan. 1998, doi: 10.1016/S0966-6362(97)00038-6.

[6] D. Richards, Jim, *Biomechanics in Clinic and Research*, 1st ed. Churchill Livingstone, London, 2008. [Online]. Available: https://www.researchgate.net/publication/234166805_Biomechanics_in_Clinic_and_Research

[7] G. Wu *et al.*, 'ISB recommendation on definitions of joint coordinate system of various joints for the reporting of human joint motion - Part I: Ankle, hip, and spine', *J. Biomech.*, vol. 35, no. 4, pp. 543–548, 2002, doi: 10.1016/S0021-9290(01)00222-6.

[8] T. R. Derrick, A. J. van den Bogert, A. Cereatti, R. Dumas, S. Fantozzi, and A. Leardini, 'ISB recommendations on the reporting of intersegmental forces and moments during human motion analysis', *J. Biomech.*, vol. 99, Jan. 2020, doi: 10.1016/J.JBIOMECH.2019.109533.

[9] H. Hobara *et al.*, 'Amputee locomotion: Spring-like leg behavior and stiffness regulation using running-specific prostheses', *J. Biomech.*, vol. 46, no. 14, pp. 2483–2489, Sep. 2013, doi: 10.1016/j.jbiomech.2013.07.009.

[10] R. J. Butler, H. P. Crowell, and I. M. Davis, 'Lower extremity stiffness: implications for performance and injury', *Clin. Biomech.*, vol. 18, no. 6, pp. 511–517, Jul. 2003, doi: 10.1016/S0268-0033(03)00071-8.

[11] F. Gondoni, 'Valutazione comparativa dei modelli per la stima di vertical e leg stiffness durante la corsa', *Master Thesis Biomedical. Engineering. Politecnico di Milano*, 2020.

[12] 'Ottobock.com Reasons for amputating'. https://www.ottobock.africa/en/your-individual-fitting/lower-limb/info-for-lower-limb-amputees/before-the-amputation/amputation-causes (accessed Aug. 01, 2022).

[13] 'MedlinePlus.gov Leg or foot amputation'. https://medlineplus.gov/ency/article/007365.htm (accessed Aug. 01, 2022).

[14] 'Agenzia Nazionale per i Servizi Sanitari Regionali. Programma Nazionale Esiti'. https://pne.agenas.it/risultati/tipo4/tab_aslT4.php?ind=59&tipo=4&area= (accessed Jul. 01, 2022).

[15] C. S. Molina and J. Faulk, *Lower Extremity Amputation*. 2022. [Online]. Available: http://www.ncbi.nlm.nih.gov/pubmed/31536201

[16] 'PamHealth.com Life after amputation: What to expect fot the new amputee'. https://pamhealth.com/company/company-updates/life-after-amputation-what-to-expect-for-the-new-amputee (accessed Aug. 01, 2022).

[17] D. Matthews, M. Sukeik, and F. Haddad, 'Return to sport following amputation.', *J. Sports Med. Phys. Fitness*, vol. 54, no. 4, pp. 481–6, Aug. 2014, [Online]. Available: http://www.ncbi.nlm.nih.gov/pubmed/25034549

[18] 'AccessiWay.com Le categorie e le classificazioni degli atleti con disabilità alle Paralimpiadi'.

https://www.accessiway.com/blog/le-categorie-e-le-classificazioni-degli-atleti-con-disabilita-alle-paralimpiadi (accessed Aug. 01, 2022).

[19] 'Paralympic.org Classification in Para Athletics'.

[20] 'Paralympics.org.uk Para athletics'. https://paralympics.org.uk/sports/para-athletics (accessed Sep. 01, 2022).

[21] B. Baum, 'Running after lower extremity amputation with daily-use and running-specific prostheses: A review of biomechanics outcomes', vol. 23, pp. 121–130, Feb. 2020.

[22] 'Hangerclinic.com Lower Limb Prosthetics'. https://hangerclinic.com/prosthetics/lower-limb/prosthetic-feet/sach-feet/ (accessed Oct. 01, 2022).

[23] H. Hobara *et al.*, 'Amputee locomotion: Lower extremity loading using running-specific prostheses', *Gait Posture*, vol. 39, no. 1, pp. 386–390, Jan. 2014, doi: 10.1016/j.gaitpost.2013.08.010.

[24] A. Gri, 'The effect of socket alignment on the running performance of elite Paralympic athletes during indoor and outdoor tests using an instrumented Running Prosthetic Foot', *Master Thesis Mechanical Engineering Universtità degli Studi di Padova*, 2019.

[25] 'Paralympic.org General rules and regulations'. https://www.paralympic.org/athletics/rules (accessed Nov. 01, 2022).

[26] 'Physiopedia.com Lower Limb Prosthetic Sockets and Suspension Systems'. https://www.physio-pedia.com/Lower_Limb_Prosthetic_Sockets_and_Suspension_Systems (accessed Oct. 01, 2022).

[27] 'Amputeecoalition.org Prosthetic knee systems'. https://www.amputee-coalition.org/resources/prosthetic-knee-systems/ (accessed Nov. 13, 2022).

[28] 'ProstheticRunning.com Running Prostheses'. https://www.prostheticrunning.com/runningprostheses (accessed Oct. 01, 2022).

[29] J. R. Tacca, O. N. Beck, P. Taboga, and A. M. Grabowski, 'Running-specific prosthesis model, stiffness and height affect biomechanics and asymmetry of athletes with unilateral leg amputations across speeds', *R. Soc. Open Sci.*, vol. 9, no. 6, Jun. 2022, doi: 10.1098/rsos.211691.

[30] F. Hadj-Moussa, C. C. Ngan, and J. Andrysek, 'Biomechanical factors affecting individuals with lower limb amputations running using running-specific prostheses: A systematic review', *Gait Posture*, vol. 92, no. October 2021, pp. 83–95, 2022, doi: 10.1016/j.gaitpost.2021.10.044.

[31] P. Taboga, E. K. Drees, O. N. Beck, and A. M. Grabowski, 'Prosthetic model, but not stiffness or height, affects maximum running velocity in athletes with unilateral transtibial amputations', *Sci. RepoRtS* |, vol. 10, p. 1763, 2020, doi: 10.1038/s41598-019-56479-8.

[32] G. L. Migliore *et al.*, 'Innovative alignment of sprinting prostheses for persons with transfemoral amputation: Exploratory study on a gold medal Paralympic athlete', *Prosthetics Orthot. Int.*, vol. 45, no. 1, pp. 46–53, Feb. 2021, doi: 10.1177/0309364620946910.

[33] 'List of world records in athletics'. https://en.wikipedia.org/wiki/List_of_world_records_in_athletics (accessed Oct. 01, 2022).

[34] 'List of IPC world records in athletics'. https://en.wikipedia.org/wiki/List_of_IPC_world_records_in_athletics (accessed Oct. 01, 2022).

[35] A. M. Grabowski, C. P. McGowan, W. J. McDermott, M. T. Beale, R. Kram, and H. M. Herr, 'Running-specific prostheses limit ground-force during sprinting', *Biol. Lett.*, vol. 6, no. 2, pp. 201–204, Apr. 2010, doi: 10.1098/rsbl.2009.0729.

[36] A. M. Grabowski, C. P. McGowan, W. J. McDermott, M. T. Beale, R. Kram, and H. M. Herr, 'Running-specific prostheses limit ground-force during sprinting', *Biol. Lett.*, vol. 6, no. 2, pp. 201–204, 2010, doi: 10.1098/rsbl.2009.0729.

[37] L. A. Sepp, B. S. Baum, E. Nelson-Wong, and A. K. Silverman, ‘Dynamic balance during running using running-specific prostheses’, *J. Biomech.*, vol. 84, pp. 36–45, Feb. 2019, doi: 10.1016/j.jbiomech.2018.12.016.

[38] P. Taboga, E. K. Drees, O. N. Beck, and A. M. Grabowski, ‘Prosthetic model, but not stiffness or height, affects maximum running velocity in athletes with unilateral transtibial amputations’, *Sci. Rep.*, vol. 10, no. 1, Dec. 2020, doi: 10.1038/s41598-019-56479-8.

[39] A. Makimoto *et al.*, ‘Ground reaction forces during sprinting in unilateral transfemoral amputees’, *J. Appl. Biomech.*, vol. 33, no. 6, pp. 406–409, Dec. 2017, doi: 10.1123/jab.2017-0008.

[40] Y. Namiki, S. Hashizume, A. Murai, Y. Kobayashi, H. Takemura, and H. Hobara, ‘Joint moments during sprinting in unilateral transfemoral amputees wearing running-specific prostheses’, *Biol. Open*, vol. 8, no. 2, Feb. 2019, doi: 10.1242/BIO.039206.

[41] R. Nagahara, M. Mizutani, A. Matsuo, H. Kanehisa, and T. Fukunaga, ‘Association of sprint performance with ground reaction forces during acceleration and maximal speed phases in a single sprint’, *J. Appl. Biomech.*, vol. 34, no. 2, pp. 104–110, Apr. 2018, doi: 10.1123/jab.2016-0356.

[42] H. Sakata, S. Hashizume, H. Takemura, and H. Hobara, ‘Braking And Propulsive Impulses Across A Range Of Running Speeds In Unilateral Transfemoral Amputees’. [Online]. Available: https://commons.nmu.edu/isbs/vol37/iss1/15

[43] N. Petrone *et al.*, ‘Collection of Structural Loads Acting on Instrumented Running Specific Prostheses during Field Tests on Elite Atletes’, Jun. 2020, p. 74. doi: 10.3390/proceedings2020049074.

[44] N. Petrone *et al.*, ‘Development of instrumented running prosthetic feet for the collection of track loads on elite athletes’, *Sensors (Switzerland)*, vol. 20, no. 20, pp. 1–18, Oct. 2020, doi: 10.3390/s20205758.

[45] N. Petrone, G. Costa, G. Foscan, F. Bettella, G. Migliore, and A. G. Cutti, ‘Conceptual Design of a New Multi-Component Test Bench for the Dynamic Characterization of Running Specific Prostheses’, Jun. 2020, p. 75. doi: 10.3390/proceedings2020049075.

[46] R. S. Alcantara, W. B. Edwards, G. Y. Millet, and A. M. Grabowski, ‘Predicting continuous ground reaction forces from accelerometers during uphill and downhill running: a recurrent neural network solution’, *PeerJ*, vol. 9, Jan. 2022, doi: 10.7717/peerj.12752.

[47] ‘Futurelearn.com Motion Capture Course’. https://www.futurelearn.com/info/courses/motion-capture-course/0/steps/272019

[48] V. Cavedon, M. Sandri, M. Pirlo, N. Petrone, C. Zancanaro, and C. Milanese, ‘Anthropometry-driven block setting improves starting block performance in sprinters.’, *PLoS One*, vol. 14, no. 3, p. e0213979, 2019, doi: 10.1371/journal.pone.0213979.

[49] G. Wu and P. R. Cavanagh, ‘ISB recommendations for standardization in the reporting of kinematic data’, *J. Biomech.*, vol. 28, no. 10, pp. 1257–1261, 1995, doi: 10.1016/0021-9290(95)00017-C.

[50] D. Mandalidis, G. Glakousakis, and P. Kalatzis, ‘An anthropometric-based method for the assessment of pelvis position in three-dimensional space’, *MethodsX*, vol. 9, p. 101616, 2022, doi: 10.1016/j.mex.2022.101616.

[51] ‘Human Gait and Clinical Movement Analysis - Figure’. https://www.researchgate.net/figure/The-types-of-motion-in-the-three-anatomical-planes-a-sagittal-plane-motion-pelvic_fig16_301935875 (accessed Nov. 10, 2022).

[52] E. S. Grood and W. J. Suntay, ‘A Joint Coordinate System for the Clinical Description of Three-Dimensional Motions: Application to the Knee’, *J. Biomech. Eng.*, vol. 105, no. 2, pp. 136–144, May 1983, doi: 10.1115/1.3138397.

APPENDIX

Appendix A: List of Acronyms

AB: Able-bodied

AL: Affected Limb

AP: Anterior-Posterior

CNS: Central Nervous System

COM: Centre of Mass

COP: Centre of Pressure

CS: Coordinate System

FEM: Finite Element Model

GRF: Ground Reaction Force

GT: Greater Trochanter

HJC: Hip Joint Centre

ILEA: Individual with Lower Extremity Amputation

JCS: Joint Coordinate System

KD: Knee Disarticulated

ML: Medial-Lateral

NAS: Non-Amputee Sprinters

OS: Olimpia Session

RAR: Resisted Accelerated Running

ROM: Range of Motion

RPF: Running Prosthetic Foot

RSP: Running Specific Prosthesis

RQ: Research Question

SSR: Steady State Running

TF/TFA: Transfemoral/ Transfemoral Amputee

TT/TTA: Transtibial/ Transtibial Amputee

UL: Unaffected Limb

V: Vertical

Appendix B: Markerset

The full markerset used in the three Olimpia Sessions is listed below. This markerset is applicable to transfemoral amputee only, while the markerset used for transtibial athletes is not reported, because trials relative to TT athlete have not been processed yet.

The column 'Marker Label' has been subdivided into two parts: on the left the markers used during OS1/OS2 and on the right the markers used in OS3. In some cases, also the acronym of the subject is reported to indicate that a marker has been used only for the specific athlete.

The symbol '<x>' stands for 'side', so to have the complete name of the marker, 'L' or 'R' must be added.

In the fourth column, those markers which are applied only in static are marked with 'X', while those points which are identified through wand calibration are marked with 'W'.

Body	**Marker Label**		Marker type	Static	Description
	OS1/2	OS3			
Head	H1	H1	Technical		Frontal
	H2	H2	Technical		Lateral right
	H3	H3	Technical		Posterior occipital extreme
	H4	H4	Technical		Lateral left
	NASION	NB	Anatomical	X	Frontal bone glabella
	CHIN	CH	Anatomical	X	Chin protuberance
	JAW	JB	Anatomical	X	Left jaw bone
		<x>AM	Anatomical	W	Acoustic meatus
Trunk	IJ	IJ	Anatomical		Jugular Notch
	PX	PX	Anatomical	W	Xiphoid Process
	T8	T8	Anatomical	X	8th Thoracic vertebra
	C7	C7	Anatomical	X	7th Cervical vertebra
		<x>TPZ	Anatomical		Base of the neck
Arm	AC<x>	<x>AC	Anatomical		Acromion
	EL<x>	<x>HLE	Anatomical		Humerus Lateral epicondyle
	HA<x>	<x>MSS	Anatomical		Midpoint of the lateral and medial styloids of the forearm
	HM3<x>		Anatomical		Third Metacarpal Head
Pelvis	<x>ASIS	<x>ASIS	Anatomical		Antero-Superior Iliac Spine
	<x>PSIS	<x>PSIS	Anatomical	X	Postero-Superior Iliac Spine
	<x>HJC	<x>HJC	Virtual		Hip joint center
		<x>PEL	Technical		Technical marker on lateral aspect of pelvis
Thigh (UL)	GT<x>	<x>GT	Anatomical		Great trochanter
	FLE<x>	<x>FLE	Anatomical		Femur lateral epicondyle
	FME<x>	<x>FME	Anatomical	X	Femur medial epicondyle
	T1<x>	<x>T1	Technical		Proximally lateral axis of the thigh
	T2<x>	<x>T2	Technical		Distally lateral axis of the thigh
	T3<x>	<x>T3	Technical		Proximally posterior axis of the thigh
		<x>T4	Technical		Distally posterior axis of the thigh
Shank (UL)	TT<x>	<x>TT	Anatomical		Tibial Tuberosity
	HF<x>	<x>HF	Anatomical		Head of Fibula
	LM<x>	<x>LM	Anatomical		Lateral Malleolus
	MM<x>	<x>MM	Anatomical	X	Medial Malleolus
	SH1<x>	<x>SH1	Technical		Technical marker on the mid shank
Socket-TF	S2<x>	<x>FAP	Technical		Proximally frontal axis of the socket

	S4<x>	<x>FAD	Technical		Distally frontal axis of the socket
	S1<x>	<x>LAP	Technical		Proximally lateral axis of the socket
	S3<x>	<x>LAD	Technical		Distally lateral axis of the socket
		<x>PAP	Technical		Proximally posterior axis of the socket
		<x>PAD	Technical		Distally posterior axis of the socket
	FME<x>		Technical	X	Femur medial epicondyle (on the socket).
	FLE<x>		Technical		Femur lateral epicondyle (on the socket).
	MIDDLE SOCKET		Technical		Midpoint between two femoral epicondyles
	GT<x>	<x>GT	Anatomical		Great trochanter
	KL<x>	<x>KL	Mechanical		Placed laterally on the prosthetic knee center of rotation
	KM<x>	<x>KM	Mechanical		Placed medially on the prosthetic knee center of rotation
		<x>WAM	Mechanical	W	Screw of the socket connector – antero-medial
		<x>WAL	Mechanical	W	Screw of the socket connector – antero-lateral
		<x>WPM	Mechanical	W	Screw of the socket connector – postero-medial
		<x>WPL	Mechanical	W	Screw of the socket connector – postero-lateral
Load Cell-TF		<x>LO1	Mechanical	W	Load cell: lateral
		<x>LO2	Mechanical	W	Load cell: anterior
		<x>LO3	Mechanical	W	Load cell: medial
		<x>LO4	Mechanical	W	Load cell: posterior
Clamp-TF	FP3(AS)	<x>CLL	Mechanical		Clamp: lateral
		<x>CLA	Mechanical	W	Clamp: anterior
	FP2 (AS)	<x>CLM	Mechanical		Clamp: medial
		<x>CLP	Mechanical	W	Clamp: posterior
Foot (UL)	CA<x>	<x>CA	Anatomical		Posterior aspect of calcaneus, just below the Achille's tendon insertion
	IMH <x>	<x>IMH	Anatomical	X	Head of the first metatarsal head
	IIMH<x>	<x>IIMH	Anatomical		Head of the second metatarsal head
	VMH<x>	<x>VMH	Anatomical		Head of the fifth metatarsal head
	F1<x>	<x>F1	Technical		On the proximal-lateral side of the midfoot
Proximal Foot	FP1	<x>FPA	Technical		Foot proximal anterior - Placed as anteriorly as possible on the mid-line of the prosthetic foot
	FP4 (AS)	<x>FPP	Technical		Foot proximal posterior - Placed posterior to the clamp on the mid-line of the prosthetic foot
	FP2 (MC)	<x>FP1	Technical		Placed on a T-frame clamped to the prosthetic foot, proximally to clamp.
	FP3 (MC)	<x>FP2	Technical		Placed on a T-frame clamped to the prosthetic foot, distally to clamp on the same line of FP1.
	FP4 (MC)	<x>FP3	Technical		Placed on a T-frame clamped to the prosthetic foot, perpendicularly downwards to the line joining FP1 and FP2.
Technical Foot		<x>FM1	Technical		Placed on the bending midpoint
		<x>FM2	Technical		Placed on the first distal bending curve
		<x>FM3	Technical		Midpoint between FM1 and FM2
Distal Foot	FD1	<x>FD1	Technical		The most distal point (tip) of the prosthetic foot
	FD2	<x>FD2	Technical		Placed medially on the foot tip
	FD3	<x>FD3	Technical		Placed laterally on the foot tip

The graphical representation of the markerset can be visualised in the figure below. In detail, it refers to the markerset employed in OS3 with the athlete Ambra Sabatini, but it is useful for the identification of markers location relative to OS1 and OS2 too, with appropriate changes to labels.

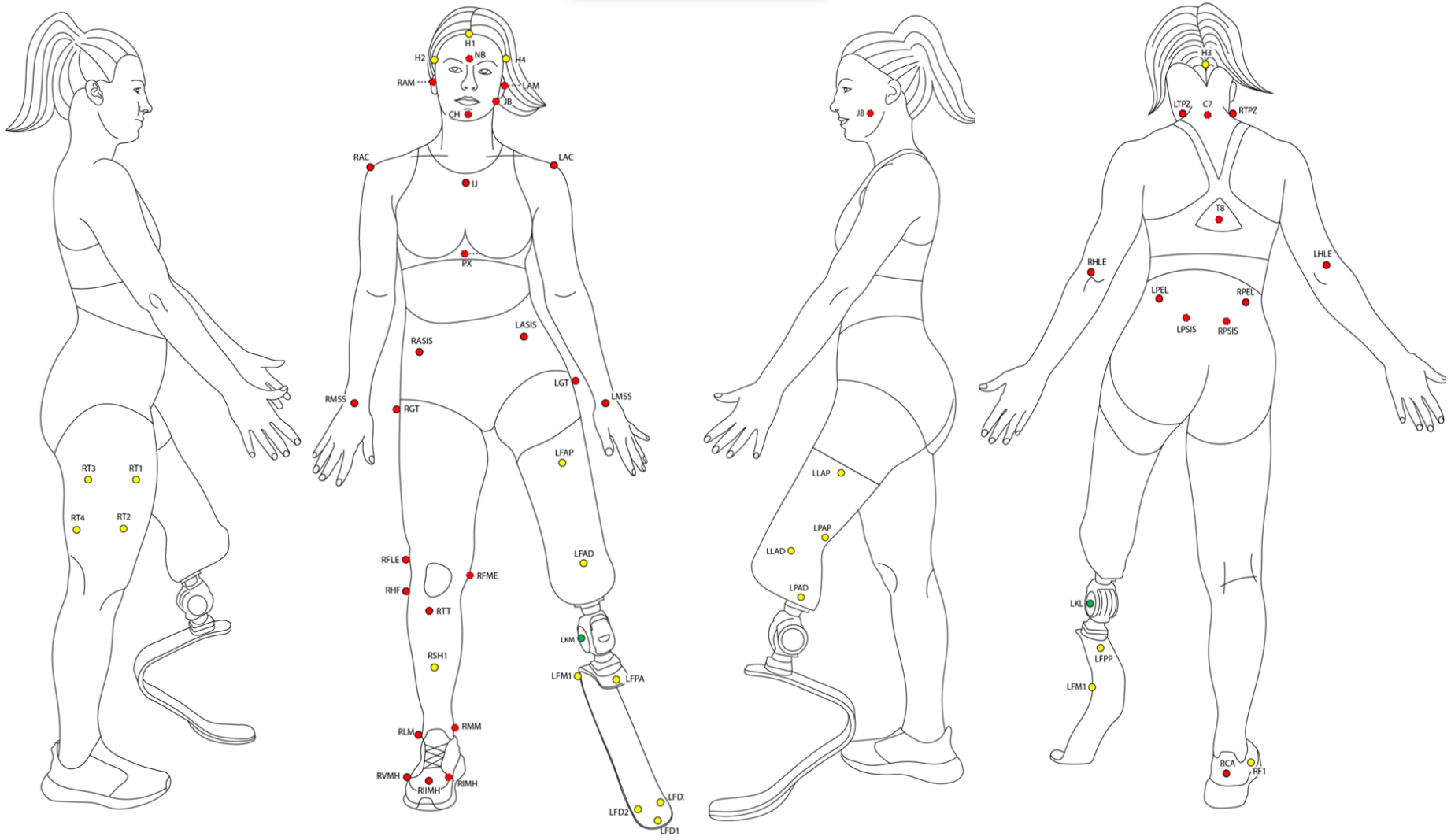
RT3
RT1
RT4
RT2
H1
H2
NB
H4
RAM
LAM
JB
CH
RAC
LAC
IJ
PX
LASIS
RASIS
LGT
RMSS
LMSS
RGT
LFAP
RFLE
RFME
RHF
RTT
RSH1
LKM
LFM1
LFPA
RLM
RMM
RVMH
RIMH
RIIMH
LFD
LFD2
LFD1
JB
LLAP
LPAP
LLAD
LPAD
H3
LTPZ
C7
RTPZ
T8
RHLE
LHLE
LPEL
RPEL
LPSIS
RPSIS
LKL
LFPP
LFM1
RCA
RF1

Appendix C: Coordinate Systems

The description of the reference systems used for the kinematic analysis is here provided. Graphical representation of the CS can be found in Figure 5.5 and Figure 5.6 of Chapter 5.

PELVIS

Axis/point	Formula	Description
$^{G}\hat{\boldsymbol{z}}_{\boldsymbol{pl}}$	$\frac{RASI - LASI}{\|RASI - LASI\|}$	Directed from LASI to RASI
$\boldsymbol{SACR}$	$\frac{LPSI + RPSI}{2}$	Midpoint between LPSI and RPSI
$^{G}\boldsymbol{O}_{\boldsymbol{pl}}$	$\frac{LASI + RASI}{2}$	Midpoint between LASI and RASI
$^{G}\hat{\boldsymbol{x}}_{\boldsymbol{temp}}$	$O_1 - SACR$	Directed from SACR to the $^{G}O_{pl}$
$^{G}\hat{\boldsymbol{y}}_{\boldsymbol{pl}}$	$\frac{^{G}\hat{z}_{pl} \times {}^{G}\hat{x}_{temp}}{\|{}^{G}\hat{z}_{pl} \times {}^{G}\hat{x}_{temp}\|}$	Perpendicular to the plane defined by LASI, RASI and SACR, pointing upward
$^{G}\hat{\boldsymbol{x}}_{\boldsymbol{pl}}$	$^{G}\hat{y}_{pl} \times {}^{G}\hat{z}_{pl}$	

THIGH

Axis/point	Formula	Description
$^{G}\boldsymbol{O}_{\boldsymbol{th}}$	$\frac{FLE + FME}{2}$	Midpoint between FLE and FME
$^{G}\hat{\boldsymbol{y}}_{\boldsymbol{th}}$	$\frac{HJC - {}^{G}O_{th}}{\|HJC - {}^{G}O_{th}\|}$	Vertical axis, joining the $^{G}O_{th}$ to the HJC
$^{G}\hat{\boldsymbol{x}}_{\boldsymbol{th}}$	$\frac{^{G}\hat{y}_{th} \times (FLE - FME)}{\|{}^{G}\hat{y}_{th} \times (FLE - FME)\|}$	Perpendicular to the plane defined by HJC, FLE, and FME, pointing forward (to be adapted for left and right sides – the formula is for right prosthetic limb)
$^{G}\hat{\boldsymbol{z}}_{\boldsymbol{th}}$	$^{G}\hat{x}_{th} \times {}^{G}\hat{y}_{th}$	

SHANK

Axis/point	Formula	Description
$^{G}\boldsymbol{O}_{\boldsymbol{tb}}$	$\frac{LM + MM}{2}$	Midpoint between
$^{G}\hat{\boldsymbol{x}}_{\boldsymbol{tb}}$	$\frac{(HF - {}^{G}O_{tb}) \times (LM - MM)}{\|(HF - {}^{G}O_{tb}) \times (LM - MM)\|}$	Perpendicular to the plane defined by LM, MM and HF, pointing forward (to be adapted for left and right sides – the formula is for right prosthetic limb)
$^{G}\hat{\boldsymbol{z}}_{\boldsymbol{tb}}$	$\frac{^{G}\hat{x}_{tb} \times (TT - {}^{G}O_{tb})}{\|{}^{G}\hat{x}_{tb} \times (TT - {}^{G}O_{tb})\|}$	Perpendicular to the plane defined by $^{G}\hat{x}_{tb}$ and the line joining the $^{G}O_{tb}$ to TT, pointing rightward (to be adapted for left and right sides – the formula is for right prosthetic limb)
$^{G}\hat{\boldsymbol{y}}_{\boldsymbol{tb}}$	$^{G}\hat{z}_{tb} \times {}^{G}\hat{x}_{tb}$	

SOCKET OS1/OS2

Axis/point	Formula	Description
$^{G}\boldsymbol{O}_{\boldsymbol{sk}}$	$\frac{MDM + MDL}{2}$	Midpoint between MDM and MDL
$^{G}\hat{\boldsymbol{y}}_{\boldsymbol{sk}}$	$\frac{HJC - {}^{G}O_{sk}}{\|HJC - {}^{G}O_{sk}\|}$	Directed from $^{G}O_{sk}$ to HJC
$^{G}\hat{\boldsymbol{z}}_{\boldsymbol{temp}}$	$\frac{MDL - MDM}{\|MDL - MDM\|}$	On the line joining MDM to MDL, pointing rightward (to be adapted for left and right sides – the formula is for right prosthetic limb)

${}^{G}\hat{x}_{sk}$	$\frac{{}^{G}\hat{y}_{sk} \times {}^{G}\hat{z}_{temp}}{\left\| {}^{G}\hat{y}_{sk} \times {}^{G}\hat{z}_{temp} \right\|}$	Perpendicular to the plane defined by HJC, MDM and MDL, pointing forward
${}^{G}\hat{z}_{sk}$	${}^{G}\hat{x}_{sk} \times {}^{G}\hat{y}_{sk}$	

SOCKET OS3

Axis/point	Formula	Description
${}^{G}O_{sp}$	$\frac{WAL + WAM + WPL + WPM}{4}$	Center of gravity of the points WAL, WAM, WPL and WPM
${}^{G}\hat{y}_{sp}$	$\frac{(WAL - WPM) \times (WAM - WPM)}{\|(WAL - WPM) \times (WAM - WPM)\|}$	Perpendicular to the plane defined by WAL, WAM and WPM
${}^{G}\hat{z}_{temp}$	$\frac{WAL - WAM}{\|WAL - WAM\|}$	On the line joining WAL and WAM, pointing rightward
${}^{G}\hat{x}_{sp}$	$\frac{{}^{G}\hat{y}_{sp} \times {}^{G}\hat{z}_{temp}}{\left\| {}^{G}\hat{y}_{sp} \times {}^{G}\hat{z}_{temp} \right\|}$	Perpendicular to the plane defined by ${}^{G}\hat{y}_{sp}$ and the line joining WAL and WAM, pointing forward
${}^{G}\hat{z}_{sp}$	${}^{gnd}\hat{x}_{sp} \times {}^{gnd}\hat{y}_{sp}$	

PROSTHETIC KNEE

Axis/point	Formula	Description
${}^{G}O_{knee}$	$\frac{KM + KL}{2}$	Midpoint between KM and KL
${}^{G}\hat{z}_{knee}$	$\frac{KL - KM}{\|KL - KM\|}$	True axis of knee flexion/extension. On the line joining KM to KL, pointing rightward (to be adapted for left and right sides – the formula is for right prosthetic knee).
${}^{G}\hat{y}_{temp}$	$\frac{HJC - {}^{G}O_{knee}}{\left\|HJC - {}^{G}O_{knee}\right\|}$	Directed from ${}^{G}O_{knee}$ to HJC
${}^{G}\hat{x}_{knee}$	$\frac{{}^{G}\hat{y}_{temp} \times {}^{G}\hat{z}_{knee}}{\left\| {}^{G}\hat{y}_{temp} \times {}^{G}\hat{z}_{knee} \right\|}$	Perpendicular to the plane defined by HJC, KM and KL, pointing forward
${}^{G}\hat{y}_{knee}$	${}^{G}\hat{z}_{knee} \times {}^{G}\hat{x}_{knee}$	

DISTAL FUNCTIONAL KNEE

It is the same as Prosthetic knee, but centred in FP1 or in midpoint between LO1, LO2, LO3, LO4

LOAD CELL

Axis/point	Formula	Description
${}^{G}O_{lc}$	$\frac{LO1 + LO2 + LO3 + LO4}{4}$	Center of mass of the load-cell markers
${}^{G}\hat{z}_{temp}$	$\frac{LO1 - LO3}{\|LO1 - LO3\|}$	On the line joining LO1 and LO3, pointing rightward (to be adapted for left and right sides – the formula is for right prosthetic limb).
${}^{G}\hat{y}_{lc}$	$\frac{{}^{gnd}\hat{z}_{temp} \times (LO2 - LO1)}{\left\| {}^{gnd}\hat{z}_{temp} \times (LO2 - LO1) \right\|}$	Perpendicular to the plane defined by LO1, LO2 and LO3
${}^{G}\hat{x}_{lc}$	$\frac{{}^{G}\hat{y}_{lc} \times {}^{G}\hat{z}_{temp}}{\left\| {}^{G}\hat{y}_{lc} \times {}^{G}\hat{z}_{temp} \right\|}$	Perpendicular to ${}^{G}\hat{y}_{lc}$ and the line joining LO1 and LO2, pointing forward
${}^{G}\hat{z}_{lc}$	${}^{G}\hat{x}_{lc} \times {}^{G}\hat{y}_{lc}$	

CLAMP

Axis/point	Formula	Description
${}^{G}\boldsymbol{O_{cl}}$	$\frac{CLA + CLL + CLM + CLP}{4}$	Center of mass of the clamp markers
${}^{G}\hat{\boldsymbol{z}}_{\boldsymbol{temp}}$	$\frac{CLL - CLM}{\|CLL - CLM\|}$	On the line joining CLL to CLM, pointing laterally
${}^{G}\hat{\boldsymbol{y}}_{\boldsymbol{cl}}$	$\frac{{}^{G}\hat{\boldsymbol{z}}_{\boldsymbol{temp}} \times (CLA - CLM)}{\|{}^{G}\hat{\boldsymbol{z}}_{\boldsymbol{temp}} \times (CL2 - CLM)\|}$	Perpendicular to the plane defined by ${}^{G}\hat{y}_{cl}$ and the line joining CLA and CLM, pointing upward (to be adapted for left and right sides – the formula is for right prosthetic foot)
${}^{G}\hat{\boldsymbol{z}}_{\boldsymbol{cl}}$	${}^{G}\hat{y}_{cl} \times {}^{G}\hat{z}_{temp}$	
${}^{G}\hat{\boldsymbol{x}}_{\boldsymbol{cl}}$	${}^{G}\hat{y}_{cl} \times {}^{G}\hat{z}_{cl}$	

FOOT

Axis/point	Formula	Description
${}^{G}\boldsymbol{O_{ft}}$	CA	
${}^{G}\hat{\boldsymbol{y}}_{\boldsymbol{ft}}$	$\frac{(VMH - CA) \times (FMH - CA)}{\|(VMH - CA) \times (FMH - CA)\|}$	Perpendicular to the plane defined by FMH, VMH and CA pointing upward (to be adapted for left and right sides – the formula is for right foot)
${}^{G}\hat{\boldsymbol{z}}_{\boldsymbol{ft}}$	$\frac{(SMH - CA) \times {}^{G}\hat{y}_{ft}}{\|(SMH - CA) \times {}^{G}\hat{y}_{ft}\|}$	Perpendicular to the plane defined by ${}^{G}\hat{y}_{ft}$ and SMH, pointing rightward (to be adapted for left and right sides – the formula is for right foot)
${}^{G}\hat{\boldsymbol{x}}_{\boldsymbol{tb}}$	${}^{G}\hat{y}_{ft} \times {}^{G}\hat{z}_{ft}$	

PROXIMAL FOOT

Axis/point	Formula	Description
${}^{G}\boldsymbol{O_{fp}}$	FPA	
${}^{G}\hat{\boldsymbol{x}}_{\boldsymbol{fp}}$	$\frac{FPA - FPP}{FPA - FPP}$	
${}^{G}\hat{\boldsymbol{n}}_{\boldsymbol{fp}}$	$\frac{(FP1 - FP2) \times (FP2 - FP3)}{\|(FP1 - FP2) \times (FP2 - FP3)\|}$	
${}^{G}\hat{\boldsymbol{y}}_{\boldsymbol{fp}}$	$\frac{{}^{G}\hat{x}_{fp} - {}^{G}\hat{n}_{fp}}{\|{}^{G}\hat{x}_{fp} - {}^{G}\hat{n}_{fp}\|}$	
${}^{G}\hat{\boldsymbol{z}}_{\boldsymbol{fp}}$	$\frac{{}^{G}\hat{x}_{fp} \times {}^{G}\hat{y}_{fp}}{\|{}^{G}\hat{x}_{fp} \times {}^{G}\hat{y}_{fp}\|}$	

DISTAL FOOT

Axis/point	Formula	Description
${}^{G}\boldsymbol{O_{fd}}$	$FD1$	
$\boldsymbol{O_1}$	$\frac{FD2 + FD3}{2}$	Midpoint between FD2 and FD3
${}^{G}\hat{\boldsymbol{x}}_{\boldsymbol{fd}}$	$\frac{(FD1 - O_1)}{\|(FD1 - O_1)\|}$	On the line joining O_1 and FD1, pointing forward
${}^{G}\hat{\boldsymbol{y}}_{\boldsymbol{fd}}$	$\frac{{}^{G}x_{fd} \times (FD2 - FD3)}{\|{}^{G}x_{fd} \times (FD2 - FD3)\|}$	Perpendicular to the plane defined by FD1, FD2 and FD3
${}^{G}\hat{\boldsymbol{z}}_{\boldsymbol{fd}}$	${}^{G}\hat{x}_{fd} \times {}^{G}\hat{y}_{fd}$	